

Quotient Quiver Subtraction

Amihay Hanany,^a Rudolph Kalveks,^a and Guhesh Kumaran^a

^a*Theoretical Physics Group, The Blackett Laboratory, Imperial College London, Prince Consort Road, SW7 2AZ, UK*

E-mail: a.hanany@imperial.ac.uk, rudolph.kalveks09@imperial.ac.uk,
guhesh.kumaran18@imperial.ac.uk

ABSTRACT: We develop the diagrammatic technique of quiver subtraction to facilitate the identification and evaluation of the $SU(n)$ hyper-Kähler quotient (HKQ) of the Coulomb branch of a $3d \mathcal{N} = 4$ unitary quiver theory. The target quivers are drawn from a wide range of theories, typically classified as “good” or “ugly”, which satisfy identified selection criteria. Our subtraction procedure uses quotient quivers that are “bad”, differing thereby from quiver subtractions based on Kraft-Procesi transitions. The simple diagrammatic procedure identifies one or more resultant quivers, the union of whose Coulomb branches corresponds to the desired HKQ. Examples include quivers whose Coulomb branches are moduli spaces of free fields, closures of nilpotent orbits of classical and exceptional type, and slices in the affine Grassmanian. We calculate the Hilbert Series and Highest Weight Generating functions for HKQ examples of low rank. For certain families of quivers, we are able to conjecture HWGs for arbitrary rank. We examine the commutation relations between quotient quiver subtraction and other diagrammatic techniques, such as Kraft-Procesi transitions, quiver folding, and discrete quotients.

ARXIV EPRINT: [2308.05853](https://arxiv.org/abs/2308.05853)

Contents

1	Introduction	1
2	Method of quotient quiver subtraction for $SU(n)$ HKQs	5
2.1	Analytic computation of $SU(n)$ HKQ	5
2.2	Rules for $SU(n)$ HKQ by quotient quiver subtraction	6
2.3	A physical interpretation of the $U(n)$ quotient quiver	9
2.4	Aspects of Quiver Theory	10
2.4.1	Unframed quivers	10
2.4.2	"Good", "Bad", and "Ugly" Quivers	11
2.4.3	Nilpotent Orbits and Slodowy Slices	11
2.4.4	The affine Grassmannian	12
3	Moduli Space of Free Fields	13
3.1	Moduli Space of Free Fields $SU(2)$ HKQ	13
3.1.1	$\mathbb{H}^4 // SU(2)$	13
3.1.2	$\mathbb{H}^9 // SU(2)$	14
3.1.3	$\mathbb{H}^{2k} // SU(2), k \geq 2$	15
3.1.4	$\mathbb{H}^{2k+1} // SU(2), k \geq 2$	16
3.2	Moduli Space of Free Fields $SU(3)$ HKQ	17
3.2.1	$\mathbb{H}^{16} // SU(3)$	17
4	A-type Orbits	18
4.1	A-type Orbit $SU(2)$ HKQ	18
4.1.1	$\overline{n.min.A_k} // SU(2)$	18
4.1.2	$\overline{max.A_k} // SU(2)$	22
4.2	A-type Orbit $SU(3)$ HKQ	23
4.2.1	$\overline{max.A_k} // SU(3)$	23
4.3	A-type Orbit $SU(n)$ HKQ	25
4.3.1	$\overline{max.A_{2k-1}} // SU(k)$	25
4.3.2	Height 2 Orbits $\overline{\mathcal{O}}_{(2^p, 1^{k-2p+1})}^{A_k} // SU(n)$	25
4.3.3	Height 2 Orbits $\overline{\mathcal{O}}_{(2^k)}^{A_{2k-1}} // SU(n)$	27
5	B-type Orbits	28
5.1	B-type Orbit $SU(2)$ HKQ	29
5.1.1	$\overline{min.B_k} // SU(2)$ for $k \geq 4$	29
5.1.2	$\overline{n.min.B_k} // SU(2)$ for $k \geq 3$	30
5.2	B-type Orbit $SU(3)$ HKQ	32
5.2.1	$\overline{\mathcal{O}}_{(2^4, 1^{2k-7})}^{B_k} // SU(3)$	32
5.3	B-type Orbit $SU(n)$ HKQ	35
5.3.1	Height 2 Orbits $\overline{\mathcal{O}}_{(2^{2p}, 1^{2k-4p+1})}^{B_k} // SU(n)$	35

6	C-type Orbits	36
7	D-type Orbits	36
7.1	D-type Orbit $SU(2)$ HKQ	37
7.1.1	$\overline{\min.D_k} // SU(2), k \geq 4$	37
7.1.2	$\overline{n.\min.D_k} // SU(2)$ for $k \geq 4$	39
7.2	D-type Orbit $SU(3)$ HKQ	42
7.2.1	$\overline{n.n.\min.D_6} // SU(3)$	42
7.3	D-type Orbit $SU(n)$ HKQ	43
7.3.1	$\overline{\mathcal{O}_{(2^{2p}, 12k-4p)}^{D_k}} // SU(n), n \leq p+1$	43
7.3.2	$\overline{\mathcal{O}_{(2^{2k})}^{D_{2k}}} // SU(n), n \leq k$	46
7.3.3	$\overline{\mathcal{O}_{(2^{2k}, 12)}^{D_{2k+1}}} // SU(n), n \leq k$	47
8	Exceptional Orbits	48
8.1	Exceptional Orbit $SU(2)$ HKQ	48
8.1.1	$\overline{sub.reg.G_2} // SU(2)$	48
8.1.2	$\overline{\min.F_4} // SU(2)$	49
8.1.3	$\overline{\min.E_6} // SU(2)$	50
8.1.4	$\overline{\min.E_7} // SU(2)$	50
8.1.5	$\overline{\min.E_8} // SU(2)$	51
8.2	Exceptional Orbit $SU(3)$ HKQ	51
8.2.1	$\overline{\min.E_7} // SU(3)$	52
8.2.2	$\overline{\min.E_8} // SU(3)$	53
8.3	Exceptional Orbit $SU(4)$ HKQ	53
8.3.1	$\overline{\min.E_8} // SU(4)$	53
9	Slices in Exceptional Affine Grassmannians	54
9.1	$SU(2)$ HKQ	55
9.1.1	$\overline{[\mathcal{W}_{E_6}]_{[1,0,0,0,0,1]}^{[1,0,0,0,0,1]}} // SU(2)$	55
9.1.2	$\overline{[\mathcal{W}_{E_6}]_{[0,0,1,0,0,0]}^{[0,0,1,0,0,0]}} // SU(2)$	56
9.1.3	$\overline{[\mathcal{W}_{E_6}]_{[0,0,0,0,0,1]}^{[0,0,0,0,0,2]}} // SU(2)$	57
9.1.4	$\overline{[\mathcal{W}_{E_6}]_{[0,0,0,0,0,1]}^{[0,0,0,1,1,0]}} // SU(2)$	58
9.1.5	$\overline{[\mathcal{W}_{E_6}]_{[0,2,0,0,0,0]}^{[1,0,0,1,0,0]}} // SU(2)$	59
9.1.6	$\overline{[\mathcal{W}_{E_7}]_{[0,0,0,0,0,0,1]}^{[0,0,0,1,0,0,0]}} // SU(2)$	60
9.1.7	$\overline{[\mathcal{W}_{E_7}]_{[1,0,0,0,0,0,0]}^{[0,1,0,0,0,0,0]}} // SU(2)$	61
9.2	$SU(3)$ HKQ	62
9.2.1	$\overline{[\mathcal{W}_{E_7}]_{[1,0,0,0,0,0,0]}^{[0,1,0,0,0,0,0]}} // SU(3)$	62
10	Miscellaneous Moduli Spaces	64
10.1	Star shaped quiver $SU(2)^5 // SU(2)$	65
10.2	Star shaped quiver $SU(2)^{N+1} // SU(2), N > 1$	65

10.3	A_{k-1} Class \mathcal{S} theory on a torus with 1 puncture	66
10.4	Extended E_6 quiver $\overline{\min.E_6} \times \mathbb{H}^2 // \text{SU}(2)$	66
11	Discussion and Conclusions	68
A	U(1) HKQs	79
B	U(n) HKQ Examples	80
B.1	U(n) HKQ of $\overline{\max.A_k}, k \geq 3$	80
B.2	U(k) HKQ of $\overline{\mathcal{W}_{A_{n+k-1}}}_{[0, \dots, 0, n-k, 0, 0, \dots, 0]}$ $_{[0, \dots, 0, 0, n-k-2, 0, \dots, 0]}$	81
C	Violation of the Junction Rule	82
D	Violation of the External Leg Rule	83

1 Introduction

A motivation for studying quiver gauge theories is that their graphical nature allows for simple diagrammatic and combinatorial operations that represent actions on the moduli spaces of vacua. As a consequence, information about the structure of these moduli spaces can often be found in an efficient way.

The notion of *magnetic quivers* has been applied to quantum field theories with eight supercharges in three, four, five, and six dimensions with great success [1–45]. This demonstrates the power of simple diagrammatic techniques on quivers in solving various problems within physics and is hence a motivation to develop further diagrammatic techniques.

Our focus is on moduli spaces constructed using the Coulomb branches of $3d \mathcal{N} = 4$ unitary quiver gauge theories. These can be described by Hilbert series (HS) computed using the monopole formula [46]. The monopole formula treats the Coulomb branch as a moduli space of dressed monopole operators and constructs a HS that captures how the generators of the Coulomb branch are charged under $\text{SU}(2)_R$ R -symmetry and their $\text{U}(1)_J$ topological symmetries. Relations between these charges encoded in the quiver can lead to enhanced global symmetries of the moduli space. We refer to a quiver gauge theory as a "magnetic quiver" for the moduli space, X , if the Coulomb branch of the magnetic quiver is X [1].

From a refined HS one can derive the Highest Weight Generating function (HWG) that enumerates the irreps (identified by Dynkin labels) of the global symmetry that appear at each order in the HS [47]. Sometimes, an HS or HWG can be expressed in a compact form using the Plethystic Exponential [48].

Diagrammatic operations on quivers include *folding*, *discrete gauging*, and *quiver subtraction*. These have been the subject of various studies. For example, the discrete actions of folding and discrete gauging of magnetic quivers were studied in [49–51], and quiver subtractions representing Kraft-Procesi (KP) transitions [52] between related moduli spaces

were studied in [53, 54]. Our aim herein is to build on ideas introduced in [28] and [55] to systematise a way of using quiver subtraction to take an $SU(n)$ HKQ from the Coulomb branch of a unitary magnetic quiver. This in turn allows us to explore the relationships between such diagrammatic HKQs and other operations.

The *folding* of a magnetic quiver corresponds to an action on the Coulomb branch which reduces it to a subspace that is invariant under some discrete action. This can be represented diagrammatically as the folding of k identical legs in a quiver around a common pivot node, with the introduction of a non-simply laced edge of multiplicity k [56], so that the pivot node is associated to long roots of the algebra of the global symmetry. Such folding reduces the dimension of the moduli space and may manifest in the HWG via identifications between highest weight fugacities. Examples of folded magnetic quivers appear in Sections 3, 5, 8, and 11.

The *discrete gauging* of a Coulomb branch involves the identification of points in the moduli space under a discrete action. The dimension of the space is not reduced, but its volume is reduced by a factor of the order of the discrete group. As a special case, the discrete gauging by S_k of the Coulomb branch of a magnetic quiver with a bouquet of $n \geq k$ $U(1)$ gauge nodes, can be implemented diagrammatically by collecting k such nodes into a single $U(k)$ node with an adjoint hypermultiplet [50]. This action was extended to quivers with a *complete graph* of $U(1)$ gauge nodes in [39].

Discrete gauging may manifest in the HWG (after assigning fugacities under the discrete action to its coefficients) as a finite group average over its terms according to the Burnside lemma [57]. Note that the characters of discrete symmetry groups commute with highest weight fugacities, and not Cartan sub-algebra (CSA) fugacities, so the HWG is essential for this analysis. Examples of magnetic quivers with discrete gauging appear in Sections 5, 8, 10, and 11.

The aforementioned examples draw not only upon magnetic quivers for free field theories, which present a simple background against which to develop our methods, but also upon magnetic quivers for the closures of nilpotent orbits, which are more intricate and merit some introductory comments.

The closures of nilpotent orbits of semi-simple Lie algebras ("nilpotent orbits" or "orbits") have deep connections to the Coulomb branches of $3d \mathcal{N} = 4$ theories and many have constructions from magnetic quivers [58, 59].

The theorem of Namikawa [60], applied to moduli spaces of $3d \mathcal{N} = 4$ theories, states that the chiral ring with generators at spin 1 of $SU(2)_R$ is a nilpotent orbit. This has been verified for the Coulomb branches of many magnetic quivers for nilpotent orbits by applying the monopole formula.

Nilpotent orbits, along with other Coulomb branches, are symplectic singularities and enjoy a stratification into a finite number of symplectic leaves [61]. This structure can be presented in a poset or Hasse diagram [5], which shows the partial order between (closures of) symplectic leaves in the moduli space. In the mathematics literature, Kraft and Procesi [52, 62] computed Hasse diagrams for nilpotent orbits of Classical groups and identified the transverse spaces, or KP transitions, between adjacent (closures of) symplectic leaves.

Prior studies [58] have shown that all orbits of A-type algebras, as well as all orbits with characteristic height [63]¹ equal to two, being located near the origin of such Hasse diagrams, have magnetic quivers, and magnetic quivers have also been identified for some higher orbits of non A-type algebras. Examples of unitary magnetic quivers for nilpotent orbits appear in Sections 4, 5, 7 and 8.

Discrete actions on the closures of nilpotent orbits of semi-simple Lie algebras were studied and classified mathematically by Kostant and Brylinski [64] and Kobak and Swann [65]. These studies found relationships between orbits through discrete actions, and a variety of their results have been replicated using magnetic quivers, through the *discrete gauging* of their Coulomb branches, including by diagrammatic methods [51].

In both *folding* and *discrete gauging* there exist diagrammatic operations on magnetic quivers, which represents their action on the Coulomb branch in a simple and efficient way without resorting to explicit formulae.

The usual diagrammatic method of *quiver subtraction* [66], which may relate multiple quivers, is more complicated, and draws on the irreducible nature of KP transitions. Importantly, KP transitions, such as A_k Kleinian singularities and g_k minimal nilpotent orbits, can be represented by unitary magnetic quivers, and *quiver subtraction* permits the deconstruction of a given unitary magnetic quiver into a partially ordered Hasse diagram or poset of magnetic quivers.

The *quiver subtraction* implementation of the KP transitions makes it very simple to compute the Hasse diagrams of moduli spaces which are symplectic singularities (but not necessarily orbits) providing their magnetic quivers are known.

KP transitions also have a physical realisation in Type IIB string theory in NS5-D5-D3 brane systems [53, 54]. This involves the movement of D3 branes, such as coinciding them with 5-branes in particular ways and brane creation/annihilation [67]. The net result of the manipulation of the branes matches that obtained by quiver subtraction.

Let us return now to our central topic of hyper-Kähler quotients. The Coulomb branch of a magnetic quiver is always a hyper-Kähler cone, so we can consider its hyper-Kähler quotient (HKQ) by some subgroup of its global symmetry. Physically, such an HKQ is a gauging [55] that incorporates the action of a moment map [59].

The result of an HKQ of some moduli space X with global symmetry $G_{\mathcal{C}}$ by a continuous symmetry $G \subset G_{\mathcal{C}}$ is denoted $X///G$ and depends on the explicit choice of embedding of G into $G_{\mathcal{C}}$. When all the generators of G are involved in the gauging, the resulting (quaternionic) dimension is $|X///G| = |X| - |G|$. However, if the subgroup G is "too large" (in terms of dimensions and structure) relative to X , then the resulting moduli space will have a (quaternionic) dimension greater than $|X| - |G|$, and we say that *incomplete Higgsing* has occurred.

Kobak and Swann [65] showed that the HKQs of classical orbits by continuous symmetry groups are hyper-Kähler, and provide several such examples, based mainly on HKQs by low rank unitary groups, where the resulting space is also an orbit. The U(1) HKQs

¹"Characteristic height" is defined as the dot product between the Characteristic of the orbit and the Coxeter Labels of the algebra.

appearing in Kobak-Swann's work can be replicated graphically using magnetic quivers and elementary *quiver subtraction* involving a $U(1)$ gauge node, as demonstrated in Appendix A.

Given the feasibility of implementing discrete actions and $U(1)$ HKQs on the Coulomb branch using magnetic quivers and diagrammatic techniques, and the consistency with established mathematical results, it is natural to ask whether classical group HKQs can also be realised diagrammatically.

In [28], the $SU(3)$ HKQ of the minimal orbit of E_8 was computed to give a double cover of the 21-dimensional orbit of E_6 . The observation was made that this HKQ could have been represented by the subtraction of the quiver $(1) - (2) - (3) - (2) - (1)$ from the *unframed* unitary magnetic quiver for the minimal orbit of E_8 , to produce a magnetic quiver for this double cover. See Section 8.

Another work [55] includes an example of the implementation of a $U(n)$ HKQ on a unitary magnetic quiver, using $3d$ mirror symmetry and Higgs-Coulomb branch dualities. This $U(n)$ HKQ can also be realised diagrammatically as the subtraction of the quiver $(1) - (2) - \dots - (n) - \dots - (2) - (1)$ from the framed unitary quiver, as we show in Appendix B.

In this paper we generalise this type of quiver subtraction into a precise procedure for an $SU(n)$ HKQ, providing a list of selection rules for the starting quivers from which such an HKQ is permissible. A full list of our rules for $SU(n)$ HKQs via *quotient quiver subtraction* will be provided in Section 2, but we can preview some key features.

In particular, we only work with those magnetic quivers where there is a *Dynkin type* embedding of $SU(n)$ into the global symmetry \mathcal{G}_C , and our diagrammatic selection rules avoid those magnetic quivers where *incomplete Higgsing* occurs, so that the resulting moduli spaces have the correct integer (quaternionic) dimension.

Notably, our rules involve the subtraction of a quotient quiver with gauge nodes of the form $(1) - (2) - \dots - (n) - \dots - (2) - (1)$. Such a quiver is "bad" in the sense of [68], and its Coulomb branch cannot therefore be computed using the monopole formula, differing thereby from the quivers for KP transitions, which are always "good". Nevertheless, such a quotient quiver can often be subtracted from a "good" or "ugly" magnetic quiver that has a corresponding "external leg" to produce valid magnetic quiver(s), whose Coulomb branches have the correct dimensions for an HKQ. We refer to our procedure as "*quotient quiver subtraction*" to avoid confusion with quiver subtraction for KP transitions.

A significant feature of our rules is that, in certain cases, they identify that the HKQ of a Coulomb branch is a union of Coulomb branches. We draw on methods similar to [36] to evaluate the HS of such unions and to illuminate their underlying structures.

To demonstrate our $SU(n)$ quotient quiver subtraction rules, we show how they can be applied to many examples of unitary magnetic quivers, with Coulomb branches drawn, inter alia, from free fields, classical or exceptional nilpotent orbits, and slices in the affine Grassmannian [69]. We find many relationships between such spaces, along with several results that have not, to the best of our knowledge, appeared in the physics or mathematics literature. We validate the results by computing HKQs through analytic methods using Weyl integration.

We find that diagrammatic HKQs provide a means of identifying relationships involving magnetic quivers that lie outside the realms of brane systems and class \mathcal{S} theories, and which have not been well studied in the literature.

Organisation of the paper In Section 2 we recap the usual method of taking an HKQ via Weyl integration and present our diagrammatic rules for $SU(n)$ quotient quiver subtraction, which simplify this calculation.

We also recap briefly on relevant aspects of quiver theory, including the method of (un)framing quivers, and the relationships between magnetic quivers, nilpotent orbits, Slodowy slices and slices in the affine Grassmannian. We also define the notation that we use.

In Section 3 we warm-up by testing our rules of $SU(n)$ quotient quiver subtraction on magnetic quivers for moduli spaces of free fields.

In Sections 4, 5, 6, 7 and 8 we apply the rules of $SU(n)$ quotient quiver subtraction to find HKQs of some classical and exceptional nilpotent orbits. We obtain many conjectures for relationships between orbits and/or slices in the affine Grassmannian. For low rank cases we check these relationships by computing HS and/or HWGs.

In Section 9 we apply the rules of $SU(n)$ quotient quiver subtraction to some slices in the affine Grassmannians of E_6 and E_7 , thereby testing that our rules remain valid when applied to complicated quivers.

In Section 10 we apply our rules to some miscellaneous families of magnetic quivers, in order to generalise results from earlier sections.

Finally, in the concluding Section 11, we compile some results and conjectures obtained by quotient quiver subtraction (see Tables 1, 2, 3 and 4). We also discuss how the diagrammatic technique of $SU(n)$ quotient quiver subtraction typically commutes with *folding* and *discrete gauging*, but not with quiver subtraction for KP transitions. Finally we identify some open problems.

The Appendices contain supplementary materials, including a discussion of situations where precise application of the selection rules is necessary to avoid pathological results. Additionally, we include examples of certain $U(n)$ HKQs that follow as a natural extension of the rules for $SU(n)$ presented in Section 2.

2 Method of quotient quiver subtraction for $SU(n)$ HKQs

2.1 Analytic computation of $SU(n)$ HKQ

The refined Hilbert series $HS_{G_{\mathcal{C}}}$ of the Coulomb branch of a magnetic quiver is first computed using the unitary monopole formula, as outlined in [46]. This formula counts monopole operators graded by their charges under $SU(2)_R$ R -symmetry and $U(1)_J$ topological symmetry. The fugacities associated to the topological symmetry can be mapped to the Cartan sub-algebra (CSA) fugacities of the global symmetry $G_{\mathcal{C}}$ of the Coulomb branch using the Cartan matrix. When expanded perturbatively, such an HS enumerates the characters of irreps of the global symmetry at each value of R -charge.

Suppose the global symmetry of the Coulomb branch is $G_C = \prod_i G_i$. If there exists an embedding of $SU(n)$ into some G_j , $G_j \hookrightarrow G'_j \times SU(n)$, then the general form for its hyper-Kähler quotient by $SU(n)$ is given by [58]:

$$\text{HS}_{G_C//SU(n)}(x_1, \dots, x_r; t) = \int_{SU(n)} d\mu_{SU(n)} \frac{\text{HS}_{G_C}(x_1, \dots, x_r; y_1, \dots, y_{n-1}; t)}{\text{PE}[\chi([1, 0, \dots, 0, 1]_{SU(n)})t^2]}, \quad (2.1)$$

where the x_i are fugacities for $G'_j \times \prod_{i \neq j} G_i$, and the y_i are fugacities for $SU(n)$. The denominator is a PE of the character of the adjoint of $SU(n)$, graded by the R -charge counting fugacity t .

The physical interpretation of this formula is the gauging, against a background of relations, of an $SU(n)$ subgroup of the global symmetry G_C of the Coulomb branch [55]. Explicitly, the formula starts with a Hilbert series, takes its quotient by symmetric products of the $SU(n)$ adjoint representation, and projects out $SU(n)$ singlets.

It follows from (2.1) that the quaternionic dimension of HS_{G_C} is reduced by at most $n^2 - 1$. There are two contributions, the first from the denominator of (2.1), which reduces the dimension by $(n^2 - 1)/2$, and the second from the Haar measure and Weyl integration, which affect the dimension up to a further reduction of $(n^2 - 1)/2$. We refer to *complete Higgsing* whenever $|\text{HS}_{G_C//SU(n)}| = |\text{HS}_{G_C}| - (n^2 - 1)$. Sometimes, however, HS_{G_C} fails to explore enough of the lattice of $SU(n)$ to saturate this dimensional reduction, and this is referred to as *incomplete Higgsing*.

Providing complete Higgsing occurs, the formula (2.1) is valid; otherwise it cannot be used, and a construction from first principles using moment maps is required. We focus herein on HKQs with complete Higgsing.

2.2 Rules for $SU(n)$ HKQ by quotient quiver subtraction

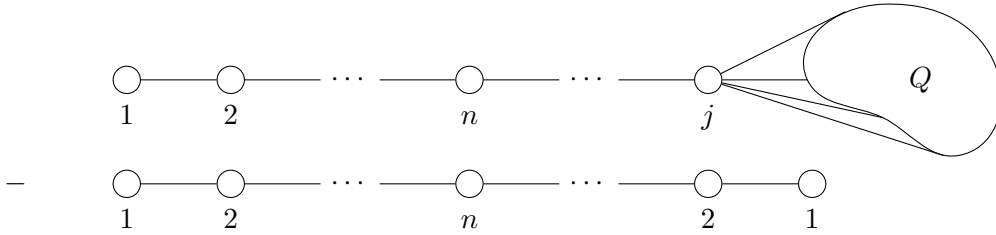


Figure 1: Schematic drawing of a valid target quiver (top) having a junction and an external leg. The target quiver for the quotient quiver subtraction must have a leg that starts as $(1) - \dots - (n)$. If the quotient quiver (bottom) overlaps a junction node of rank j on the target quiver, this must align with a node of rank $2 \leq j$ on the quotient quiver. The remainder of the target quiver, denoted Q , can take any "good" or "ugly" form.

When carrying out $SU(n)$ HKQ by quotient quiver subtraction, we find it convenient to work with unframed quivers as intermediates, and to subtract between unframed magnetic quivers to obtain a framed result.

We define the $U(n)$ *quotient quiver* as the unframed quiver $(1) - (2) - \dots - (n) - \dots - (2) - (1)$ and the *target quiver* as the unitary magnetic quiver for which the $SU(n)$ hyper-Kähler quotient of its Coulomb branch is desired. The procedure for performing an $SU(n)$ HKQ by quotient quiver subtraction is then as follows. At each stage of the procedure there are selection rules (in bold) that should be applied before continuing.

1. Select a "good" or "ugly" unitary magnetic quiver as the target.

Long Framing Rule The target quiver must be framed only on long nodes, otherwise unframing will give an ambiguous result.

2. Transform the target quiver into its unframed form.

External Leg Rule The unframed target quiver must have at least one external leg with gauge nodes of $(1) - (2) - \dots - (n)$. For a non-simply laced target quiver, this leg must correspond to long roots. Multiple legs may give a choice of HKQs.

3. Align the quotient quiver against this external leg and subtract its gauge nodes from the target.

Single Edge Rule The edges of the quotient quiver are simply laced and can only be subtracted from a section of the target quiver with single edges.

Junction Rule If the quotient quiver extends beyond a junction in the target quiver, the junction must align with a trailing node of 2 in the quotient quiver, as drawn in Figure 1.

Union Rule If the quotient quiver extends past the junction, then all possible alignments must lead to valid diagrams.

Adjoint Hypers Rule Any nodes with an adjoint hypermultiplet must survive the quotient quiver subtraction.

4. Restore the original balance of all surviving gauge nodes by attaching flavours.

Rebalancing Rule The resulting framed quiver(s) must contain no node (gauge or flavour) with negative rank.

5. If a particular alignment of the quotient quiver breaks the target into disconnected pieces, then its contribution to the moduli space is the Cartesian product of the Coulomb branches of these disjoint magnetic quivers.

6. If the target quiver contains a junction, and there are multiple possible alignments of the quotient quiver, each alignment is taken as yielding a different quiver, and the desired moduli space is the union of the Coulomb branches of these magnetic quivers.

By way of explanatory comments:

- Recall that the Hilbert series from applying the monopole formula to a simply laced magnetic quiver is insensitive to the choice of framing, and that for a non-simply laced quiver, the HS is insensitive to choice of framing amongst long nodes [70]. Quiver subtraction requires compatible framing, so that the framing on the target quiver and the quotient quiver need to be aligned before subtraction, if this is possible, by judicious shifts in framing. Alternatively, one can work with unframed quivers in both cases, and this is the diagrammatic approach that we find simpler for $SU(n)$ HKQs.
- The [External Leg Rule](#) requires that an external leg of $(1) - (2) - \dots - (n)$ must be available for subtraction of the quotient quiver. By construction, this leg has a chain of $n - 1$ balanced nodes and so contains the Dynkin diagram of A_{n-1} , thereby ensuring that there is a Dynkin type embedding of $SU(n)$, and permitting comparison with the result from Weyl integration. The sum of the ranks of the (unframed) quotient quiver is n^2 and so, when it is subtracted, the (quaternionic) dimension of the framed target quiver's Coulomb branch is reduced by $n^2 - 1$ (allowing for the dimension 1 increase from the initial unframing). This matches with the expectation from Weyl integration for an $SU(n)$ HKQ whenever there is complete Higgsing.
- The unframing of the target quiver re-introduces the center-of-mass $U(1)$ to the global symmetry. Thus the subtraction of the $U(n)$ quotient quiver (of dimension n^2) from the unframed target quiver is consistent with an $SU(n)$ HKQ.
- The [External Leg Rule](#) also requires the external leg to lie within the long roots of the target quiver. This is because the quotient quiver corresponds to long roots and so cannot be subtracted from short roots.
- Empirically, we find that quotient quiver subtraction does not match Weyl integration under violation of the [Adjoint Hypers Rule](#).
- The [Single Edge Rule](#) forbids the quotient quiver being aligned against a part of the target quiver with non-simply laced edges or multiple hypers. This is because quiver subtraction is undefined in these cases.
- The [Rebalancing Rule](#) ensures that the resulting quiver will not have any nodes (gauge or flavour) with negative rank. This is because magnetic quivers with negative rank nodes do not have an interpretation.
- The [Junction Rule](#) is an empirical rule for target quivers where the quotient quiver extends past a junction. If this rule is violated, then we have found that incomplete Higgsing occurs under Weyl integration and we are unable to validate the result from quiver subtraction. Conversely, the requirement that a junction should align with a node of at most rank 2 on the quotient quiver leads to any alternative resulting quivers having an intersection related by A-type Kleinian singularities; and this appears to be sufficient to ensure complete Higgsing.
- The [Union Rule](#) ensures that the union of the Coulomb branches of the alternative magnetic quivers can be constructed.

- The interpretation of the Coulomb branch of disconnected quivers is the natural one of a Cartesian product of Coulomb branches. In terms of HS, it is the usual multiplicative product.
- In a magnetic quiver each gauge node is associated to a different root fugacity, and the requirement of a Dynkin type embedding fixes a specific labelling of the nodes by fugacities. So even if alternative alignments of the quotient quiver are related by outer automorphism, they represent different moduli spaces, and have to be treated as distinct components of the union.
- A trivial comment is that if multiple $SU(n)$ HKQ are to be computed then one simply does quiver subtraction for each $SU(n)$ HKQ in turn. However, as we will discuss in Section 11, the order in which these are carried out may matter.

Some examples that illustrate pathological outcomes from violating the selection rules are contained in Appendices C and D.

Whenever alternative magnetic quivers result from quotient quiver subtraction, it remains to find their union. We compute the Hilbert series for the union of the Coulomb branches of a set of quivers $\{Q_i\}$, where $i = 1, \dots, n$, using the *Unions of Cones* formula [36]:

$$\begin{aligned} \text{HS}(\mathcal{C}(Q_1 \cup Q_2 \cup \dots \cup Q_n)) &= \sum_i \text{HS}(\mathcal{C}(Q_i)) - \sum_{1 \leq i < j \leq n} \text{HS}(\mathcal{C}(Q_i \cap Q_j)) \\ &+ \dots + \sum_{1 \leq i_1 < i_2 < \dots < i_p \leq n} (-1)^{p-1} \text{HS}(\mathcal{C}(Q_{i_1} \cap \dots \cap Q_{i_p})) + \dots \end{aligned} \tag{2.2}$$

The magnetic quivers for the intersections can be found by carrying out Kraft-Procesi quiver subtractions from each component of the union down to a common quiver.

This decomposition of the union as a signed sum of Coulomb branches is the reason quotient quiver subtraction provides additional insight into the structure of an HKQ compared with Weyl integration. While it is a challenge to decompose a moduli space into its constituent parts from an HS alone, with quotient quiver subtraction, each alignment directly identifies the magnetic quiver for each constituent part of the moduli space.

We test our conjecture that the $SU(n)$ HKQ of the Coulomb branch of the target quiver corresponds to the union of Coulomb branches from different possible alignments with many examples in the course of this work. To validate a quotient quiver subtraction, we compare the results to those from an $SU(n)$ HKQ by Weyl integration. We do this using the Dynkin type embedding of $SU(n)$ into $G_{\mathcal{C}}$ associated with the external leg, all as described further in each example.

2.3 A physical interpretation of the $U(n)$ quotient quiver

As mentioned, the $U(n)$ quotient quiver is “bad”, so its Coulomb branch is not computable with the monopole formula. However, we can go to the Type IIB Hanany-Witten brane system [67] for the $U(n)$ quotient quiver which is drawn in Figure 2. It is clear that from

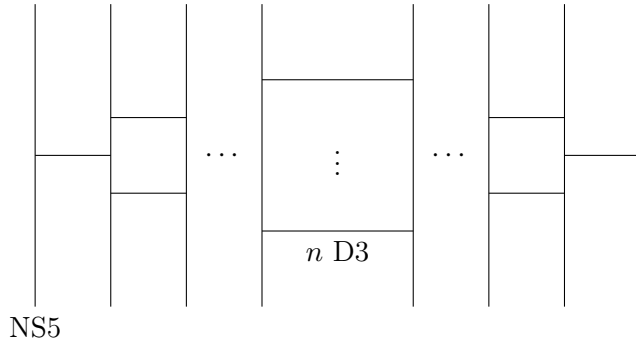


Figure 2: Type IIB brane system for the $U(n)$ quotient quiver. There are $2n$ NS5 branes with $2n - 1$ intervals on which D3 brane branes are suspended.

the point of view of the NS5 brane that this is the moduli space of an $SU(2n)$ monopole with magnetic charges $(1, 2, \dots, n, \dots, 2, 1)$. The moduli space of such a monopole has been found in the mathematics literature as $T^*SL(n)$ [71, 72]. The moduli space $T^*SL(n)$ is smooth and compact and it is at present unclear how this is connected to the $SU(n)$ HKQ, a singular operation, of Coulomb branches which are also singular and non-compact.

An alternative viewpoint is that the $U(n)$ quotient quiver can be framed as a $4d \mathcal{N} = 2$ Class \mathcal{S} theory consisting of two maximal punctures of A_{n-1} ².

2.4 Aspects of Quiver Theory

It is helpful to summarise key aspects of the theory and notational conventions that surround the magnetic quivers appearing in this paper. These include the method of *unframing*, as well as some canonical moduli spaces, such as nilpotent orbits, Slodowy slices, and Affine Grassmannian slices, many of which have magnetic quivers.

2.4.1 Unframed quivers

In any quiver gauge theory there exists an overall center-of-mass $U(1)$ symmetry that is gauged away by the choice of framing i.e. specification of flavours. In the monopole formula this is reflected in the choice of origin for the system of monopole charges, and such a choice is indeed necessary for the monopole formula to evaluate without divergence.

However, as observed in [70], this choice of origin, providing it is made amongst monopole charges associated with long roots, does not affect the Coulomb branch calculation in a fundamental manner, since the impact on the refined HS can be compensated by a suitable choice of map between node and CSA fugacities. This in turn makes it possible to treat framed unitary magnetic quivers within equivalence classes represented by an *unframed* quiver that only contains gauge nodes, as discussed in [73].

A framed unitary quiver can be converted to its *unframed* representative as follows.

1. Replace every flavour node of n by a flavour node of 1, increasing the multiplicity of direct links between it and other nodes by a factor of n to compensate.

²We thank Tudor Dimofte for discussions about this point.

2. Redraw the diagram to superimpose all the flavour nodes of 1.
3. Convert the flavour node of 1 to a U(1) gauge node.

This introduction of an overall U(1) gauge node in place of the flavour nodes is the crucial first step in the procedure for SU(n) HKQ by quotient quiver subtraction in Section 2. A framed quiver that is equivalent to the original can be recovered from the unframed quiver by setting any one of the monopole charges chosen among the long roots to zero.

2.4.2 "Good", "Bad", and "Ugly" Quivers

The terms "good", "bad", and "ugly", coined and defined in [68], are related to the R -charges of monopole operators. These follow directly from the structure of a quiver by computation of the "balance" of each gauge node. The balance b_i of a U(n_i) gauge node, having adjacent nodes (gauge or flavour) with ranks $\{r_j\}$ and link multiplicities $\{m_j\}$, is defined as:

$$b_i = \sum_{j \in \text{adjacent}} m_j r_j - 2n_i. \quad (2.3)$$

A quiver is termed "good" if all gauge nodes have non-negative balance, "ugly" if any gauge node has balance of -1 (but not less), or "bad" if any gauge node has balance less than -1 . The monopole formula will usually converge for a "good" or "ugly" theory, but not for a "bad" theory. A node is termed "balanced" if its balance is 0. In a "good" or "ugly" theory, if a (sub)set of balanced gauge nodes forms a Dynkin diagram, then a factor of this group appears in the Coulomb branch global symmetry [20]. This is due to the coincidence that additional monopole operators appear on the Coulomb branch when the balance condition is satisfied.

2.4.3 Nilpotent Orbits and Slodowy Slices

The nilpotent orbits of a Lie algebra \mathfrak{g} are in one-to-one correspondence with the different possible embeddings $G \hookrightarrow \text{SU}(2)$, due to theorems of Jacobson-Morozov [74, 75] and Kostant [76]. Knowledge of all of the embeddings of SU(2) into a Lie group G , as classified by Dynkin [77], is then sufficient to find all of its nilpotent orbits.

Each such embedding specifies the construction of a nilpotent orbit of G and is easily represented using characters. We define a map ρ which takes the simple root fugacities of G , $\{z_1, \dots, z_{\text{rank}(G)}\}$, and the CSA fugacities of G , $\{x_1, \dots, x_{\text{rank}(G)}\}$, into the CSA fugacity x of SU(2):

$$\rho : \{x_1, \dots, x_{\text{rank}(G)}\} \rightarrow \{x^{w_1}, \dots, x^{w_{\text{rank}(G)}}\}, \quad (2.4)$$

$$\rho : \{z_1, \dots, z_{\text{rank}(G)}\} \rightarrow \{x^{q_1}, \dots, x^{q_{\text{rank}(G)}}\}, \quad (2.5)$$

where the exponents q_i and w_j are necessarily related by the Cartan matrix of G :

$$q_i = \sum_j A_{ij} w_j. \quad (2.6)$$

These maps can be used to decompose irreps of G into irreps of SU(2) and this permits the labelling of nilpotent orbits in any one of a number of equivalent ways [76]:

1. By the *Characteristic*, or *root map*, set of ordered exponents $\{q_1, \dots, q_{\text{rank}(G)}\}$,
2. By the *weight map* set of ordered exponents $\{w_1, \dots, w_{\text{rank}(G)}\}$,
3. By the *partition*³ which enumerates the dimensions and multiplicity of $\text{SU}(2)$ irreps in the vector/fundamental of G under the map ρ .

A typical way of labelling the closures of nilpotent orbits is by group and partition data as $\overline{\mathcal{O}}_\rho^G$, where the overline clarifies that we are referring to the closure of the orbit. The partition data allows the nilpotent orbits of G to be organised as a Hasse diagram, and certain orbits in this poset carry canonical names. These include the minimal orbit $\overline{\text{min.}G}$, "next to" minimal orbits $\overline{n.\text{min.}G}$ (where we can use $n.$ multiple times to indicate how far an orbit is from the minimal), the sub-regular orbit $\overline{\text{sub.reg.}G}$ and the maximal or regular orbit $\overline{\text{max.}G}$ (also termed the nilcone \mathcal{N}).

Nilpotent orbits have been studied extensively in the quiver gauge theory literature [58, 59]. Notably, there exist unitary magnetic quivers for any orbit of A-type or any orbit of G that has a Characteristic height of 2. These are all balanced quivers of Dynkin type. A magnetic quiver for a height 2 orbit can be constructed by taking the Dynkin diagram of G , numbering each node in the usual way following [78], then using the weight map to assign the rank of the $U(w_i)$ gauge node at position i , and the root map to assign the attached flavours q_i .

Nilpotent orbits have transverse spaces formed by the generators of the Lie algebra \mathfrak{g} which are not included in the embedding ρ . These spaces are termed Slodowy slices, or Slodowy intersections if restricted by a superior orbit in the poset. Each such transverse space within \mathfrak{g} is defined by a pair of orbits and is notated $\mathcal{S}_{\rho,\sigma}^G$, where the slice is taken from σ to ρ . Many Slodowy slices and intersections possess unitary magnetic quivers of Dynkin type, but these are not generally balanced. For further background on Slodowy slices and intersections see [79, 80].

2.4.4 The affine Grassmannian

While we do not attempt a systematic account of the relationship between quivers and affine Grassmannian spaces, for which the reader is referred to [69], it is noteworthy that many of the quivers that result from the quotient quiver subtraction examples herein turn out to be slices in an affine Grassmannian. Indeed, any framed unitary magnetic quiver, whose gauge nodes take the form of the Dynkin diagram of some Lie group G , and which is "good" in the sense of [68] has a Coulomb branch that is a slice in the affine Grassmannian of G . This is denoted $[\mathcal{W}_{\mathfrak{g}}]_{\mathbf{b}}^{\mathbf{f}}$, where the vectors $\mathbf{f} \equiv [f_1, \dots, f_{\text{rank}(G)}]$ and $\mathbf{b} \equiv [b_1, \dots, b_{\text{rank}(G)}]$ represent flavour nodes and the balances of gauge nodes, respectively.

The flavour and balance vectors contain the same information as the flavour and gauge nodes of a unitary magnetic quiver. The ranks of the quiver gauge nodes $U(r_i)$ can thus be recovered from the affine Grassmannian slice $[\mathcal{W}_{\mathfrak{g}}]_{\mathbf{b}}^{\mathbf{f}}$ by introducing the vector

³ $(\dots, n_i^{m_i}, \dots)$ denotes a partition where the superscript m_i gives the multiplicity of the dimension n_i in the partition.

$\mathbf{r} \equiv [r_1, \dots, r_{\text{rank}(G)}]$, specialising (2.3) to the case where the quiver is of Dynkin type, and rearranging to obtain:

$$\mathbf{r} = A_{\mathfrak{g}}^{-1} \cdot (\mathbf{f} - \mathbf{b}), \quad (2.7)$$

where $A_{\mathfrak{g}}$ is the Cartan matrix for G .

Without going into too many technical details about the affine Grassmannian, in order to ensure that the corresponding magnetic quiver is "good", it is necessary that the vector $\mathbf{f} - \mathbf{b}$ lies in the positive coroot lattice of G , where the lattice is written in a basis of fundamental weights of G .

The global symmetry of an Affine Grassmannian slice $[\overline{\mathcal{W}_{\mathfrak{g}}}]_{\mathbf{b}}^{\mathbf{f}}$ is generally some proper subgroup of G , matching G only in the case where the balance vector is trivial. The magnetic quivers for nilpotent orbits of A-type and/or of height 2 constitute such examples where $\mathbf{b} = \mathbf{0}$.

The ability of the affine Grassmannian to construct a wide range of "good" theories entails that some moduli spaces known by different names also have a description as an affine Grassmannian slice. Thus, the affine Grassmannian contains magnetic quivers for some nilpotent orbits, Slodowy slices and Slodowy intersections, amongst others. We deploy these various descriptions as appropriate.

3 Moduli Space of Free Fields

We begin with magnetic quivers for some of the moduli spaces of free fields and apply the rules presented in Section 2 to compute the $SU(n)$ HKQ of the Coulomb branch using $SU(n)$ quotient quiver subtraction. Additionally, we compare $SU(n)$ quotient quiver subtraction where the explicit embedding used will be given when studying each example.

3.1 Moduli Space of Free Fields $SU(2)$ HKQ

3.1.1 $\mathbb{H}^4 // SU(2)$

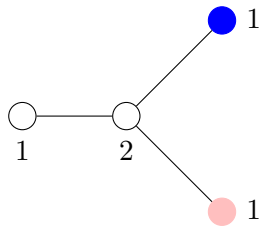


Figure 3: Unframed magnetic quiver \mathcal{Q}_3 for \mathbb{H}^4 .

The magnetic quiver \mathcal{Q}_3 for \mathbb{H}^4 is drawn in Figure 3, where we have introduced colours to distinguish nodes which have different fugacities. The quiver \mathcal{Q}_3 can also be identified as the $T_3 [SU(2)]$ theory. The global symmetry of its Coulomb branch is $SU(2)^3$.

We carry out quiver subtraction by aligning the $U(2)$ quotient quiver along the uncoloured nodes and ending on either the blue or pink node. These alternatives give the

following quivers:

$$\mathcal{Q}_{3a} = \begin{array}{c} \square \ 2 \\ | \\ \bullet \ 1 \end{array} ; \quad \mathcal{Q}_{3b} = \begin{array}{c} \square \ 2 \\ | \\ \bullet \ 1 \end{array} . \quad (3.1)$$

To calculate the union of \mathcal{Q}_{3a} and \mathcal{Q}_{3b} diagrammatically, we note that their intersection is at the origin, so the HWG of the union follows from standard results for A_1 magnetic quivers [81]:

$$HWG[\mathcal{C}(\mathcal{Q}_{3a} \cup \mathcal{Q}_{3b})] = PE[\mu^2 t^2] + PE[\nu^2 t^2] - 1 \quad (3.2)$$

$$= PE[(\mu^2 + \nu^2)t^2 - \mu^2 \nu^2 t^4], \quad (3.3)$$

where μ and ν are highest weight fugacities for each of the two $SU(2)$ subgroups. This is the D_2 minimal orbit.

The unrefined HS evaluates as:

$$HS[\mathcal{C}(\mathcal{Q}_{3a} \cup \mathcal{Q}_{3b})] = \frac{1 - t^4}{(1 - t^2)^3} + \frac{1 - t^4}{(1 - t^2)^3} - 1 \quad (3.4)$$

$$= \frac{1 + 4t^2 - 4t^4}{(1 - t^2)^2}, \quad (3.5)$$

which is of quaternionic dimension 1.

Considering the outer automorphism symmetry, the HKQ may be computed explicitly using Weyl integration by choosing any factor of $SU(2)$ to implement the quotient. This replicates the results HS and HWG above and so we find that the diagrammatic and analytic integration methods lead to the same result:

$$HS[\mathcal{C}(\mathcal{Q}_3)///SU(2)] = HS[\mathcal{C}(\mathcal{Q}_{3a} \cup \mathcal{Q}_{3b})] \quad (3.6)$$

3.1.2 $\mathbb{H}^9///SU(2)$

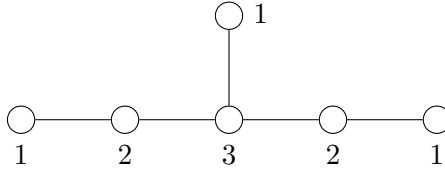


Figure 4: Unframed magnetic quiver \mathcal{Q}_4 for \mathbb{H}^9 .

The magnetic quiver \mathcal{Q}_4 for the \mathbb{H}^9 is shown in Figure 4.

The Coulomb branch has an $SU(3)^2 \times U(1)$ global symmetry, with the two $SU(3)$ being equivalent under outer automorphism. The quiver subtraction of the $U(2)$ quotient quiver is determined by aligning it along one of the factors of $SU(3)$, as shown in Figure 5. Applying the monopole formula to \mathcal{Q}_5 yields the HKQ from quiver subtraction, which we present as an unrefined HS:

$$HS[\mathbb{H}^9///SU(2)] = HS[\mathcal{C}(\mathcal{Q}_5)] = \frac{(1 + t^2)(1 + 8t^2 + t^4)}{(1 - t)^6(1 - t^2)^6} \quad (3.7)$$

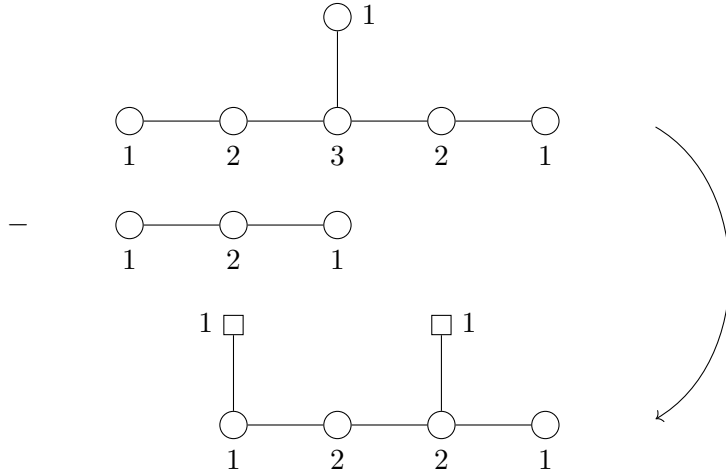


Figure 5: Subtraction of the $U(2)$ quotient quiver from \mathcal{Q}_4 to produce \mathcal{Q}_5 .

This HS can be identified as the product $a_3 \times \mathbb{H}^3$ of the $SU(4)$ minimal orbit with a 3 (quaternionic) dimensional moduli space of free fields.

To confirm this using Weyl integration, we use the embedding of $A_2 \leftrightarrow A_1 \times U(1)$ which decomposes the fundamental as:

$$[1, 0]_{A_2} \rightarrow [1]_{A_1}(1) + [0]_{A_1}(-2), \quad (3.8)$$

where the integer in the round brackets is the $U(1)$ charge. The result of the Weyl integration matches the quiver subtraction.

3.1.3 $\mathbb{H}^{2k} // SU(2), k \geq 2$

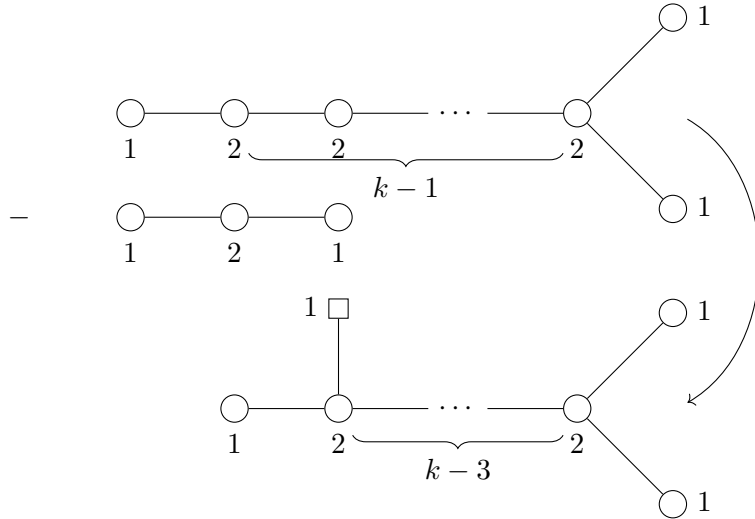


Figure 6: One subtraction of the $U(2)$ quotient quiver from the magnetic quiver \mathcal{Q}_6 for \mathbb{H}^{2k} to produce the magnetic quiver \mathcal{Q}_{28} for $\overline{min.D_k}$.

The unframed magnetic quiver \mathcal{Q}_6 for \mathbb{H}^{2k} is drawn in the top of Figure 6. This quiver takes the form of the finite D_{k+2} Dynkin diagram. The Coulomb branch has a $SO(2k) \times SU(2)$ global symmetry. Although there are two ends from which a $U(2)$ quotient quiver may be subtracted in accordance with the rules in Section 2, consider the possibility drawn in Figure 6, which results in the magnetic quiver \mathcal{Q}_{28} for $\overline{\min.D_k}$. We conjecture that

$$\mathbb{H}^{2k} // SU(2) = \overline{\min.D_k}, \quad k \geq 2. \quad (3.9)$$

We have tested the conjecture in (3.9) for $k = 2, \dots, 6$, finding agreement with Weyl integration. The first member of the family, $k = 2$, was evaluated in Section 3.1.1. The Weyl integration is performed with respect to the fugacity for the $SU(2)$ in the Coulomb branch global symmetry of \mathcal{Q}_6 .

The result (3.9) is in accordance with gauging the $SU(2)$ flavour symmetry of the quiver $[SU(2)] - [D_k]$ to give the electric quiver $(SU(2)) - [D_k]$ and comparing their Higgs branches.

3.1.4 $\mathbb{H}^{2k+1} // SU(2), k \geq 2$

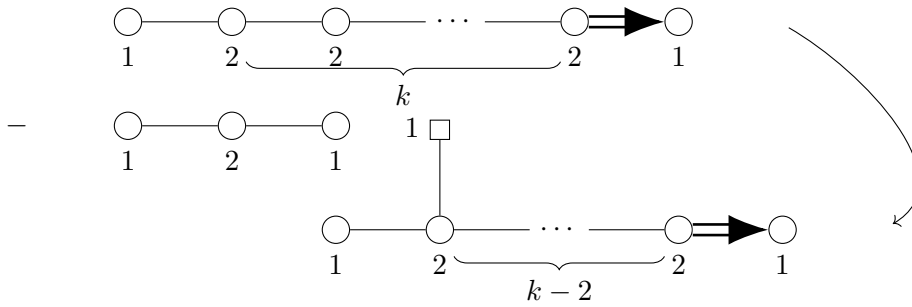


Figure 7: Subtraction of the $U(2)$ quotient quiver from the magnetic quiver \mathcal{Q}_7 for \mathbb{H}^{2k+1} to produce the magnetic quiver \mathcal{Q}_{19} for $\overline{\min.B_k}$.

The unframed magnetic quiver \mathcal{Q}_7 for \mathbb{H}^{2k+1} is drawn in the top of Figure 7. This quiver takes the form of the finite B_{k+2} Dynkin diagram. The Coulomb branch has a $SO(2k+1) \times SU(2)$ global symmetry. There is only one place from which a $U(2)$ quotient quiver may be subtracted in accordance with the rules in Section 2. This is shown in Figure 7 and results in the magnetic quiver \mathcal{Q}_{19} for $\overline{\min.B_k}$. We conjecture that

$$\mathbb{H}^{2k+1} // SU(2) = \overline{\min.B_k}, \quad k \geq 2. \quad (3.10)$$

We have tested the conjecture in (3.10) for $k = 1, \dots, 5$, finding agreement with Weyl integration. The Weyl integration is performed with respect to the fugacity for the $SU(2)$ in the Coulomb branch global symmetry of \mathcal{Q}_7 .

The result (3.10) is in accordance with gauging the $SU(2)$ flavour symmetry of the quiver $[SU(2)] - [B_k]$ to give the electric quiver $(SU(2)) - [B_k]$ and comparing their Higgs branches.

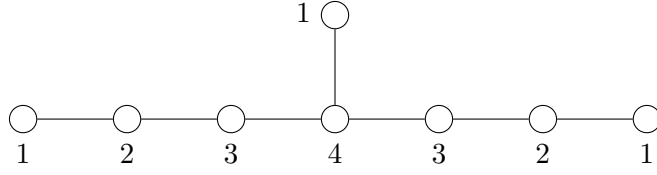


Figure 8: Unframed magnetic quiver \mathcal{Q}_8 for \mathbb{H}^{16} .

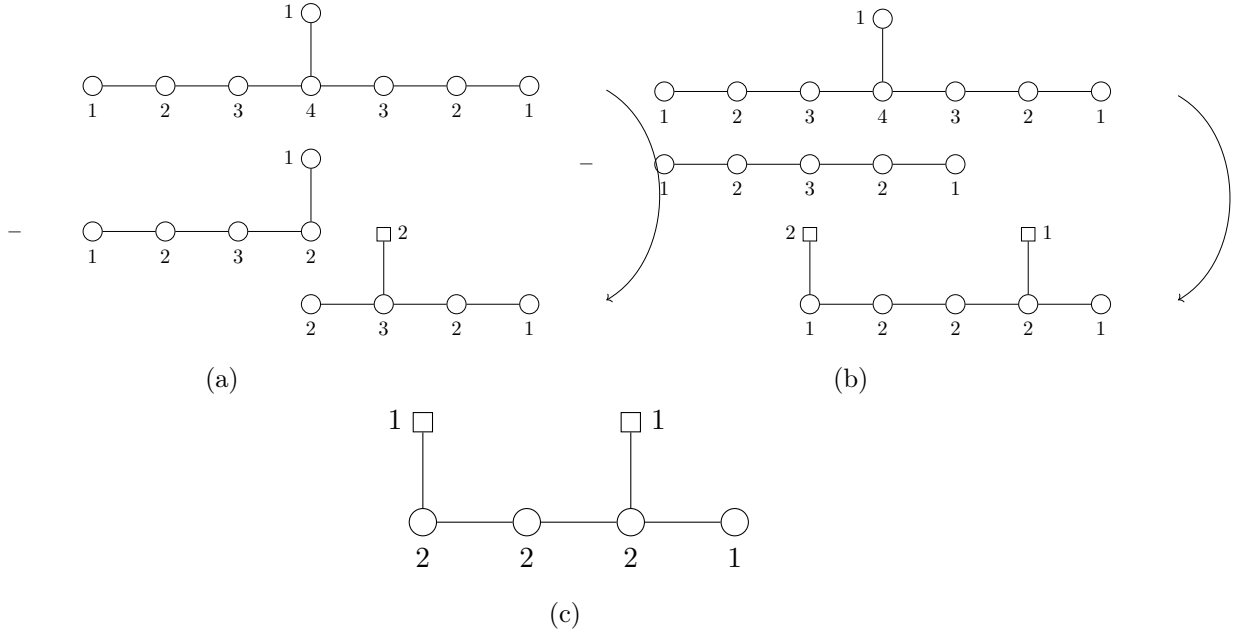


Figure 9: Both alignments of the $U(3)$ quotient quiver against \mathcal{Q}_8 producing \mathcal{Q}_{9a} and \mathcal{Q}_{9b} . Their intersection, reached via A_1 KP transitions, is quiver \mathcal{Q}_{9c} .

3.2 Moduli Space of Free Fields $SU(3)$ HKQ

3.2.1 $\mathbb{H}^{16}///SU(3)$

A magnetic quiver \mathcal{Q}_8 for \mathbb{H}^{16} is shown in Figure 8.

The Coulomb branch has an $SU(4)^2 \times U(1)$ global symmetry, with an outer automorphism between the factors of $SU(4)$. An $U(3)$ quotient quiver may be removed from either long leg, but as the quotient quiver extends past a junction, there are two possible alignments as shown in Figure 9a and Figure 9b. These produce quivers \mathcal{Q}_{9a} and \mathcal{Q}_{9b} respectively. We expect the HKQ to be the Coulomb branch of the union of \mathcal{Q}_{9a} and \mathcal{Q}_{9b} .

$$\mathbb{H}^{16}///SU(3) = \mathcal{C} \left(\begin{array}{cccc} & \square 2 & & \\ & | & & \\ \circ & - & \circ & - & \circ & - & \circ \\ 2 & & 3 & & 2 & & 1 \end{array} \right) \cup \mathcal{C} \left(\begin{array}{cccc} 2 \square & & & \square 1 \\ | & & & | \\ \circ & - & \circ & - & \circ & - & \circ \\ 1 & & 2 & & 2 & & 2 & & 1 \end{array} \right). \quad (3.11)$$

The intersection of these quivers \mathcal{Q}_{9c} is related to \mathcal{Q}_{9a} and \mathcal{Q}_{9b} by an A_1 Kraft-Processi

transition. The monopole formula can be used to compute the HS of each part of the union. The combination yields the 8 (quaternionic) dimensional HS:

$$HS = \frac{(1+t^2)^2(1+5t^2+t^4)}{(1-t)^8(1-t^2)^8} + \frac{\left(\begin{array}{l} 1+2t+13t^2+28t^3+62t^4+88t^5+128t^6+132t^7 \\ +128t^8+88t^9+62t^{10}+28t^{11}+13t^{12}+2t^{13}+t^{14} \end{array} \right)}{(1-t)^6(1-t^2)^6(1-t^3)^4} - \frac{(1+t^2)(1+8t^2+t^4)}{(1-t)^8(1-t^2)^6} \quad (3.12)$$

$$= \frac{\left(\begin{array}{l} 1+4t+18t^2+56t^3+151t^4+320t^5+581t^6+856t^7+1044t^8+1012t^9 \\ +790t^{10}+460t^{11}+177t^{12}+4t^{13}-46t^{14}-36t^{15}-15t^{16}-4t^{17}-t^{18} \end{array} \right)}{(1-t)^4(1-t^2)^8(1-t^3)^4}, \quad (3.13)$$

where the HS in order in (3.12) are for the Coulomb branches of \mathcal{Q}_{9a} , \mathcal{Q}_{9b} , and \mathcal{Q}_{9c} respectively.

Explicit computation of the HKQ by Weyl integration may be done with the following embedding of $A_3 \leftrightarrow A_2 \times U(1)$, which decomposes the fundamental as:

$$[1, 0, 0]_{A_3} \rightarrow [1, 0]_{A_2}(1) + [0, 0]_{A_2}(-3). \quad (3.14)$$

The result matches the Hilbert series from the quotient quiver subtraction.

4 A-type Orbits

Here we look at A-type nilpotent orbits and some of the HKQs one can take using $U(n)$ quotient quiver subtraction as described in Section 2. There are many orbits for which an $SU(n)$ HKQ can be computed, although we cannot use quiver subtraction to take the $SU(n)$ HKQ of any A-type orbit. For example, the magnetic quivers for $\overline{\min.A_k}$ only contain nodes of rank 1, and so do not permit the subtraction of an $U(n)$ quotient quiver – this would violate the [External Leg Rule](#).

The examples we use to illustrate the quotient quiver subtraction procedure include the $SU(2)$ HKQ of $\overline{n.\min.A_k}$, which we generalise to show how to take the $SU(n)$ quotient of any height 2 orbit of A-type, and the $SU(2)$ and $SU(3)$ HKQs of $\overline{\max.A_k}$, which we generalise for $\overline{\max.A_{2n-1}}//SU(n)$. Many other examples are possible.

To check the results of quiver subtraction using Hilbert Series (and/or HWGs) derived from Weyl integration, we employ an embedding of $A_k \leftrightarrow A_{k-n} \times A_{n-1} \times U(1)$ which decomposes the fundamental of A_k as:

$$[1, 0, \dots, 0]_{A_k} \rightarrow [1, 0, \dots, 0]_{A_{k-n}}(n) + [1, 0, \dots, 0]_{A_{n-1}}(n-k-1), \quad (4.1)$$

where we have used $()$ to denote $U(1)$ charges and suppressed any singlets.

4.1 A-type Orbit $SU(2)$ HKQ

4.1.1 $\overline{n.\min.A_k}//SU(2)$

The magnetic quivers for $\overline{n.\min.A_k}$, with $k \geq 4$, meet the criteria for an $SU(2)$ quiver subtraction. (We note in passing that the unframed magnetic quiver for $\overline{n.\min.A_3}$, shown

in Figure 10, has a double link, and so not all alignments of the U(2) quotient quiver are consistent with the [Single Edge Rule](#), and the quiver subtraction fails.)

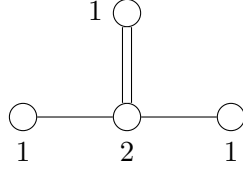


Figure 10: Unframed magnetic quiver \mathcal{Q}_{10} for $\overline{n.min.A_3}$.

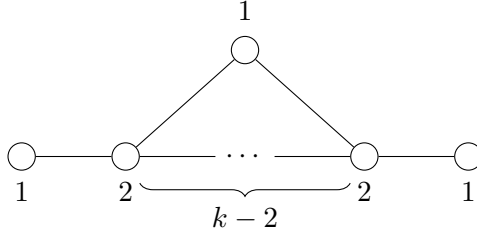


Figure 11: Unframed magnetic quiver \mathcal{Q}_{11} for $\overline{n.min.A_k}$ for $k \geq 4$.

A magnetic quiver \mathcal{Q}_{11} for $\overline{n.min.A_k}$ is drawn in Figure 11. We wish to carry out quiver subtraction to find the SU(2) HKQ. There is one special case for $k = 4$ to consider before generalising. There are two possible alignments of the U(2) quotient quiver and so the result is a union of Coulomb branches. The quiver subtractions (once an end node has been chosen) are as shown in Figure 12, and result in the framed quivers \mathcal{Q}_{12a} and \mathcal{Q}_{12b} .

We can identify the Coulomb branches of these quivers as the orbit $\overline{\mathcal{O}}_{(3)}^{A_2}$ and the affine Grassmannian slice $\overline{[\mathcal{W}_{D_3}]_{[0,0,2]}}^{[0,1,3]}$. These are 3 (quaternionic) dimensional moduli spaces, with global symmetries SU(3) and SU(3) \times U(1), respectively.⁴ We conjecture that:

$$\overline{n.min.A_4} // \text{SU}(2) = \overline{\mathcal{O}}_{(3)}^{A_2} \cup \overline{[\mathcal{W}_{D_3}]_{[0,0,2]}}^{[0,1,3]}. \quad (4.2)$$

To compute this union, we first find the intersection of \mathcal{Q}_{12a} and \mathcal{Q}_{12b} . This is a magnetic quiver \mathcal{Q}_{12c} for $\overline{min.A_2}$, reached in both cases by an A_2 Kraft-Procesi transition.

Thus, the conjecture leads to an HWG for the union as the signed sum of HWGs:

$$\begin{aligned} HWG \left[\overline{\mathcal{O}}_{(3)}^{A_2} \cup \overline{[\mathcal{W}_{D_3}]_{[0,0,2]}}^{[0,1,3]} \right] &= PE \left[\mu_1 \mu_2 t^2 + \mu_1 \mu_2 t^4 + (\mu_1^3 + \mu_2^3) t^6 - \mu_1^3 \mu_2^3 t^{12} \right] \\ &\quad + PE \left[(1 + \mu_1 \mu_2) t^2 + \left(\mu_2 q^2 + \frac{\mu_1}{q^2} \right) t^4 - \mu_1 \mu_2 t^8 \right] \\ &\quad - PE \left[\mu_1 \mu_2 t^2 \right], \end{aligned} \quad (4.3)$$

where $\mu_{1,2}$ are highest weight fugacities for A_2 , q is a fugacity for U(1) charges, and the three PEs encode the HWGs for $\overline{\mathcal{O}}_{(3)}^{A_2}$, $\overline{[\mathcal{W}_{D_3}]_{[0,0,2]}}^{[0,1,3]}$, and the intersection $\overline{min.A_2}$, respectively. The results (4.2) and (4.3) are confirmed by Weyl integration.

⁴This slice in the affine Grassmannian of D_3 can also be identified as the Slodowy intersection $\mathcal{S}_{(4,1^2),(2^3)}^{A_5}$.

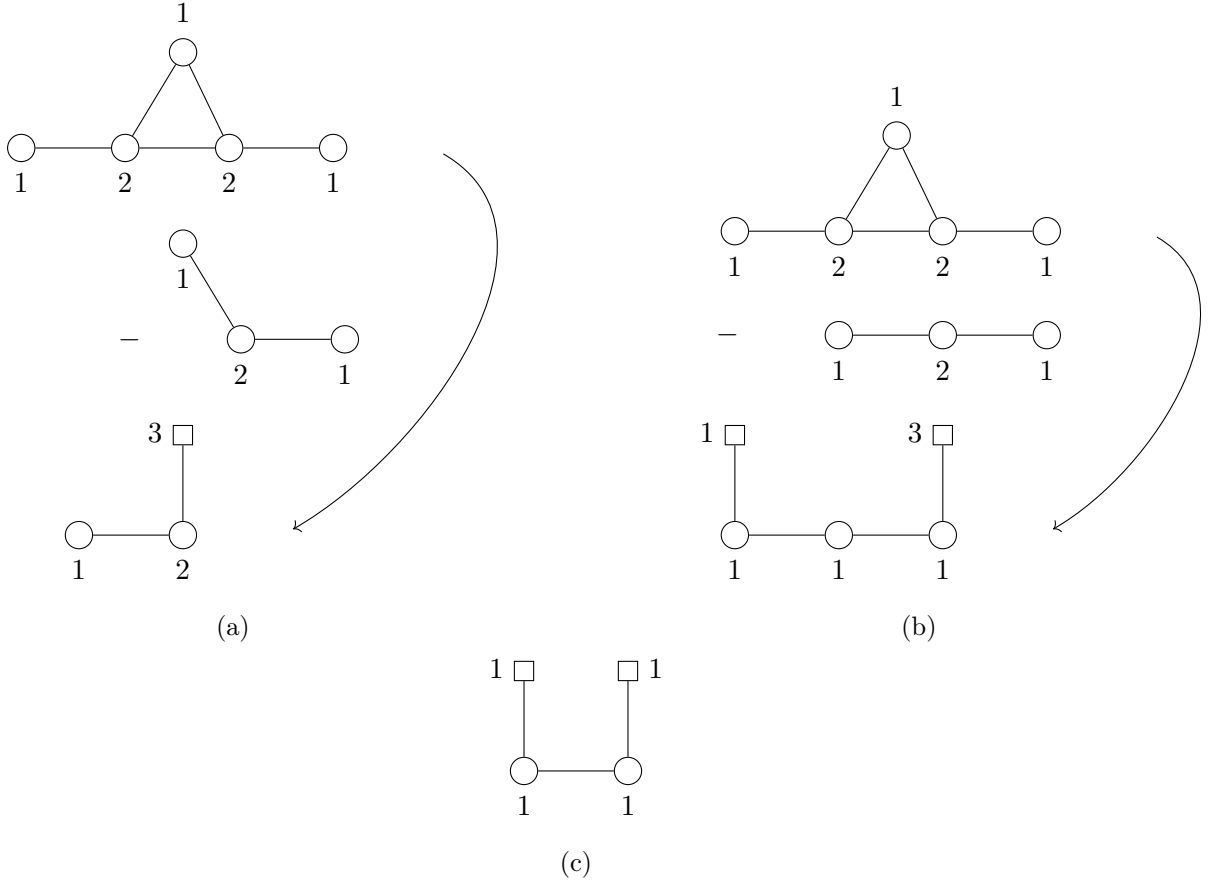


Figure 12: Both alignments of the $U(2)$ quotient quiver against the unframed magnetic quiver \mathcal{Q}_{11} for $\overline{\min.A_4}$ to give the quivers \mathcal{Q}_{12a} and \mathcal{Q}_{12b} . Their intersection, reached via A_2 Kraft-Procesi transitions, is quiver \mathcal{Q}_{12c} .

Now consider the general case for $\overline{n.\min.A_k}$, $k \geq 5$. There are two possible alignments of the $U(2)$ quotient quiver, as shown in Figure 13.

These yield the quivers \mathcal{Q}_{13a} and \mathcal{Q}_{13b} respectively. We identify their Coulomb branches as the orbit $\overline{\mathcal{O}}_{(3,1^{k-4})}^{A_{k-2}}$ and the affine Grassmannian slice $\overline{[\mathcal{W}_{D_{k-1}}]_{[0,0,\dots,2]}^{[0,1,\dots,2]}}$, which have global symmetries A_{k-2} and $A_{k-2} \times U(1)$, respectively. So, based on quiver subtraction, we conjecture that:

$$\overline{n.\min.A_k} // \text{SU}(2) = \overline{\mathcal{O}}_{(3,1^{k-4})}^{A_{k-2}} \cup \overline{[\mathcal{W}_{D_{k-1}}]_{[0,0,\dots,2]}^{[0,1,\dots,2]}}, \quad k \geq 5. \quad (4.4)$$

In order to evaluate the union, we note that quivers \mathcal{Q}_{13a} and \mathcal{Q}_{13b} are both related by an A_1 KP transition to the magnetic quiver \mathcal{Q}_{13c} for $\overline{n.\min.A_{k-2}}$. So, we evaluate the

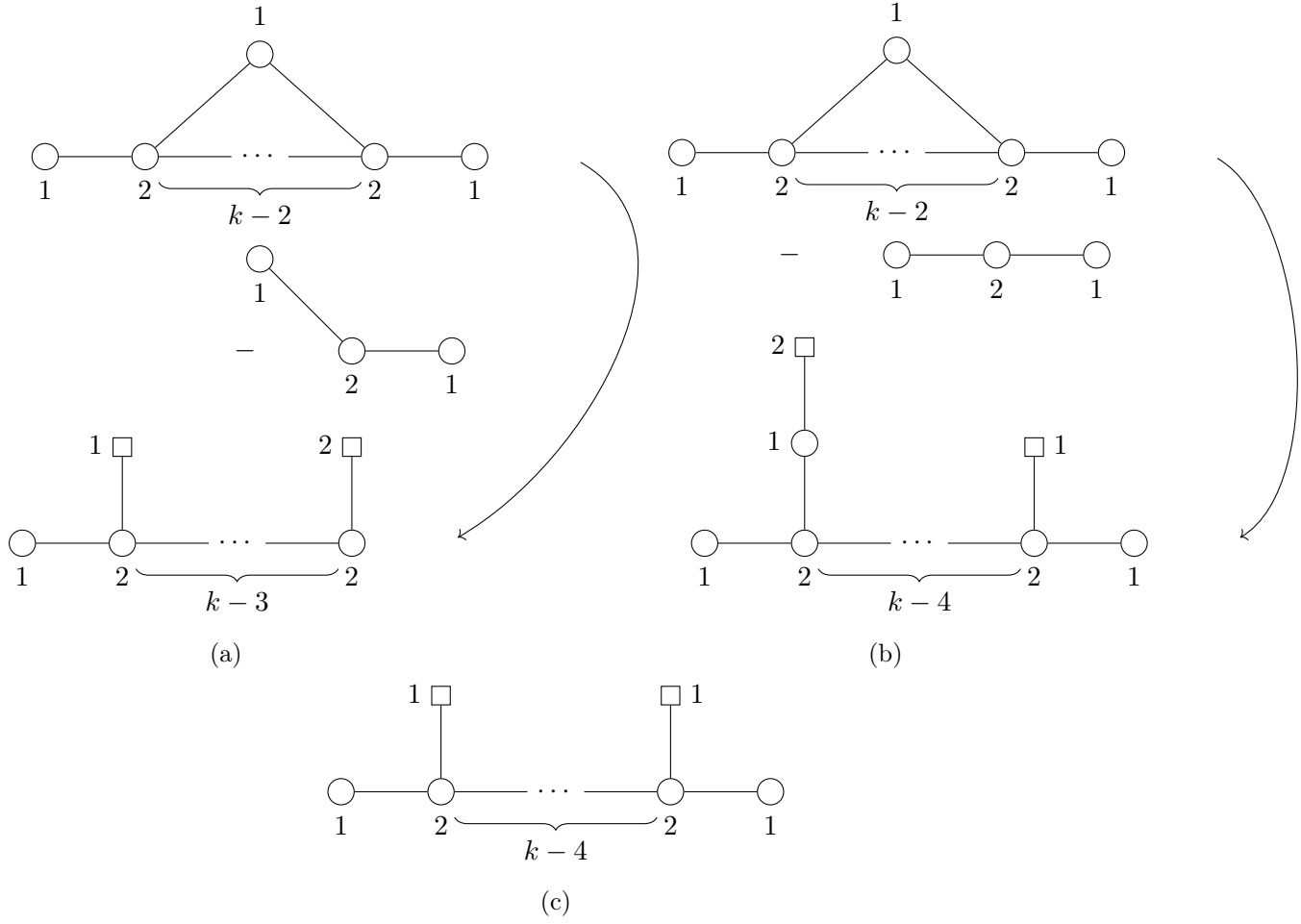


Figure 13: Both alignments of the $U(2)$ quotient quiver against the unframed magnetic quiver \mathcal{Q}_{11} for $\overline{\min.A_k}$ for $k \geq 5$ to give the quivers \mathcal{Q}_{13a} and \mathcal{Q}_{13b} . Their intersection, reached via A_1 Kraft-Procesi transitions, is quiver \mathcal{Q}_{13c} .

HWG as:

$$\begin{aligned}
& HWG \left[\overline{\mathcal{O}}_{(3,1^{k-4})}^{A_{k-2}} \cup \overline{[\mathcal{W}_{D_{k-1}}]_{[0,0,\dots,2]}}^{[0,1,\dots,2]} \right] \\
&= PE \left[\sum_{i=1}^2 \mu_i \mu_{k-1-i} t^{2i} + \mu_1 \mu_{k-2} t^4 + (\mu_1^2 \mu_{k-3} + \mu_2 \mu_{k-2}^2) t^6 - \mu_1^2 \mu_2 \mu_{k-3} \mu_{k-2}^2 t^{12} \right] \\
&+ PE \left[t^2 + \sum_{i=1}^2 \mu_i \mu_{k-1-i} t^{2i} + \left(\mu_2 q^2 + \frac{\mu_{k-3}}{q^2} \right) t^4 - \mu_2 \mu_{k-3} t^8 \right] \\
&- PE \left[\sum_{i=1}^2 \mu_i \mu_{k-1-i} t^{2i} \right], \quad k \geq 5, \tag{4.5}
\end{aligned}$$

where $\mu_{1,2,\dots,k-2}$ are highest weight fugacities for A_{k-2} and q is a fugacity for $U(1)$ charges.

In principle, the HWG (4.5) can be checked for any given value of k using Weyl inte-

gration. We have evaluated the cases for $k \leq 8$ and found these to be consistent with the conjecture (4.4). However, the nice decomposition of the HWG as a sum of polynomial PEs is only manifest under the quiver subtraction approach.

4.1.2 $\overline{max.A_k} // SU(2)$

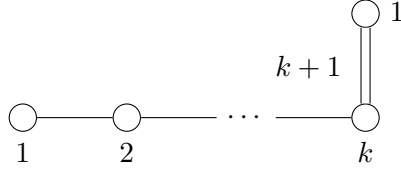


Figure 14: Unframed magnetic quiver \mathcal{Q}_{14} for $\overline{max.A_k}$ for $k \geq 1$.

A magnetic quiver \mathcal{Q}_{14} for $\overline{max.A_k}$ is shown in Figure 14. The label $k + 1$ next to the multiple edges indicates that there are $k + 1$ hypermultiplets transforming in the bifundamental of the $U(k)$ and $U(1)$ gauge groups. For $k \geq 3$, this magnetic quiver meets the criteria in Section 2 for quiver subtraction by an $SU(2)$ HKQ.

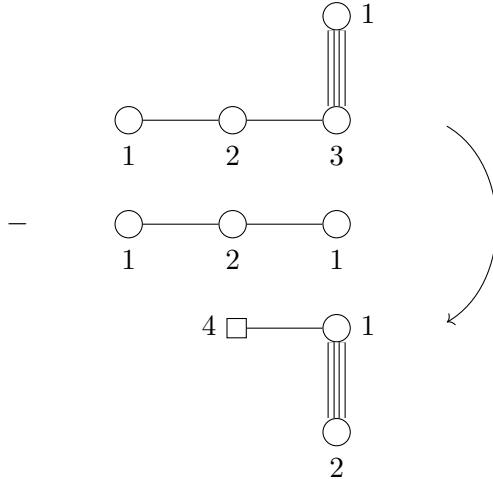


Figure 15: Subtraction of the $U(2)$ quotient quiver from the magnetic quiver \mathcal{Q}_{14} for $\overline{max.A_3}$ to give quiver \mathcal{Q}_{15} .

There is a special case for $k = 3$. Figure 15 shows the subtraction of the $U(2)$ quotient quiver from the unframed magnetic quiver for $\overline{max.A_3}$, which results in the framed quiver \mathcal{Q}_{15} .

In order to decipher the Coulomb branch of \mathcal{Q}_{15} , we note that this quiver is simply laced, so we can choose to shift the framing to the gauge node of rank 1, such that the quiver decouples into a pair of quivers, $(2) - [4]$ and $(1) - [4]$. We can identify their Coulomb branches as the Slodowy slices $\mathcal{S}_{\mathcal{N},(2^2)}^{A_3}$ [79] and $\mathbb{C}^2/\mathbb{Z}_4$ [5], respectively. Thus, we obtain the result (verified by Weyl integration):

$$\overline{max.A_3} // \text{SU}(2) = \mathcal{C} \left(\begin{array}{c} \square 4 \\ | \\ \textcircled{2} \text{---} \textcircled{1} \end{array} \right) = \mathcal{C} \left(\begin{array}{c} \square 4 \\ | \\ \textcircled{2} \end{array} \otimes \begin{array}{c} \square 4 \\ | \\ \textcircled{1} \end{array} \right) = \mathcal{S}_{\mathcal{N},(2^2)}^{A_3} \otimes \mathbb{C}^2 / \mathbb{Z}_4 \quad (4.6)$$

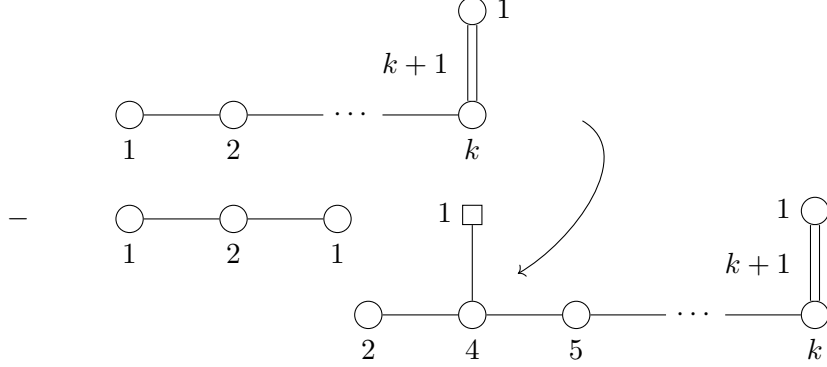


Figure 16: Subtraction of the U(2) quotient quiver from the magnetic quiver \mathcal{Q}_{14} for $\overline{max.A_k}$ to give quiver \mathcal{Q}_{16} .

Now consider the general case for $k > 3$. The subtraction of the U(2) quotient quiver from the unframed magnetic quiver for $\overline{max.A_k}$ is shown in Figure 16. The Coulomb branch of the resulting quiver \mathcal{Q}_{16} is the affine Grassmannian slice $[\mathcal{W}_{D_{k-1}}]_{[0,0,\dots,2]}^{[k+1,0,\dots,0]}$, (as can be seen by shifting the framing to the gauge node of rank 1 with $k+1$ links). This has (quaternionic) dimension $k(k+1)/2 - 3$ and a global symmetry $\text{SU}(k-1) \times \text{U}(1)$.

Thus, we have obtained the general conjecture:

$$\overline{max.A_k} // \text{SU}(2) = \mathcal{C} \left(\begin{array}{c} \square k+1 \\ | \\ \textcircled{k} \text{---} \dots \text{---} \textcircled{5} \text{---} \textcircled{4} \text{---} \textcircled{2} \\ | \\ \textcircled{1} \end{array} \right) = [\mathcal{W}_{D_{k-1}}]_{[0,0,\dots,2]}^{[k+1,0,\dots,0]}, \quad k \geq 4. \quad (4.7)$$

We have checked (4.6) and (4.7) explicitly for $k \leq 7$, using Weyl integration, with the embeddings (4.1).

4.2 A-type Orbit SU(3) HKQ

4.2.1 $\overline{max.A_k} // \text{SU}(3)$

For $k \geq 5$, the magnetic quivers \mathcal{Q}_{14} for $\overline{max.A_k}$ permit subtraction of an U(3) quotient quiver.

There is a special case for $k = 5$. Upon performing the quiver subtraction and shifting the framing, as before, we obtain:

$$\overline{max.A_5} // SU(3) = \mathcal{C} \left(\begin{array}{c} \square 6 \\ | \\ \textcircled{2} \text{---} \textcircled{4} \text{---} \textcircled{1} \\ \text{6} \end{array} \right) = \mathcal{C} \left(\begin{array}{c} \square 6 \\ | \\ \textcircled{1} \end{array} \otimes \begin{array}{c} \square 6 \\ | \\ \textcircled{2} \text{---} \textcircled{4} \end{array} \right), \quad (4.8)$$

where the index above the multiple edge connecting the nodes of rank 4 and 1 indicates an edge multiplicity of 6. We observe that the $U(3)$ quotient quiver saturates the magnetic quiver for $\overline{max.A_5}$, with the result that the latter decouples as the product of two moduli spaces. The Coulomb branch of (1) – [6] is the A_5 Kleinian singularity $\mathbb{C}^2/\mathbb{Z}_6$ and the Coulomb branch of (2) – (4) – [6] is $\mathcal{S}_{A_5, (2^3)}^{\mathcal{N}}$, the Slodowy slice to the orbit of A_5 labelled by partition (2^3) . The combined moduli space is 7 (quaternionic) dimensional and has an $SU(3) \times U(1)$ global symmetry. Thus, we have obtained the result that:

$$\overline{max.A_5} // SU(3) = \mathcal{S}_{A_5, (2^3)}^{\mathcal{N}} \otimes \mathbb{C}^2/\mathbb{Z}_6. \quad (4.9)$$

The next case is that for $k = 6$. Performing the quiver subtraction, we find the magnetic quiver for $[\mathcal{W}_{A_4}]_{[0,0,0,4]}^{[0,0,7,0]}$ whose Coulomb branch is 13 (quaternionic) dimensional and has an $SU(4) \times U(1)$ global symmetry. We conclude that

$$\overline{max.A_6} // SU(3) = \mathcal{C} \left(\begin{array}{c} \square 7 \\ | \\ \textcircled{2} \text{---} \textcircled{4} \text{---} \textcircled{6} \text{---} \textcircled{1} \end{array} \right) = [\mathcal{W}_{A_4}]_{[0,0,0,4]}^{[0,0,7,0]} \quad (4.10)$$

Finally, for $k \geq 7$ we obtain the general result

$$\overline{max.A_k} // SU(3) = \mathcal{C} \left(\begin{array}{c} \square k+1 \\ | \\ \textcircled{2} \text{---} \textcircled{4} \text{---} \textcircled{6} \text{---} \textcircled{7} \text{---} \dots \text{---} \textcircled{k} \\ \text{1} \end{array} \right), \quad k \geq 7, \quad (4.11)$$

where we have made the choice to frame the node of $k + 1$, instead of the node added for rebalancing. The resulting quiver has a global symmetry of $SU(k - 2) \times U(1)$ on its Coulomb branch. For the cases $k = 7, 8, 9, 10$, these Coulomb branches are slices in the affine Grassmannians $[\overline{\mathcal{W}_{D_5}}]_{[0,0,0,4]}^{[0,0,0,8,0]}$, $[\overline{\mathcal{W}_{E_6}}]_{[0,0,0,0,4]}^{[0,0,0,0,9,0]}$, $[\overline{\mathcal{W}_{E_7}}]_{[0,0,0,0,0,4]}^{[0,0,0,0,0,10,0]}$, and $[\overline{\mathcal{W}_{E_8}}]_{[0,0,0,0,0,0,4]}^{[0,0,0,0,0,0,11,0]}$, respectively.

Two things must be noted; the first is that all of the balance vectors are of the form $[0, \dots, 0, 4]$ and the flavour vectors for k is of the form $[0, \dots, 0, k + 3, 0]$. The second point to note is that the gauge nodes in the resulting quiver for $\overline{max.A_k} // SU(3)$ forms the E_{k-2} Dynkin diagram and so this particular HKQ gives an E -sequence.

4.3 A-type Orbit $SU(n)$ HKQ

4.3.1 $\overline{max.A_{2k-1}}//SU(k)$

The maximal orbits $\overline{max.A_{2k-1}}$ are saturated by HKQs of type $SU(k)$, and this gives rise to decoupling into a product space. The cases $\overline{max.A_3}//SU(2)$ and $\overline{max.A_5}//SU(3)$ analysed earlier are the lowest rank members of this family, which generalises to all $k \geq 2$.

We carry out the subtraction of an $U(k)$ quotient quiver from the magnetic quiver for the maximal orbit $\overline{max.A_{2k-1}}$ using the rules, followed by a frame shift to manifest the global symmetry. We obtain the product of two magnetic quivers:

$$\overline{max.A_{2k-1}}//SU(k) = \mathcal{C} \left(\begin{array}{c} \begin{array}{c} \square \\ | \\ \circ \\ 1 \end{array} \quad \otimes \quad \begin{array}{c} \circ \\ \text{---} \circ \\ \text{---} \circ \\ \text{---} \dots \\ \text{---} \circ \\ 2k-2 \end{array} \end{array} \right). \quad (4.12)$$

The Coulomb branch of the first quiver is the A_{2k-1} Kleinian singularity or $\mathbb{C}^2/\mathbb{Z}_{2k}$, which has the global symmetry $U(1)$. (It can also be identified as the Slodowy slice $\mathcal{S}_{\mathcal{N},(2^k)}^{A_{2k-1}}$.) The second quiver is also a Slodowy slice to an orbit of A_{2k-1} , labelled this time by the partition (2^k) , which has the global symmetry A_{k-1} . Thus we obtain the result:

$$\overline{max.A_{2k-1}}//SU(k) = \mathbb{C}^2/\mathbb{Z}_{2k} \otimes \mathcal{S}_{\mathcal{N},(2^k)}^{A_{2k-1}}. \quad (4.13)$$

The combined moduli space has quaternionic dimension $k^2 - k + 1$ and its global symmetry is $A_{k-1} \times U(1)$. The Hilbert series of this product space can be found using the formulae in [1].

4.3.2 Height 2 Orbits $\overline{\mathcal{O}}_{(2^p, 1^{k-2p+1})}^{A_k} // SU(n)$

We consider the two-parameter family of orbits of A_k that are given by a partition of $k + 1$ of the form $(2^p, 1^{k-2p+1})$, for some integer p . These are all height 2 orbits, have the property that their HWGs are PEs of a polynomial, and take a known form derivable from the orbit partition data [58].

The magnetic quiver \mathcal{Q}_{17} for this two-parameter family is drawn in Figure 17. All

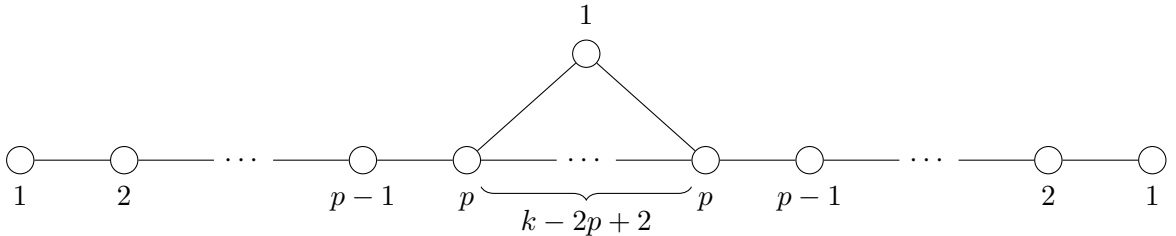


Figure 17: Unframed magnetic quiver \mathcal{Q}_{17} for the orbit of A_k with partition $(2^p, 1^{k-2p+1})$ of $k + 1$.

$$\overline{\mathcal{O}}_{(2^p)}^{A_{2p-1}} // SU((p+1)/2) = \mathcal{C} \left(\begin{array}{c} \text{Quiver Diagram} \\ \text{---} \\ n = (p+1)/2 \end{array} \right), \quad (4.18)$$

The quiver diagram consists of a horizontal chain of nodes. From left to right, the nodes are: a circle with '2' below it, a circle with '4' below it, an ellipsis, a circle with 'p-1' below it, a circle with 'p-1' below it, a circle with 'p-2' below it, an ellipsis, and a circle with '1' below it. Above the 'p-1' node is a circle with '1' above it, which is connected to a square with '2' above it. Above the second 'p-1' node is a square with '1' above it.

The Coulomb branch of the resulting quiver $\mathcal{Q}_{(4.18)}$ has global symmetry $SU((3p-1)/2) \times U(1)$ as the balanced gauge nodes along the bottom form the Dynkin diagram of $A_{3(p+1)/2}$ and the top gauge node of 1 is overbalanced with balance $2p-2$.

5 B-type Orbits

Here we consider nilpotent orbits of B-type algebras and the possible $SU(n)$ HKQs that one can take using the quiver subtraction procedure described in Section 2.

In particular, we take the examples of magnetic quivers for the orbits $\overline{min.B_k}$ and $n.min.B_k$ computing their $SU(2)$ HKQs. We also study the magnetic quiver for the orbit $\overline{\mathcal{O}}_{(2^4, 1^{2k-7})}^{B_k}$ under an $SU(3)$ HKQ. These orbits are all height 2 and have magnetic quivers that are flavoured on a long node. Based on this analysis we provide a conjecture that extends to all valid $SU(n)$ HKQs of such orbits. In each case we specify the conditions on the values of k and n which follow from the quotient quiver subtraction rules in Section 2.

The results for HKQs from quiver subtraction can be validated by comparison with explicit computations using Weyl integration. For the $SU(2)$ HKQs, we use the embedding $B_k \hookrightarrow B_{k-2} \times D_2$, which decomposes the vector of B_k as:

$$[1, 0, 0]_{B_3} \rightarrow [2]_{B_1} + [1, 1]_{D_2}, \quad (5.1)$$

$$[1, 0, \dots, 0]_{B_{k \geq 4}} \rightarrow [1, 0, \dots, 0]_{B_{k-2}} + [1, 1]_{D_2}, \quad (5.2)$$

where the singlets have been suppressed. In the above branching, the embedding is symmetric in the two factors of A_1 inside D_2 and so we can perform the HKQ w.r.t either. For the $SU(3)$ HKQ, we use the embedding of $B_k \hookrightarrow B_{k-3} \times A_2 \times U(1)$, under which the vector of B_k decomposes as:

$$[1, 0, \dots, 0]_{B_k} \rightarrow [1, 0, \dots, 0]_{B_{k-3}}(0) + [1, 0]_{A_2}(1) + [0, 1]_{A_2}(-1), \quad (5.3)$$

where the $U(1)$ charge is given by $()$.

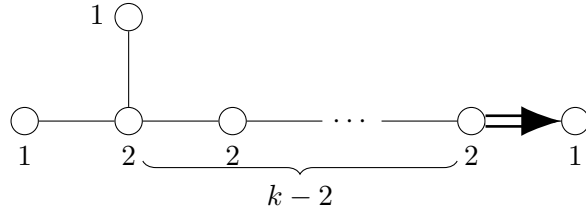


Figure 19: Unframed magnetic quiver \mathcal{Q}_{19} for $\overline{\min.B_k}$.

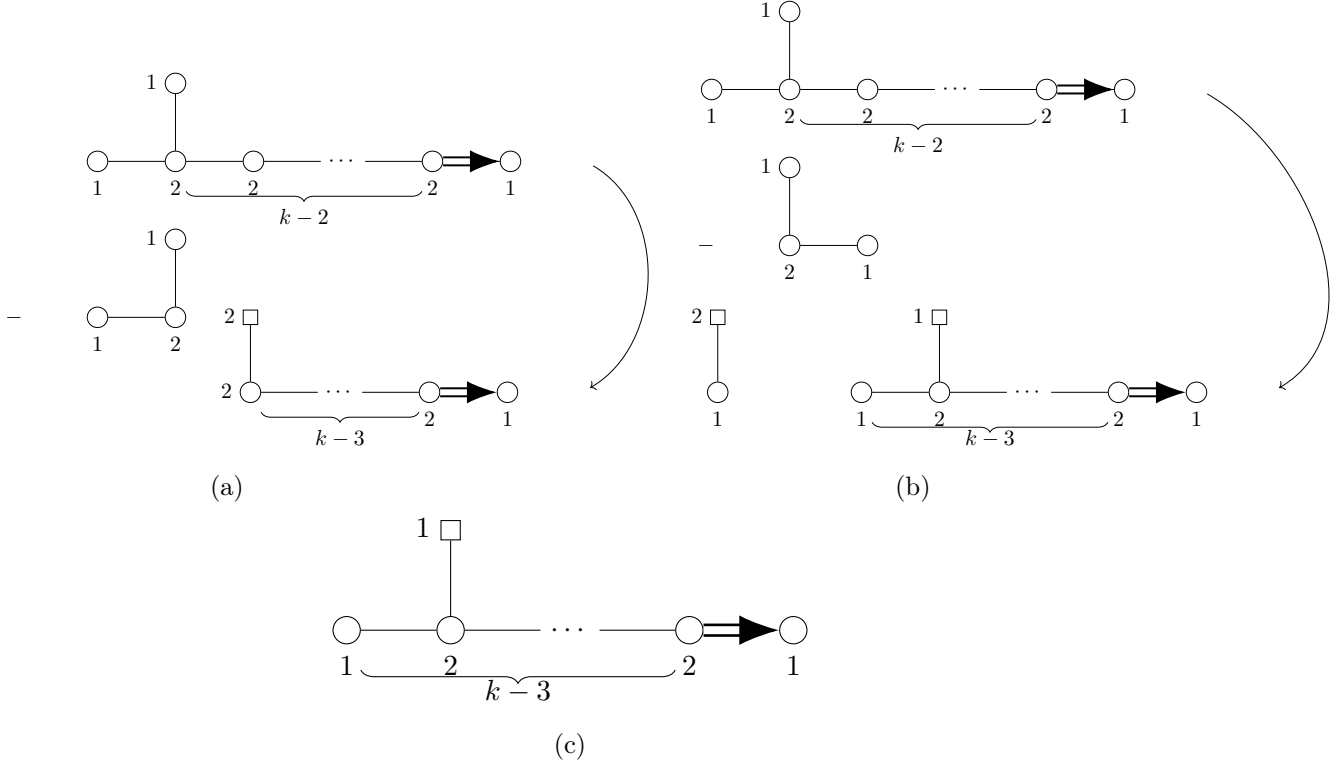


Figure 20: Both alignments of the $U(2)$ quotient quiver against the unframed magnetic quiver \mathcal{Q}_{19} for $\overline{\min.B_k}$, giving the quivers \mathcal{Q}_{20a} and \mathcal{Q}_{20b} . Their intersection, reached via A_1 KP transitions, is quiver \mathcal{Q}_{20c} .

5.1 B-type Orbit $SU(2)$ HKQ

5.1.1 $\overline{\min.B_k} // SU(2)$ for $k \geq 4$

An unframed magnetic quiver \mathcal{Q}_{19} for the orbit $\overline{\min.B_k}$ is shown in Figure 19. Only the cases for $k \geq 4$ respect all of the selection rules in Section 2. (The case $k = 3$ would require the alignment of the $U(2)$ quotient quiver with a non-simply laced edge in order to comply with the [Union Rule](#), and this would in turn violate the [Single Edge Rule](#).)

Considering the permissible cases for $k \geq 4$, there are two possible alignments of the $U(2)$ quotient quiver, as shown in Figure 20, and these result in the quivers \mathcal{Q}_{20a} and \mathcal{Q}_{20b} . The Coulomb branches of \mathcal{Q}_{20a} and \mathcal{Q}_{20b} are $\overline{n.\min.B_{k-2}}$ and $\overline{\min.A_1 \otimes \min.B_{k-2}}$,

respectively. Thus we conjecture that:

$$\overline{\min.B_k} // \text{SU}(2) = \overline{n.\min.B_{k-2}} \cup (\overline{\min.A_1} \otimes \overline{\min.B_{k-2}}), k \geq 4. \quad (5.4)$$

\mathcal{Q}_{20a} and \mathcal{Q}_{20b} are both related to their intersection \mathcal{Q}_{20c} , which is a magnetic quiver for $\overline{\min.B_{k-2}}$, by A_1 Kraft-Procesi transitions.

The HWG corresponding to the Hilbert Series of this union follows from the HWGs for its components and intersection, according to the unions of cones formula 2.2:

$$\begin{aligned} \text{HWG} [\overline{n.\min.B_{k-2}} \cup (\overline{\min.A_1} \otimes \overline{\min.B_{k-2}})] &= PE[\mu_2 t^2 + \mu_1^2 t^4] + PE[\nu^2 t^2] PE[\mu_2 t^2] - PE[\mu_2 t^2] \\ &= PE [(\mu_2 + \nu^2) t^2 + \mu_1^2 t^4 - \mu_1^2 \nu^2 t^6], \quad (5.5) \end{aligned}$$

where $\mu_{1,2}$ are highest weight fugacities for B_{k-2} and ν is a highest weight fugacity for A_1 . The first line gives the signed sum of the HWGs for $\overline{n.\min.B_{k-2}}$, $\overline{\min.A_1} \otimes \overline{\min.B_{k-2}}$, and $\overline{\min.B_{k-2}}$ respectively. As we see, this form of the HWG is easily reached using the diagrammatic technique of quotient quiver subtraction. Conveniently, the component HWGs all share a common $PE[\mu_2 t^2]$ term and this allows the recombination into a single PE, as in the second line.

We have checked the agreement between quiver subtraction and Weyl integration for $k \leq 8$ (using the embedding in (5.2)).

5.1.2 $\overline{n.\min.B_k} // \text{SU}(2)$ for $k \geq 3$

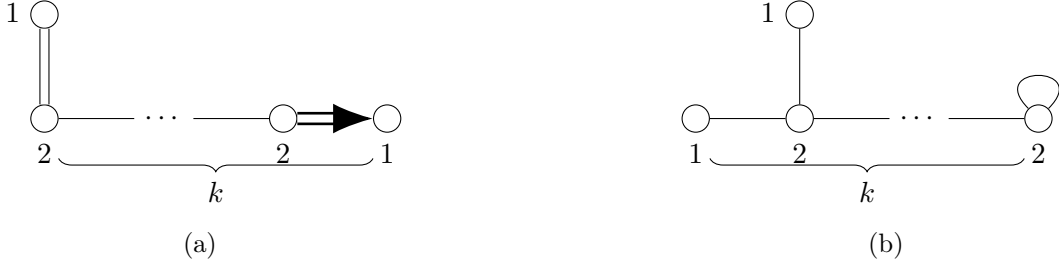


Figure 21: Alternative unframed magnetic quivers \mathcal{Q}_{21a} and \mathcal{Q}_{21b} for the $\overline{n.\min.B_k}$ for $k \geq 2$. Only \mathcal{Q}_{21b} is amenable to the $\text{SU}(n)$ HKQ quiver subtraction rules.

A typical unframed magnetic quiver \mathcal{Q}_{21a} for $\overline{n.\min.B_k}$ is drawn in Figure 21a. However, the presence of the double link means that this violates the [External Leg Rule](#) for $\text{SU}(2)$ quiver subtraction. Instead, we consider an alternative magnetic quiver \mathcal{Q}_{21b} for $\overline{n.\min.B_k}$, as shown in Figure 21b; this does permit the subtraction of the $\text{U}(2)$ quotient quiver while respecting all of the selection rules in Section 2 for $k \geq 3$. Note that the case for $k = 2$ violates the [Adjoint Hypers Rule](#).

First, there is a special case for $k = 3$. In this case there are two alignments, with the quiver subtractions as shown in Figure 22, producing quivers \mathcal{Q}_{22a} and \mathcal{Q}_{22b} . We identify the Coulomb branches of these as $\text{Sym}^2(\mathbb{C}^2/\mathbb{Z}_2) \simeq \text{Sym}^2(\overline{\min.A_1})$ [31] and $\overline{\min.A_1} \otimes \overline{\min.A_1}$, since the adjoint hypermultiplet on a $\text{U}(1)$ gauge node makes a trivial contribution to the monopole formula. We find:

$$\overline{n.\min.B_3} // \text{SU}(2) = \text{Sym}^2(\overline{\min.A_1}) \cup (\overline{\min.A_1} \otimes \overline{\min.A_1}). \quad (5.6)$$

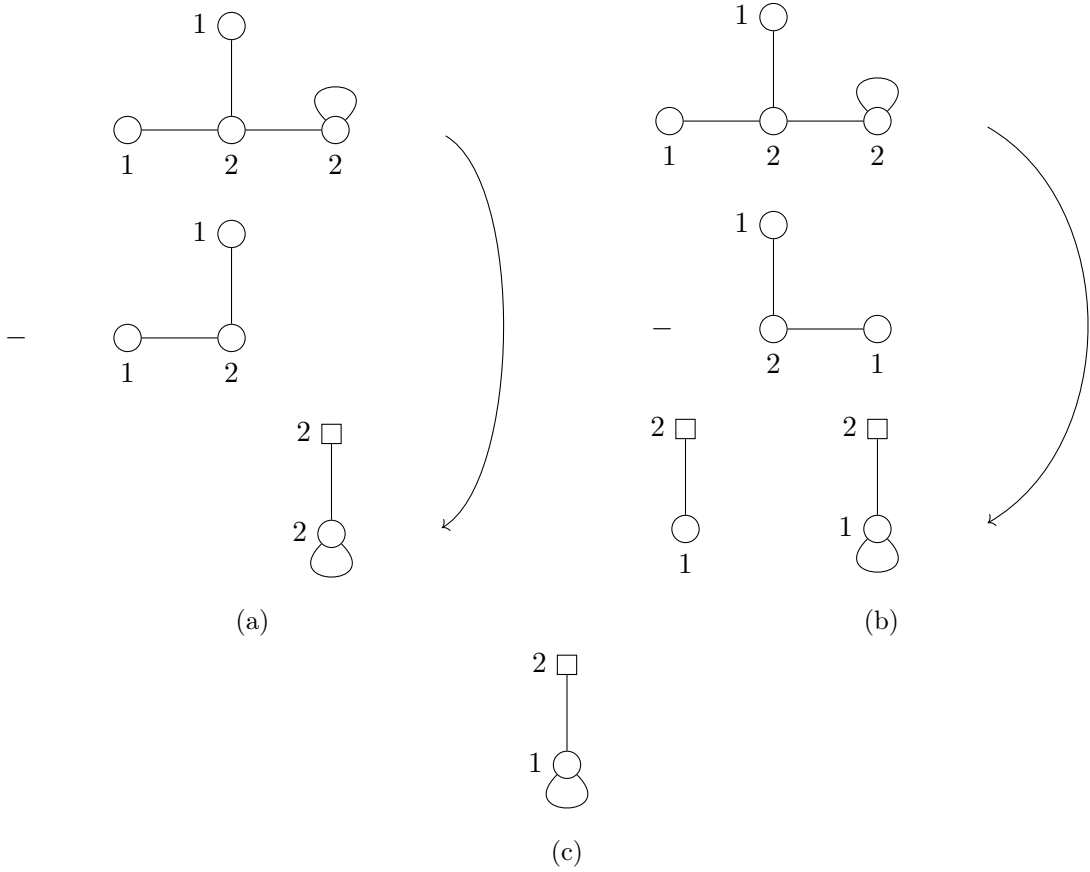


Figure 22: Both alignments of the $U(2)$ quotient quiver against the unframed magnetic quiver \mathcal{Q}_{21b} for $\overline{n.min.B_3}$, giving the quivers \mathcal{Q}_{22a} and \mathcal{Q}_{22b} . Their intersection, reached via A_1 KP transitions, is quiver \mathcal{Q}_{22c} .

To compute the union, we note that there is an A_1 Kraft-Procesi transition from each quiver to their intersection \mathcal{Q}_{22c} which is a magnetic quiver for $\overline{min.A_1}$. The HWG for the components can be computed, and using the union of cones formula (2.2) one finds that:

$$\begin{aligned}
 HWG [Sym^2 (\overline{min.A_1}) \cup (\overline{min.A_1} \otimes \overline{min.A_1})] &= PE[\mu^2 t^2 + (1 + \mu^4)t^4 + \mu^4 t^6 - \mu^8 t^{12}] \\
 &\quad + PE[\mu^2 t^2] PE[\nu^2 t^2] - PE[\mu^2 t^2], \quad (5.7)
 \end{aligned}$$

where μ is a highest weight fugacity for the common A_1 shared by the Coulomb branches of \mathcal{Q}_{22a} and \mathcal{Q}_{22b} , and ν is the highest weight fugacity for the A_1 in the Coulomb branch of \mathcal{Q}_{22b} only. We have checked this explicitly using the embedding (5.1) and Weyl integration.

Now we consider the more general case for $k \geq 4$. As shown in Figure 23, there are two possible alignments of the $U(2)$ quotient quiver, which produce quivers \mathcal{Q}_{23a} and \mathcal{Q}_{23b} . The Coulomb branches of these are identified as $\overline{n.min.D_{k-2}/\mathbb{Z}_2}$ and $\overline{min.A_1} \otimes \overline{n.min.B_{k-2}}$, respectively. The HKQ is the union of the Coulomb branches of these quivers. We conjecture:

$$\overline{n.min.B_k} // SU(2) = \overline{n.min.D_{k-2}/\mathbb{Z}_2} \cup (\overline{min.A_1} \otimes \overline{n.min.B_{k-2}}), \quad k \geq 4. \quad (5.8)$$

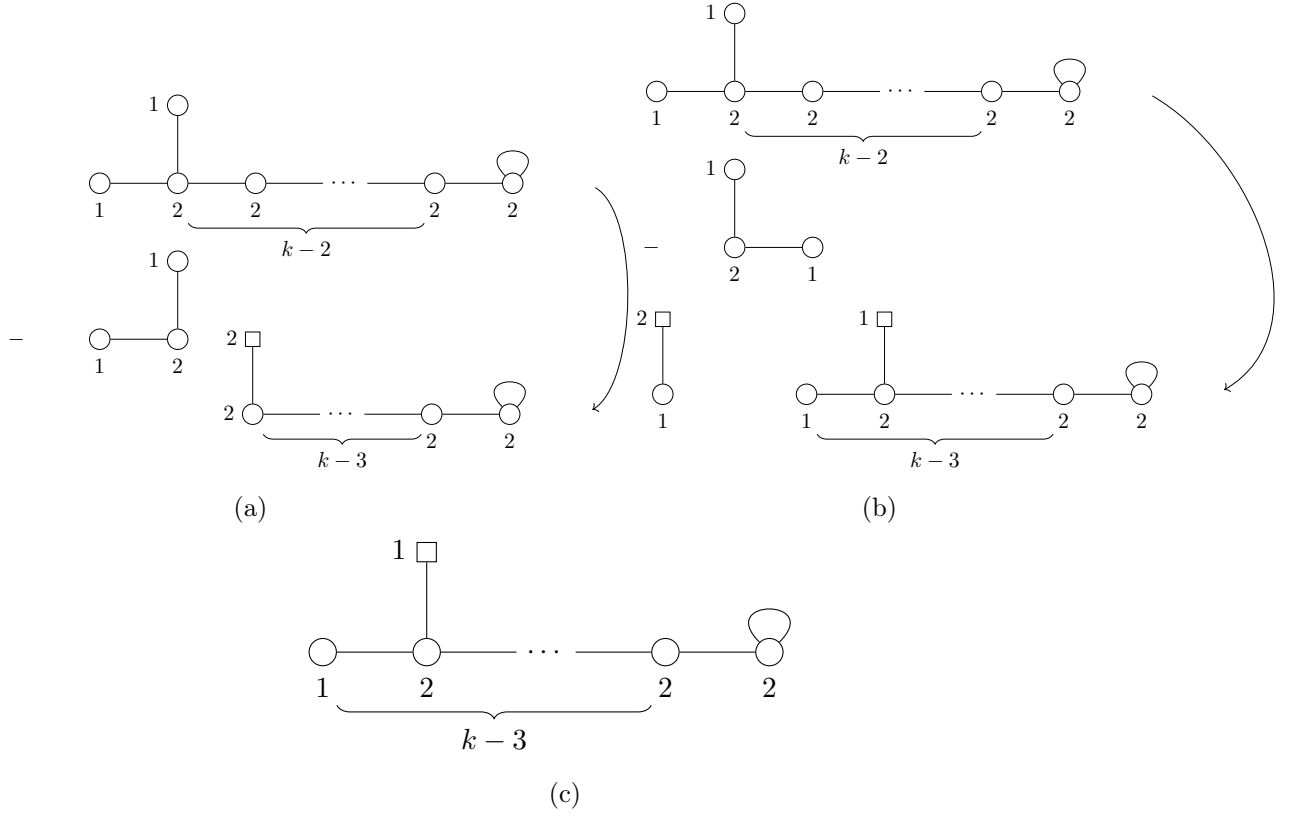


Figure 23: Both alignments of the $U(2)$ quotient quiver against the unframed magnetic quiver \mathcal{Q}_{21b} for $\overline{n.min.B_{k \geq 4}}$, giving the quivers \mathcal{Q}_{23a} and \mathcal{Q}_{23b} . Their intersection, reached via A_1 KP transitions, is quiver \mathcal{Q}_{23c} .

We can perform an A_1 KP transition on each quiver to give the intersection \mathcal{Q}_{23c} which is a magnetic quiver for $\overline{n.min.B_{k-2}}$. The HWG for the union can be found as the signed sum (2.2) of the component HWGs:

$$\begin{aligned}
& HWG[\overline{n.min.D_{k-2}/\mathbb{Z}_2} \cup (\overline{min.A_1} \otimes \overline{n.min.B_{k-2}})] \\
&= PE [\mu_2 t^2 + (2\mu_1^2 + 1) t^4 + \mu_1^2 t^6 - \mu_1^4 t^{12}] + PE[\nu^2 t^2] PE [\mu_2 t^2 + \mu_1^2 t^4] - PE [\mu_2 t^2 + \mu_1^2 t^4]
\end{aligned} \tag{5.9}$$

where $\mu_{1,2}$ are highest weight fugacities for B_k and ν is a highest weight fugacity for A_1 . The component HWGs are those for $\overline{n.min.D_{k-2}/\mathbb{Z}_2}$, $\overline{min.A_1} \otimes \overline{n.min.B_{k-2}}$, and $\overline{n.min.B_{k-2}}$, respectively. We have checked this explicitly using the embedding (5.2) and Weyl integration.

5.2 B-type Orbit $SU(3)$ HKQ

5.2.1 $\overline{\mathcal{O}}_{(2^4, 12k-7)}^{B_k} // SU(3)$

The magnetic quiver \mathcal{Q}_{24} for the orbit $\overline{\mathcal{O}}_{(2^4, 12k-7)}^{B_k}$ is shown in Figure 24. This quiver only respects the rules in Section 2 for $SU(3)$ quiver subtraction when $k \geq 6$.

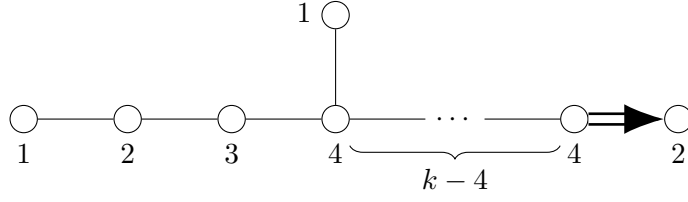


Figure 24: Unframed magnetic quiver \mathcal{Q}_{24} for the $\overline{\mathcal{O}}_{(2^4, 12k-7)}^{B_k}$.

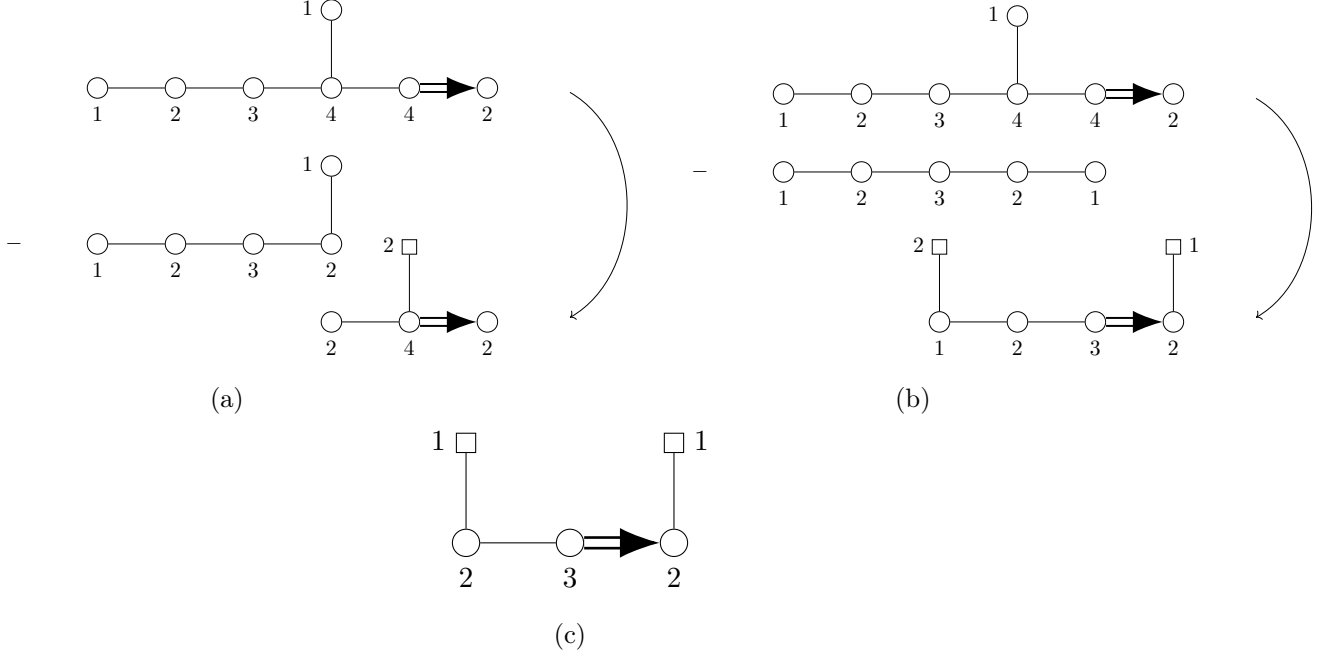


Figure 25: Both alignments of the $U(3)$ quotient quiver against \mathcal{Q}_{24} for $k = 6$ giving the quivers \mathcal{Q}_{25a} and \mathcal{Q}_{25b} . Their intersection, reached via A_1 KP transitions, is quiver \mathcal{Q}_{25c} .

The case for $k = 6$ is special. There are two alignments, shown in Figure 25, which produce quivers \mathcal{Q}_{25a} and \mathcal{Q}_{25b} . We identify the Coulomb branches of these quivers as $\overline{[\mathcal{W}_{B_3}]_{[0,0,0]}^{[0,2,0]}}$ and $\overline{[\mathcal{W}_{B_4}]_{[2,0,0,0]}^{[2,0,0,1]}}$, which have global symmetries of $SO(7)$ and $SO(7) \times U(1)$ respectively. We conclude:

$$\overline{\mathcal{O}}_{(2^4, 1^5)}^{B_6} // \text{SU}(3) = \overline{[\mathcal{W}_{B_3}]_{[0,0,0]}^{[0,2,0]}} \cup \overline{[\mathcal{W}_{B_4}]_{[2,0,0,0]}^{[2,0,0,1]}}. \quad (5.10)$$

Once again there is an A_1 KP transition from each of the two quivers to their intersection, \mathcal{Q}_{25c} which is a magnetic quiver for $\overline{[\mathcal{W}_{B_3}]_{[0,0,0]}^{[1,0,1]}}$, the double cover of the orbit $\overline{\mathcal{O}}_{(3^2, 1)}^{B_3}$ [82].

The HWG of the union in (5.10) can be computed as:

$$\begin{aligned}
& HWG \left(\overline{[\mathcal{W}_{B_3}]_{[0,0,0]}}^{[0,2,0]} \cup \overline{[\mathcal{W}_{B_4}]_{[2,0,0,0]}}^{[2,0,0,1]} \right) \tag{5.11} \\
&= \begin{pmatrix} 1 + \mu_2 t^6 + \mu_1 \mu_3^2 t^8 + \mu_1 \mu_2 \mu_3^2 t^{10} - \mu_1 \mu_2 \mu_3^2 t^{12} \\ - \mu_1 \mu_2^2 \mu_3^2 t^{14} - \mu_1^2 \mu_2 \mu_3^4 t^{16} - \mu_1^2 \mu_2^2 \mu_3^4 t^{22} \end{pmatrix} PE [\mu_2 t^2 + (1 + \mu_1^2 + \mu_2 + \mu_3^2) + 2\mu_1 \mu_3^2 t^6 + \mu_2^2 t^8] \\
&+ \begin{pmatrix} 1 + \mu_1 \mu_3^2 t^6 - \mu_1^2 t^8 - 2\mu_1 \mu_3^2 t^{10} - (\mu_1^2 \mu_3^2 t^{10})/q - \mu_1^2 \mu_3^2 q t^{10} - \mu_3^4 t^{12} \\ - (\mu_1 \mu_3^4 t^{12})/q - \mu_1 \mu_3^4 q t^{12} + \mu_1^3 \mu_3^2 t^{14} + (\mu_1^2 \mu_3^2 t^{14})/q + \mu_1^2 \mu_3^2 q t^{14} \\ + 2\mu_1^2 \mu_3^4 t^{16} + (\mu_1 \mu_3^4 t^{16})/q + \mu_1 \mu_3^4 q t^{16} + \mu_1 \mu_3^6 t^{18} - \mu_1^2 \mu_3^4 t^{20} - \mu_1^3 \mu_3^6 t^{26} \end{pmatrix} \\
&\times PE [(1 + \mu_2) t^2 + (\mu_1^2 + \mu_1 q + \mu_1/q + \mu_2 + \mu_3^2) t^4 + (\mu_3^2 q + \mu_3^2/q + \mu_1 \mu_3^2) t^6] \\
&- PE [\mu_2 t^2 + (\mu_1^2 + \mu_2 + \mu_3^2) t^4 + 2\mu_1 \mu_3^2 t^6 - \mu_1^2 \mu_3^4 t^{12}], \tag{5.12}
\end{aligned}$$

where the constituent HWG in the signed sum (5.12) are for; $\overline{[\mathcal{W}_{B_3}]_{[0,0,0]}}^{[0,2,0]}$, $\overline{[\mathcal{W}_{B_4}]_{[2,0,0,0]}}^{[2,0,0,1]}$, and their intersection $\overline{[\mathcal{W}_{B_3}]_{[0,0,0]}}^{[1,0,1]}$ respectively. The HS for the HKQ in (5.10) can be computed using the embedding (5.3) and is matching with the HS of the union in (5.10) thereby verifying (5.10), however the HWG of the HKQ in (5.10) is difficult to compute and the expression as a signed sum (5.12) is conjectured to be the correct answer. The advantage of the method of $U(n)$ quotient quiver subtraction to aid in computations is clear, as the computation of the HWG for the HKQ (5.10) has been broken down into smaller computations. Now we consider the more general case for $k \geq 7$. There are again two

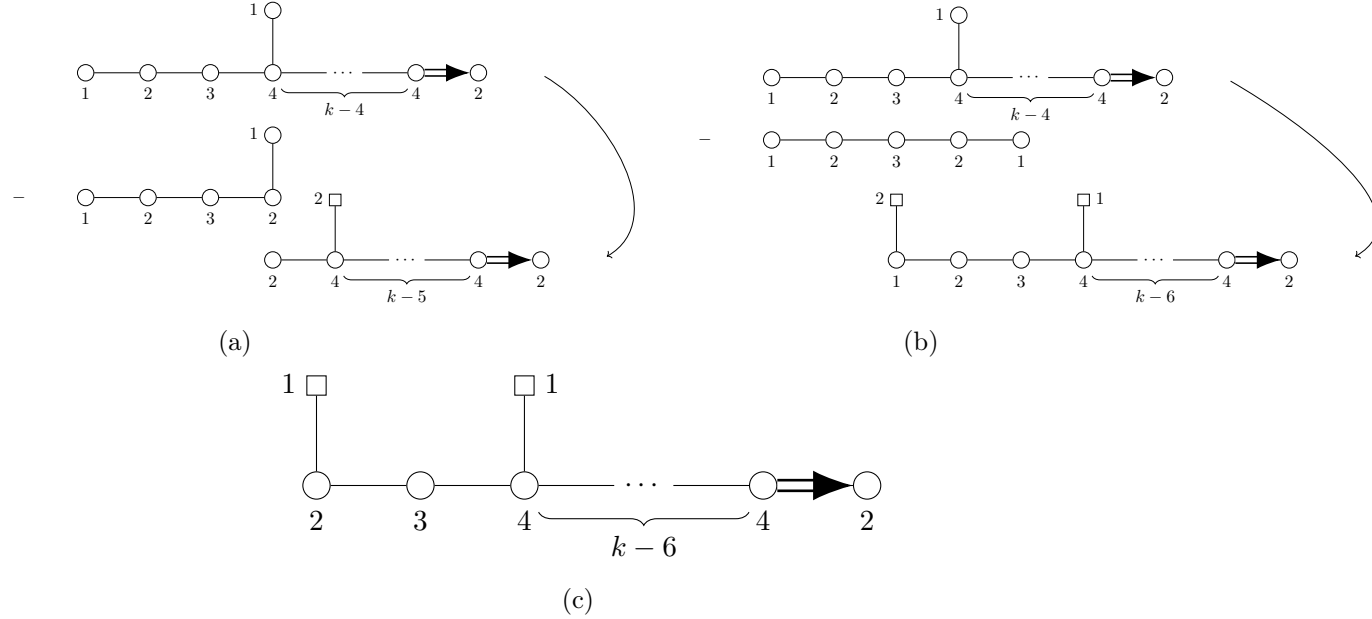


Figure 26: Both alignments of the $U(3)$ quotient quiver against \mathcal{Q}_{24} for $k \geq 7$ giving quivers \mathcal{Q}_{26a} and \mathcal{Q}_{26b} . Their intersection, reached via A_1 KP transitions, is quiver \mathcal{Q}_{26c} .

possible alignments of the $U(3)$ quotient quiver against \mathcal{Q}_{24} which results in the quivers \mathcal{Q}_{26a} and \mathcal{Q}_{26b} . The Coulomb branches of these are $\overline{[\mathcal{W}_{B_{k-3}}]_{[0,\dots,0]}}^{[0,2,0,\dots,0]}$ and $\overline{[\mathcal{W}_{B_{k-2}}]_{[2,0,\dots,0]}}^{[2,0,0,1,0,\dots,0]}$,

where the cases for $k = 4$ and $k \geq 5$ are slightly different and singlets have been suppressed for the latter. In both cases all factors of A_1 are isomorphic in the decomposition and the $SU(2)$ HKQ can be taken w.r.t any of them.

7.1 D-type Orbit $SU(2)$ HKQ

7.1.1 $\overline{\min.D_k} // SU(2), k \geq 4$

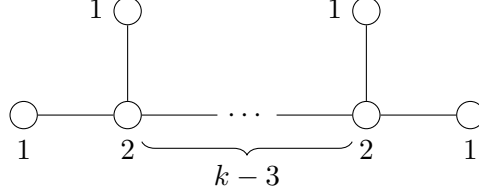


Figure 28: Unframed magnetic quiver \mathcal{Q}_{28} for $\overline{\min.D_k}$.

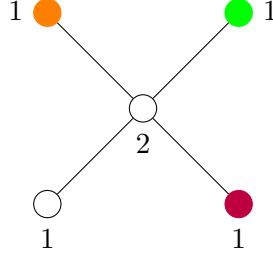


Figure 29: Unframed magnetic quiver \mathcal{Q}_{29} for $\overline{\min.D_4}$ with three nodes of rank 1 coloured.

The unframed magnetic quiver \mathcal{Q}_{28} for $\overline{\min.D_k}$ is drawn in Figure 28. The cases for $k \geq 4$ are all compatible with the rules for $SU(2)$ quiver subtraction in 2.

We first consider the special case of $k = 4$. Since the $U(2)$ quotient quiver ends on nodes which are related by outer automorphism, we draw the magnetic quiver \mathcal{Q}_{29} for $\overline{\min.D_4}$ in Figure 29 using different colours to distinguish the nodes of rank 1.

The subtraction of the $U(2)$ quotient quiver, aligned with the uncoloured nodes and each coloured node in turn, gives the resulting quivers \mathcal{Q}_{29a} , \mathcal{Q}_{29b} and \mathcal{Q}_{29c} :

$$\mathcal{Q}_{29a} = \begin{array}{c} \square \ 2 \\ | \\ \bullet \ 1 \end{array} \otimes \begin{array}{c} \square \ 2 \\ | \\ \bullet \ 1 \end{array}; \quad \mathcal{Q}_{29b} = \begin{array}{c} \square \ 2 \\ | \\ \bullet \ 1 \end{array} \otimes \begin{array}{c} \square \ 2 \\ | \\ \bullet \ 1 \end{array}; \quad \mathcal{Q}_{29c} = \begin{array}{c} \square \ 2 \\ | \\ \bullet \ 1 \end{array} \otimes \begin{array}{c} \square \ 2 \\ | \\ \bullet \ 1 \end{array} \quad (7.3)$$

Thus, we find from quiver subtraction that:

$$\overline{\min.D_4} // SU(2) = (\overline{\min.A_1} \otimes \overline{\min.A_1}) \cup (\overline{\min.A_1} \otimes \overline{\min.A_1}) \cup (\overline{\min.A_1} \otimes \overline{\min.A_1}). \quad (7.4)$$

Each pair of quivers in the union is related to its intersection by an A_1 KP transition,

$$\mathcal{Q}_{29a} \cap \mathcal{Q}_{29b} = \begin{array}{c} \square 2 \\ | \\ \bullet 1 \end{array} ; \quad \mathcal{Q}_{29a} \cap \mathcal{Q}_{29c} = \begin{array}{c} \square 2 \\ | \\ \bullet 1 \end{array} ; \quad \mathcal{Q}_{29b} \cap \mathcal{Q}_{29c} = \begin{array}{c} \square 2 \\ | \\ \bullet 1 \end{array}, \quad (7.5)$$

and further A_1 KP transitions yield their trivial three-way intersection. The HWG for this union is thus given by the signed sum of HWGs:

$$\begin{aligned} & HWG[(\overline{\min.A_1} \otimes \overline{\min.A_1}) \cup (\overline{\min.A_1} \otimes \overline{\min.A_1}) \cup (\overline{\min.A_1} \otimes \overline{\min.A_1})] \\ &= \left(\frac{1}{1 - \mu^2 t^2} \frac{1}{1 - \nu^2 t^2} - \frac{1}{1 - \rho^2 t^2} + \mu \rightarrow \nu \rightarrow \rho \right) + 1 \end{aligned} \quad (7.6)$$

$$= PE [(\mu^2 + \nu^2 + \rho^2) t^2 - \mu^2 \nu^2 \rho^2 t^6], \quad (7.7)$$

where μ, ν , and ρ are highest weight fugacities for each remaining factor of $SU(2)$. In (7.6) we have written the result from the union of cones formula (2.2) using shorthand notation. Due to cancellations of invariants under the outer automorphism group this simplifies further to (7.7). The result is easily checked by Weyl integration using the embedding (7.1) and we find agreement with quiver subtraction.

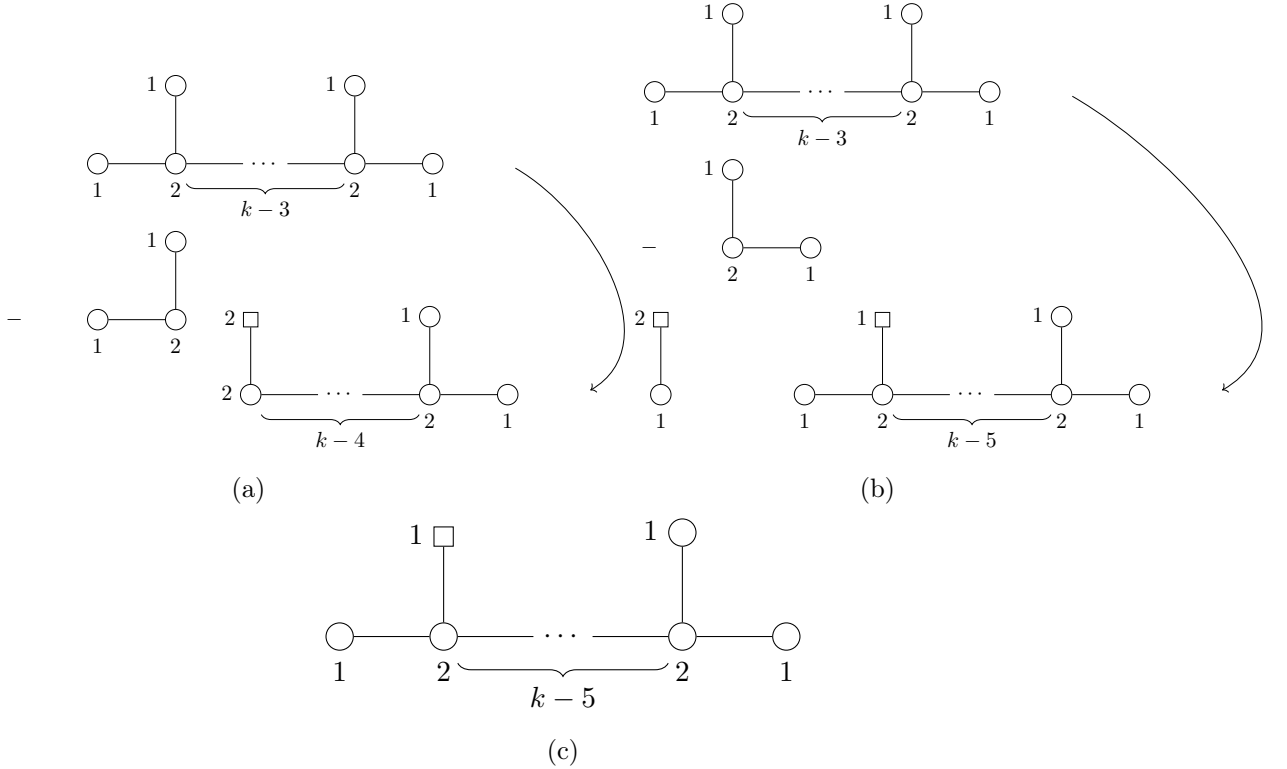


Figure 30: Both alignments of the $U(2)$ quotient quiver against \mathcal{Q}_{28} for $k \geq 5$ producing quivers \mathcal{Q}_{30a} and \mathcal{Q}_{30b} . Their intersection, reached via A_1 KP transitions, is quiver \mathcal{Q}_{30c} .

Now we consider the more general case for $k \geq 5$. There are two choices of alignment for the $U(2)$ quotient quiver against \mathcal{Q}_{28} . These are shown in Figure 30 and produce quivers

\mathcal{Q}_{30a} and \mathcal{Q}_{30b} , whose Coulomb branches are $\overline{n.min.D_{k-2}}$ and $\overline{min.A_1} \otimes \overline{min.D_{k-2}}$. We conjecture:

$$\overline{min.D_k} // \text{SU}(2) = \overline{n.min.D_{k-2}} \cup (\overline{min.A_1} \otimes \overline{min.D_{k-2}}), k \geq 5. \quad (7.8)$$

The intersection of \mathcal{Q}_{30a} and \mathcal{Q}_{30b} is a magnetic quiver \mathcal{Q}_{30c} for $\overline{min.D_{k-2}}$, reached in both cases by an A_1 KP transition. The HWG of the union is thus the signed sum of component HWGs:

$$\begin{aligned} \text{HWG} [\overline{n.min.D_{k-2}} \cup (\overline{min.A_1} \otimes \overline{min.D_{k-2}})] &= PE[\mu_2 t^2 + \mu_1^2 t^4] + PE[\mu_2 t^2] PE[\nu^2 t^2] \\ &\quad - PE[\mu_2 t^2] \quad (7.9) \\ &= PE [(\mu_2 + \nu^2) t^2 + \mu_1^2 t^4 - \mu_1^2 \nu^2 t^6], \quad (7.10) \end{aligned}$$

where $\mu_{1,2}$ are highest weight fugacities for D_{k-2} and ν is a highest weight fugacity for A_1 . The first line (7.9) follows the union of cones formula (2.2), giving the HWGs for $\overline{n.min.D_{k-2}}$ and $\overline{min.A_1} \otimes \overline{min.D_{k-2}}$, less the HWG for intersection $\overline{min.D_{k-2}}$. Each term has a common $PE[\mu_2 t^2]$ term, permitting the simplification into (7.10). This is easily checked by Weyl integration using the embedding (7.2) and we find agreement with quiver subtraction.

7.1.2 $\overline{n.min.D_k} // \text{SU}(2)$ for $k \geq 4$

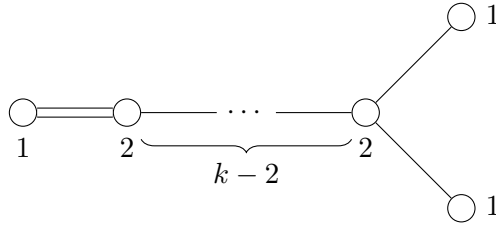


Figure 31: Unframed magnetic quiver \mathcal{Q}_{31} for $\overline{n.min.D_k}$.

An unframed magnetic quiver \mathcal{Q}_{31} for the $\overline{n.min.D_k}$ is shown in Figure 31. We consider the subtraction of a $U(2)$ quotient quiver.

First consider the special case for $k = 4$. There are two possible alignments, as shown in Figure 32, producing quivers \mathcal{Q}_{32a} and \mathcal{Q}_{32b} . The Coulomb branches of these quivers can be identified as $\overline{n.min.B_2}/\mathbb{Z}_2$ (which has a D_2 global symmetry) and $\overline{min.A_1} \otimes \overline{max.D_2}$. The former is suggested by [70] and verified by direct computation using the monopole formula. The latter can be seen by moving the framing on the quiver $[2] - (1) = (1)$. We conjecture that:

$$\overline{n.min.D_4} // \text{SU}(2) = \overline{n.min.B_2}/\mathbb{Z}_2 \cup (\overline{min.A_1} \otimes \overline{max.D_2}), \quad (7.11)$$

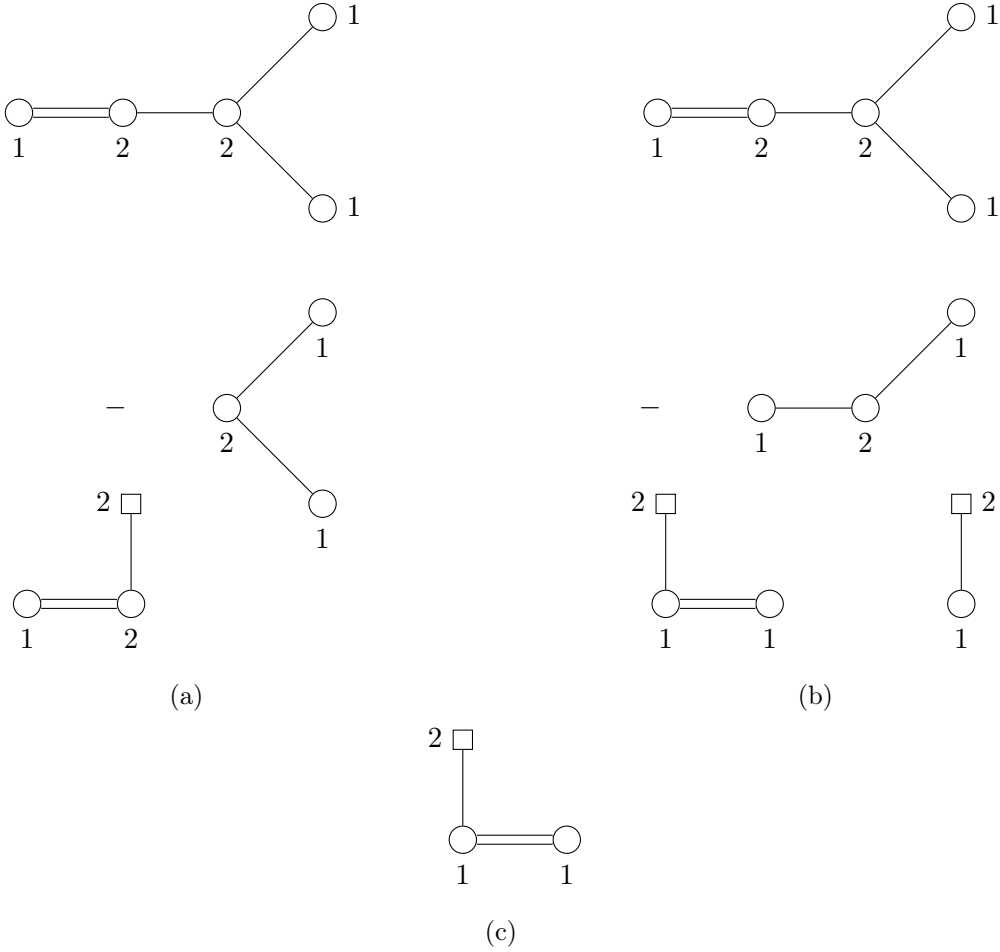


Figure 32: Both alignments of the $U(2)$ quotient quiver against \mathcal{Q}_{31} for $\overline{n.min.D_4}$ producing quivers \mathcal{Q}_{32a} and \mathcal{Q}_{32b} . Their intersection, reached via A_1 KP transitions, is quiver \mathcal{Q}_{32c} .

To compute the union, we note that the intersection is \mathcal{Q}_{32c} , a magnetic quiver for $\overline{max.D_2}$, reached in both cases by an A_1 KP transition. This yields the HWG as the signed sum:

$$\begin{aligned}
 HWG \left[\overline{n.min.B_2}/\mathbb{Z}_2 \cup \overline{min.A_1} \otimes \overline{max.D_2} \right] &= PE[(\mu_1^2 + \mu_1\mu_2 + \mu_2^2)t^2 + (1 + \mu_1\mu_2)t^4 - \mu_1^2\mu_2^2t^8] \\
 &\quad + PE[(\mu_1^2 + \mu_2^2 + \nu^2)t^2] - PE[(\mu_1^2 + \mu_2^2)t^2],
 \end{aligned} \tag{7.12}$$

where the $\mu_{1,2}$ are highest weight fugacities for D_2 , and ν is a highest weight fugacity for A_1 . The PE terms in (7.12) are HWGs for $\overline{n.min.B_2}/\mathbb{Z}_2$ (expressed in D_2 fugacities), $\overline{min.A_1} \otimes \overline{max.D_2}$, and their intersection $\overline{max.D_2}$, respectively. The result from quiver subtraction can be confirmed by using Weyl integration with the embedding (7.1). We point out that this form of the HWG is exactly the same as in (5.7) and will explore the relationship between the HKQs of B-type and D-type orbits further in Section 11.

Now consider the more general case for $k \geq 5$. There are two alignments of the $U(2)$ quotient quiver against \mathcal{Q}_{31} , as shown in Figure 33, and these produce quivers \mathcal{Q}_{33a}

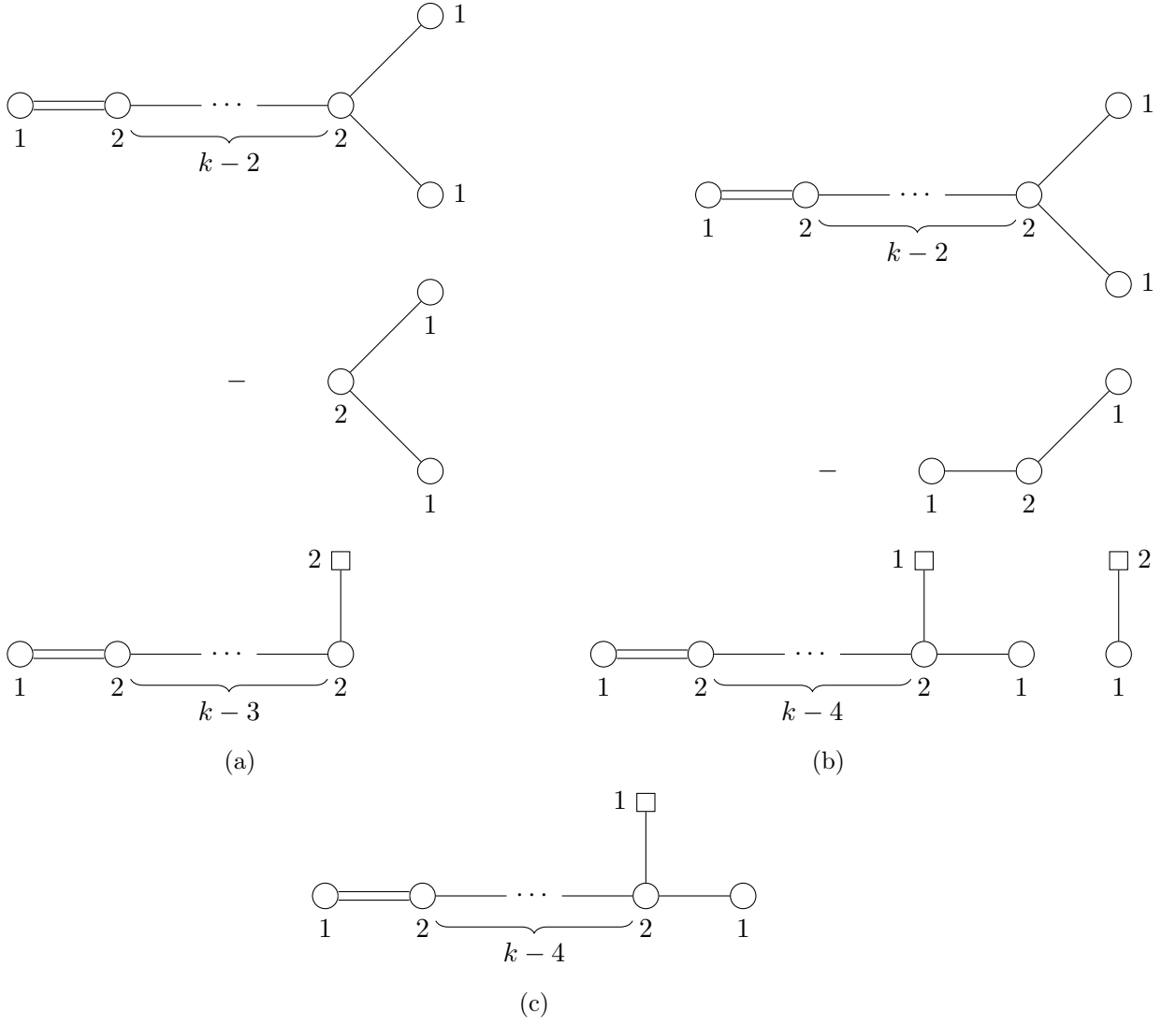


Figure 33: Both alignments of the $U(2)$ quotient quiver against \mathcal{Q}_{31} for $k \geq 5$ producing quivers \mathcal{Q}_{33a} and \mathcal{Q}_{33b} . Their intersection, reached via A_1 KP transitions, is quiver \mathcal{Q}_{33c} .

and \mathcal{Q}_{33b} , whose Coulomb branches can be identified as $\overline{n.min.B_{k-2}/\mathbb{Z}_2}$ and $\overline{n.min.D_{k-2}}$, respectively. We conjecture that:

$$\overline{n.min.D_k} // \text{SU}(2) = \overline{n.min.B_{k-2}/\mathbb{Z}_2} \cup (\overline{min.A_1} \otimes \overline{n.min.D_{k-2}}) \quad (7.13)$$

The intersection \mathcal{Q}_{33c} is a magnetic quiver for $\overline{n.min.D_{k-2}}$, as can be seen by moving the framing onto the node of rank 1 with the double hyper. The HWG for this hyper-Kähler quotient follows as:

$$\begin{aligned} \text{HWG}[\overline{n.min.D_k} // \text{SU}(2)] &= PE[\mu_2 t^2 + (2\mu_1^2 + 1)t^4 + \mu_1^2 t^6 - \mu_1^4 t^{12}] + PE[\nu^2 t^2] PE[\mu_2 t^2 + \mu_1^2 t^4] \\ &\quad - PE[\mu_2 t^2 + \mu_1^2 t^4]. \end{aligned} \quad (7.14)$$

where $\mu_{1,2}$ are highest weight fugacities for D_k and ν is a highest weight fugacity for A_1 . The first PE term is the HWG for $\overline{n.min.B_{k-2}/\mathbb{Z}_2}$, the second term is the HWG for $\overline{minA_1 \otimes n.minD_{k-2}}$, and the third is the HWG for $\overline{n.min.D_{k-2}}$.

7.2 D-type Orbit SU(3) HKQ

7.2.1 $\overline{n.n.min.D_6}/\text{SU}(3)$

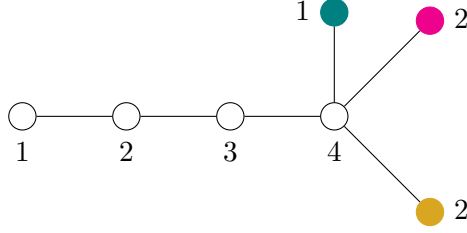


Figure 34: Magnetic quiver \mathcal{Q}_{34} for the $\overline{n.n.min.D_6}$.

The magnetic quiver \mathcal{Q}_{34} for the $\overline{n.n.min.D_6}$ is shown in Figure 34. We have used different colours for the nodes attached to the node of rank 4. We consider an SU(3) HKQ by the subtraction of the U(3) quotient quiver. There are three alignments in which the quotient quiver starts on the uncoloured nodes and ends on the teal, magenta, and gold nodes. The respective resulting quivers \mathcal{Q}_{34a} , \mathcal{Q}_{34b} , and \mathcal{Q}_{34c} are:

$$\mathcal{Q}_{34a} = \begin{array}{c} 2 \square \\ | \\ \color{magenta}{\bullet} 2 \\ | \\ \color{magenta}{\bullet} 2 \end{array} \text{ --- } \begin{array}{c} \square 2 \\ | \\ \circ 2 \\ | \\ \circ 2 \end{array} \text{ --- } \begin{array}{c} \square 2 \\ | \\ \color{gold}{\bullet} 2 \\ | \\ \color{gold}{\bullet} 2 \end{array} ; \quad \mathcal{Q}_{34b} = \begin{array}{c} 2 \square \\ | \\ \color{teal}{\bullet} 1 \\ | \\ \circ 2 \\ | \\ \color{magenta}{\bullet} 1 \end{array} \text{ --- } \begin{array}{c} \square 2 \\ | \\ \circ 2 \\ | \\ \circ 2 \end{array} \text{ --- } \begin{array}{c} \square 2 \\ | \\ \color{gold}{\bullet} 2 \\ | \\ \color{gold}{\bullet} 2 \end{array} ; \quad \mathcal{Q}_{34c} = \begin{array}{c} 2 \square \\ | \\ \color{teal}{\bullet} 1 \\ | \\ \circ 2 \\ | \\ \color{gold}{\bullet} 1 \end{array} \text{ --- } \begin{array}{c} \square 2 \\ | \\ \circ 2 \\ | \\ \circ 2 \end{array} \text{ --- } \begin{array}{c} \square 2 \\ | \\ \color{magenta}{\bullet} 2 \\ | \\ \color{magenta}{\bullet} 2 \end{array} . \quad (7.15)$$

We compute the two-way intersections to be:

$$\mathcal{Q}_{34a} \cap \mathcal{Q}_{34b} = \begin{array}{c} 1 \square \\ | \\ \color{magenta}{\bullet} 1 \\ | \\ \circ 2 \\ | \\ \color{gold}{\bullet} 2 \end{array} \text{ --- } \begin{array}{c} \square 2 \\ | \\ \circ 2 \\ | \\ \circ 2 \end{array} \text{ --- } \begin{array}{c} \square 2 \\ | \\ \color{gold}{\bullet} 2 \\ | \\ \color{gold}{\bullet} 2 \end{array} ; \quad \mathcal{Q}_{34a} \cap \mathcal{Q}_{34c} = \begin{array}{c} 1 \square \\ | \\ \color{gold}{\bullet} 1 \\ | \\ \circ 2 \\ | \\ \color{magenta}{\bullet} 2 \end{array} \text{ --- } \begin{array}{c} \square 2 \\ | \\ \circ 2 \\ | \\ \circ 2 \end{array} \text{ --- } \begin{array}{c} \square 2 \\ | \\ \color{magenta}{\bullet} 2 \\ | \\ \color{magenta}{\bullet} 2 \end{array} ; \quad \mathcal{Q}_{34b} \cap \mathcal{Q}_{34c} = \begin{array}{c} 2 \square \\ | \\ \color{teal}{\bullet} 1 \\ | \\ \circ 2 \\ | \\ \color{magenta}{\bullet} 1 \end{array} \text{ --- } \begin{array}{c} \square 1 \\ | \\ \circ 2 \\ | \\ \color{gold}{\bullet} 1 \end{array} , \quad (7.16)$$

and, finally the three-way intersection is:

$$\mathcal{Q}_{34a} \cap \mathcal{Q}_{34b} \cap \mathcal{Q}_{34c} = \begin{array}{c} 2 \square \\ | \\ \color{magenta}{\bullet} 1 \\ | \\ \circ 2 \\ | \\ \color{gold}{\bullet} 1 \end{array} . \quad (7.17)$$

All of the quivers share a global symmetry of $D_3 \times U(1)$, although the U(1) may be trivial. The quiver subtraction and Weyl integration are found to give consistent results. The HWGs for these quivers are not particularly illuminating, so we present some unrefined HS

to illustrate the details of the construction:

$$\text{HS}[\mathcal{Q}_{34a}] = \frac{\left(1 + 9t^2 + 54t^4 + 194t^6 + 471t^8 + 771t^{10} + 916t^{12} + 771t^{14} + 471t^{16} + 194t^{18} + 54t^{20} + 9t^{22} + t^{24}\right)}{(1-t^2)^{12}(1+t^2)^6} \quad (7.18)$$

$$\text{HS}[\mathcal{Q}_{34b}] = \text{HS}[\mathcal{Q}_{34c}] = \frac{\left(1 + 8t^2 + 43t^4 + 128t^6 + 238t^8 + 288t^{10} + 238t^{12} + 128t^{14} + 43t^{16} + 8t^{18} + t^{20}\right)}{(1-t^2)^{12}(1+t^2)^4} \quad (7.19)$$

$$\text{HS}[\mathcal{Q}_{34a} \cap \mathcal{Q}_{34b}] = \text{HS}[\mathcal{Q}_{34a} \cap \mathcal{Q}_{34c}] = \frac{(1+t^2)(1+4t^2+10t^4+4t^6+t^8)}{(1-t^2)^{10}} \quad (7.20)$$

$$\text{HS}[\mathcal{Q}_{34b} \cap \mathcal{Q}_{34c}] = \frac{\left(1 + 11t^2 + 57t^4 + 170t^6 + 324t^8 + 398t^{10} + 324t^{12} + 170t^{14} + 57t^{16} + 11t^{18} + t^{20}\right)}{(1-t^2)^{10}(1+t^2)^5} \quad (7.21)$$

$$\text{HS}[\mathcal{Q}_{34a} \cap \mathcal{Q}_{34b} \cap \mathcal{Q}_{34c}] = \frac{(1+t^2)^2(1+5t^2+t^4)}{(1-t^2)^8}. \quad (7.22)$$

Then one can check that

$$\begin{aligned} \text{HS}[\text{HKQ}] &= \text{HS}[\mathcal{Q}_{34a}] + \text{HS}[\mathcal{Q}_{34b}] + \text{HS}[\mathcal{Q}_{34c}] - \text{HS}[\mathcal{Q}_{34a} \cap \mathcal{Q}_{34b}] - \text{HS}[\mathcal{Q}_{34a} \cap \mathcal{Q}_{34c}] \\ &\quad - \text{HS}[\mathcal{Q}_{34b} \cap \mathcal{Q}_{34c}] + \text{HS}[\mathcal{Q}_{34a} \cap \mathcal{Q}_{34b} \cap \mathcal{Q}_{34c}] \end{aligned} \quad (7.23)$$

$$= \frac{\left(1 + 10t^2 + 76t^4 + 365t^6 + 1188t^8 + 2571t^{10} + 3675t^{12} + 3315t^{14} + 1701t^{16} + 267t^{18} - 176t^{20} - 90t^{22} - 2t^{24} + 6t^{26} + t^{28}\right)}{(1-t^2)^{12}(1+t^2)^6} \quad (7.24)$$

7.3 D-type Orbit $\text{SU}(n)$ HKQ

Quiver subtraction allows us to conjecture a general construction for any permissible hyper-Kähler quotient of a height 2 orbit of D_k by $\text{SU}(n)$. The structure of the quiver subtraction differs depending on whether the spinor nodes are involved.

7.3.1 $\overline{\mathcal{O}}_{(2^{2p}, 1^{2k-4p})}^{D_k} // \text{SU}(n), n \leq p+1$

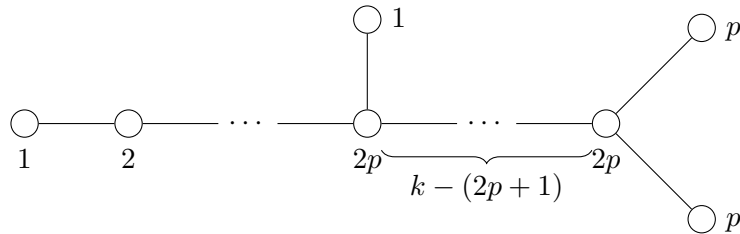


Figure 35: Unframed magnetic quiver \mathcal{Q}_{35} for the orbit of D_k labelled by the partition $(2^{2p}, 1^{2k-4p})$ of $2k$.

First, consider the orbit of D_k with partition $(2^{2p}, 1^{2k-4p})$ of $2k$, where $k \geq 2p + 2$, for which an unframed magnetic quiver \mathcal{Q}_{35} is given in Figure 35. To be consistent with the rules of quiver subtraction, the $U(n)$ quotient quiver can only be subtracted from the leg that starts $(1) - (2) - \dots - (2p) - \dots$; this puts a constraint on the values of n . The length of the $U(n)$ quotient quiver is $2n - 1$ and the length of the leg $(1) - (2) - \dots - (2p)$, up to the junction with the rank 1 node, is $2p$. Since the rules permit the quotient quiver to run past this junction by one node at most, the constraint becomes $2n - 1 \leq 2p + 1 \implies n \leq p + 1$. There are two cases; one for $n < p + 1$ and a special case for $n = p + 1$.

If $n < p + 1$, then there is only one alignment of the $U(n)$ quotient quiver. The result of the quiver subtraction is:

$$\overline{\mathcal{O}}_{(2^{2p}, 1^{2k-4p})}^{D_k} // \text{SU}(n) = \mathcal{C} \left(\begin{array}{c} \text{1} \square \\ | \\ \text{2} \circ - \text{4} \circ - \dots - \text{2n-2} \circ - \text{2n-1} \circ - \dots - \text{2p} \circ - \dots - \text{2p} \circ \\ \underbrace{\hspace{10em}}_{k - (2p + 1)} \\ \text{1} \circ \\ | \\ \text{2p} \circ - \dots - \text{2p} \circ \\ \underbrace{\hspace{10em}}_{k - (2p + 1)} \\ \text{p} \circ \\ \diagup \\ \text{p} \circ \\ \diagdown \end{array} \right), \quad (7.25)$$

This magnetic quiver has a global symmetry of $SO(2k - 2n) \times U(1)$.

In the saturated case of $n = p + 1$ this further degenerates to two special cases. The first is for $k > 2p + 2$, there are two alignments of the $U(n)$ quotient quiver and so the $SU(n)$ HKQ is a union according to the rules in 2. We find:

$$\overline{\mathcal{O}}_{(2^{2p}, 1^{2k-4p})}^{D_k} // \text{SU}(p + 1) = \mathcal{C} \left(\begin{array}{c} \text{2} \square \\ | \\ \text{2} \circ - \text{4} \circ - \dots - \text{2p-2} \circ - \text{2p} \circ - \dots - \text{2p} \circ \\ \underbrace{\hspace{10em}}_{k - (2p + 1)} \\ \text{2p} \circ - \dots - \text{2p} \circ \\ \underbrace{\hspace{10em}}_{k - (2p + 1)} \\ \text{p} \circ \\ \diagup \\ \text{p} \circ \\ \diagdown \end{array} \right) \cup \mathcal{C} \left(\begin{array}{c} \text{2} \square \\ | \\ \text{1} \circ \\ | \\ \text{2p-2} \circ - \text{2p-1} \circ - \text{2p} \circ - \dots - \text{2p} \circ \\ \underbrace{\hspace{10em}}_{k - (2p + 1)} \\ \text{1} \square \\ | \\ \text{2p} \circ - \dots - \text{2p} \circ \\ \underbrace{\hspace{10em}}_{k - (2p + 1)} \\ \text{p} \circ \\ \diagup \\ \text{p} \circ \\ \diagdown \end{array} \right) \quad (7.26)$$

The first quiver in the union is the affine Grassmannian slice $\overline{[\mathcal{W}_{D_{k-n}}]_{[0, \dots, 0, 1, 0, \dots, 0]}}_{[0, \dots, 0]}$ where the 1 in the flavour vector is in the p^{th} position. This moduli space has a global symmetry of $SO(2k - 2n)$. There is no particular name for the second moduli space but it has a global symmetry of $SO(2k - 2n) \times U(1)$.

The case for $k = 2p + 2$ has three possible alignments of the $SU(p + 1)$ quotient quiver and so the HKQ is also a union according to the rules in Section 2. We find:

$$\begin{aligned}
\overline{\mathcal{O}}_{(2^{2p}, 1^2)}^{D_{2p+2}} // \text{SU}(p+1) = \mathcal{C} & \left(\begin{array}{c} \text{Diagram 1} \\ \text{Diagram 2} \\ \text{Diagram 3} \end{array} \right) \\
\cup \mathcal{C} & \left(\begin{array}{c} \text{Diagram 4} \\ \text{Diagram 5} \end{array} \right) .
\end{aligned} \tag{7.27}$$

The diagrams are Dynkin diagrams for the Lie algebra $\mathfrak{so}(2p+2)$. They consist of a horizontal chain of nodes with ranks 2, 4, ..., $2p-2$. From the node of rank $2p-2$, two additional nodes branch out: one of rank p and one of rank p . Each of these rank p nodes is connected to a square node of rank 2. In Diagram 1, the top rank p node is black. In Diagram 2, the top rank p node is black and there is a vertical chain of nodes (square 2, circle 1, circle $2p-2$) attached to the top rank p node. In Diagram 3, the bottom rank p node is black and there is a vertical chain of nodes (square 2, circle 1, circle $2p-2$) attached to the bottom rank p node.

The nodes of rank p attached to the node of rank $2p-2$ are identical under an outer automorphism and so we fill one of these nodes black and leave the other unfilled. The first Coulomb branch in the union (7.27) is the affine Grassmannian slice $\overline{[\mathcal{W}_{D_{p+1}}]_{[0, \dots, 0]}^{[0, \dots, 0, 2, 2]}}$ which has an $SO(2p+2)$ global symmetry. The final two moduli spaces in the union (7.27) are identical but have slightly different fugacities as made clear by the colouring of the nodes. This moduli space does not have any particular name but does have a global symmetry of $SO(2p+2) \times U(1)$.

alignments and so the HKQ is a union:

$$\overline{\mathcal{O}}_{(2^{2k})}^{D_{2k}} // \text{SU}(n) \mathcal{S} = \mathcal{C} \left(\begin{array}{c} \text{Diagram 1} \\ \text{Diagram 2} \end{array} \right) \cup \mathcal{C} \left(\begin{array}{c} \text{Diagram 3} \end{array} \right). \quad (7.29)$$

Both quivers in the union have an $SO(2k) \times U(1)$ global symmetry.

7.3.3 $\overline{\mathcal{O}}_{(2^{2k}, 1^2)}^{D_{2k+1}} // \text{SU}(n), n \leq k$

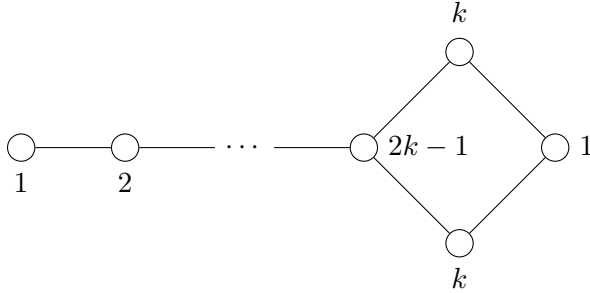


Figure 37: Unframed magnetic quiver \mathcal{Q}_{37} for $\overline{\mathcal{O}}_{(2^{2k}, 1^2)}^{D_{2k+1}}$.

Finally, consider the possible $\text{SU}(n)$ quiver subtractions from the magnetic quiver \mathcal{Q}_{37} for $\overline{\mathcal{O}}_{(2^{2k}, 1^2)}^{D_{2k+1}}$. Recalling that the junction, located at the node of rank $2k - 1$ in \mathcal{Q}_{37} , must occur on a node of 2 on the quotient quiver in accordance with the [Junction Rule](#), we find that $n \leq k$.

Considering first the general case $n < k$, there is only one alignment of the $U(n)$

quotient quiver and we find

$$\overline{\mathcal{O}}_{(2^{2k}, 1^2)}^{D_{2k}} // \text{SU}(n) = \mathcal{C} \left(\begin{array}{cccccccc} & & & & & & & k \\ & & & & & & & \circ \\ & & & & 1 & & & \circ \\ & & & & \square & & & \circ \\ & & & & | & & & \circ \\ \circ & \text{---} & \circ & \text{---} & \dots & \text{---} & \circ & \text{---} & \dots & \text{---} & \circ & \text{---} & \circ \\ 2 & & 4 & & & & 2n-2 & & 2n-1 & & & & 2k-1 & & 1 \\ & & & & & & & & & & & & \circ & \text{---} & \circ \\ & & & & & & & & & & & & \circ & & \circ \\ & & & & & & & & & & & & k & & k \end{array} \right), \quad (7.30)$$

where the Coulomb branch has an $SO(4k + 2 - 2n) \times U(1)$ global symmetry.

For the special case $n = k$ there is again only one alignment of the $U(k)$ quotient quiver which results in

$$\overline{\mathcal{O}}_{(2^{2k}, 1^2)}^{D_{2k}} // \text{SU}(k) = \mathcal{C} \left(\begin{array}{cccccccc} & & & & & & & k \\ & & & & & & & \circ \\ & & & & & & & \square & 1 \\ & & & & & & & | & \\ & & & & & & & \circ & \\ & & & & & & & \circ & \\ \circ & \text{---} & \circ & \text{---} & \dots & \text{---} & \circ & \text{---} & \circ & \text{---} & \circ & \text{---} & \circ & \text{---} & \circ \\ 2 & & 4 & & & & 2k-2 & & 1 & & & & \circ & \text{---} & \circ \\ & & & & & & & & & & & & \circ & & \circ \\ & & & & & & & & & & & & k & & k \end{array} \right), \quad (7.31)$$

the global symmetry of the Coulomb branch here is $SO(2k + 2) \times U(1)$.

8 Exceptional Orbits

We now consider the possible $SU(n)$ HKQs that one can take from exceptional orbits using quiver subtraction. Unlike, the classical case, there are no families of exceptional orbits, so these orbits are considered on a case-by-case basis. We believe the following is an exhaustive list of the magnetic quivers for exceptional orbits amenable to this approach.

We examine the $SU(2)$ HKQs of $\overline{sub.reg.G_2}$, $\overline{min.F_4}$, $\overline{min.E_6}$, $\overline{min.E_7}$, and $\overline{min.E_8}$. We also study the $SU(3)$ HKQ of $\overline{min.E_7}$ and $\overline{min.E_8}$ (the latter was first computed in [28]). Finally we consider the $SU(4)$ HKQ of $\overline{min.E_8}$.

The relevant embedding of $SU(n)$ into the fundamental will be given when studying each example.

8.1 Exceptional Orbit $SU(2)$ HKQ

8.1.1 $\overline{sub.reg.G_2} // \text{SU}(2)$

An unframed magnetic quiver for the $\overline{sub.reg.G_2}$ is drawn in at the top of Figure 38, which shows the subtraction of the $U(2)$ quotient quiver to result in the quiver \mathcal{Q}_{38} . The Coulomb branch of \mathcal{Q}_{38} is $Sym^2(\overline{min.A_1})$ [56] (it is also the orbifold $\mathbb{C}^4/\mathcal{D}_4$, where \mathcal{D}_4 is the dihedral group of order 8.). We conclude:

$$\overline{sub.reg.G_2} // \text{SU}(2) = Sym^2(\overline{min.A_1}). \quad (8.1)$$

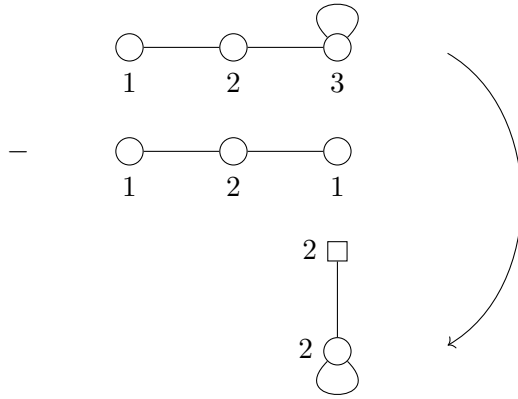


Figure 38: Quiver subtraction of the $U(2)$ quotient quiver from an unframed magnetic quiver for $\overline{sub.reg.G_2}$ to produce quiver \mathcal{Q}_{38} .

The result (8.1) can be verified using the embedding of $G_2 \leftrightarrow A_1 \times A_1$, which decomposes the fundamental of G_2 as:

$$[0, 1]_{G_2} \rightarrow [0; 2]_{A_1 \times A_1} + [1; 1]_{A_1 \times A_1}. \quad (8.2)$$

Note that the two factors of A_1 are not symmetric in this embedding. It is clear from the quiver subtraction that we must preserve the fugacity label associated to the node of rank 3 in the magnetic quiver for $\overline{sub.reg.G_2}$. This corresponds to performing the HKQ with respect to the first factor of A_1 in (8.2).

8.1.2 $\overline{min.F_4} // SU(2)$

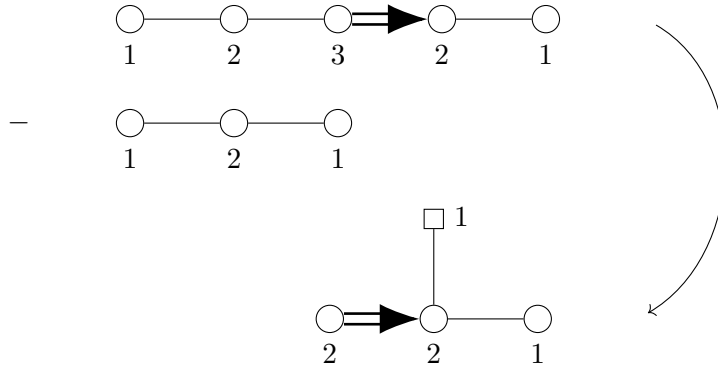


Figure 39: Quiver subtraction of the $U(2)$ quotient quiver from an unframed magnetic quiver for $\overline{min.F_4}$ to produce to produce quiver \mathcal{Q}_{39} .

An unframed magnetic quiver for $\overline{min.F_4}$ is shown at the top of Figure 39, together with the subtraction of the $U(2)$ quotient quiver to result in quiver \mathcal{Q}_{39} . Note that the subtraction occurs on the long side, in accordance with the [External Leg Rule](#). The Coulomb branch of \mathcal{Q}_{39} is $\overline{n.min.C_3}$. We conclude that:

$$\overline{min.F_4} // SU(2) = \overline{n.min.C_3}. \quad (8.3)$$

We have checked this explicitly using the embedding of $F_4 \hookrightarrow C_3 \times A_1$, where the fundamental of F_4 decomposes in the following way:

$$[0, 0, 0, 1]_{F_4} \rightarrow [0, 1, 0; 0]_{C_3 \times A_1} + [1, 0, 0; 1]_{C_3 \times A_1}. \quad (8.4)$$

8.1.3 $\overline{\min.E_6} // \text{SU}(2)$

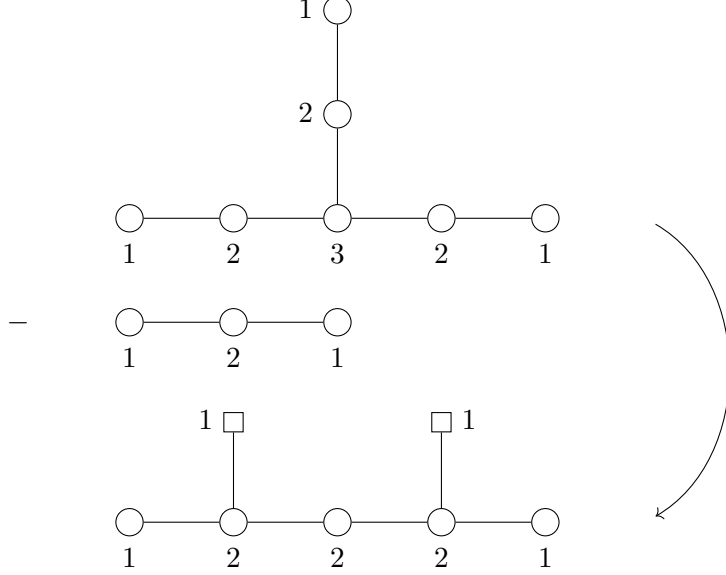


Figure 40: Quiver subtraction of the $\text{U}(2)$ quotient quiver from an unframed magnetic quiver for $\overline{\min.E_6}$ to produce quiver \mathcal{Q}_{40} .

A magnetic quiver for $\overline{\min.E_6}$ is shown at the top of Figure 40, together with the subtraction of the $\text{U}(2)$ quotient quiver to result in the quiver \mathcal{Q}_{40} . The Coulomb branch of \mathcal{Q}_{40} is $\overline{n.\min.A_5}$. We conclude that:

$$\overline{\min.E_6} // \text{SU}(2) = \overline{n.\min.A_5}. \quad (8.5)$$

There is an embedding of $E_6 \hookrightarrow A_5 \times A_1$ where the fundamental of E_6 decomposes in the following way:

$$[1, 0, 0, 0, 0]_{E_6} \rightarrow [0, 1, 0, 0, 0; 0]_{A_5 \times A_1} + [0, 0, 0, 0, 1; 1]_{A_5 \times A_1}. \quad (8.6)$$

We have used this to compute the HKQ explicitly by Weyl integration and find agreement with quiver subtraction.

8.1.4 $\overline{\min.E_7} // \text{SU}(2)$

An unframed magnetic quiver for $\overline{\min.E_7}$ is shown at the top of Figure 41, followed by the subtraction of the $\text{U}(2)$ quotient quiver to give \mathcal{Q}_{41} . The Coulomb branch of \mathcal{Q}_{41} is $\overline{n.n.\min.D_6}$. We conclude that:

$$\overline{\min.E_7} // \text{SU}(2) = \overline{n.n.\min.D_6}. \quad (8.7)$$

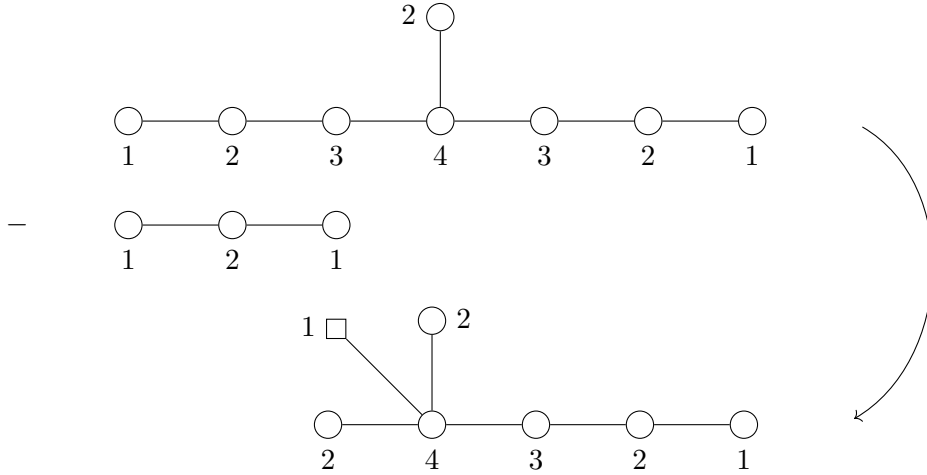


Figure 41: Quiver subtraction of the $U(2)$ quotient quiver from an unframed magnetic quiver for $\overline{min.E_7}$ to produce quiver \mathcal{Q}_{41} .

We have checked this explicitly using the embedding of $E_7 \hookrightarrow D_6 \times A_1$ which decomposes the fundamental as:

$$[0, 0, 0, 0, 0, 1, 0]_{E_7} \rightarrow [0, 0, 0, 0, 0, 1; 0]_{D_6 \times A_1} + [1, 0, 0, 0, 0, 0; 1]_{D_6 \times A_1}. \quad (8.8)$$

This example verifies the Higgs branch side of the $4d \mathcal{N} = 2$ duality proposed in [83], which says that $Sp(2)$ with 6 flavours at infinite coupling is dual to the $SU(2)$ gauging of the rank 1 E_7 SCFT.

The $3d$ mirror of the latter theory is the quiver given at the top of Figure 41 and the $SU(2)$ gauging is implemented by the $U(2)$ quotient quiver subtraction. The resulting quiver \mathcal{Q}_{41} is the $3d$ mirror of $Sp(2)$ with 6 flavours.

8.1.5 $\overline{min.E_8} // SU(2)$

An unframed magnetic quiver for $\overline{min.E_8}$ is given at the top of Figure 42 followed by the subtraction of the $U(2)$ quotient quiver to produce \mathcal{Q}_{42} . The Coulomb branch of \mathcal{Q}_{42} is $\overline{n.min.E_7}$. We conclude that:

$$\overline{min.E_8} // SU(2) = \overline{n.min.E_7}. \quad (8.9)$$

We have checked this explicitly using the Dynkin-type embedding of $E_8 \hookrightarrow E_7 \times A_1$ under which the fundamental of E_8 decomposes as:

$$[0, 0, 0, 0, 0, 0, 1, 0]_{E_8} \rightarrow [1, 0, 0, 0, 0, 0, 0; 0]_{E_7 \times A_1} + [0, 0, 0, 0, 0, 1, 0; 1]_{E_7 \times A_1} + [0, 0, 0, 0, 0, 0, 0; 2]_{E_7 \times A_1}. \quad (8.10)$$

8.2 Exceptional Orbit $SU(3)$ HKQ

It is important to note that $\overline{min.E_6}$ is not amenable to subtraction by the $U(3)$ quotient quiver as the junction occurs on a node of rank 3 on the quotient quiver as opposed to a node of rank 2 as required by the [Junction Rule](#).

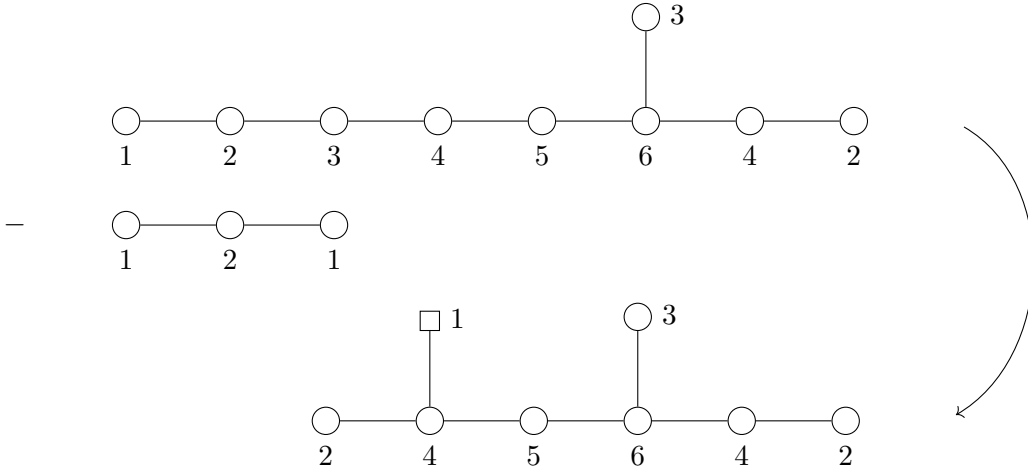


Figure 42: Quiver subtraction of the $U(2)$ quotient quiver from an unframed magnetic quiver for $\overline{\min.E_8}$ to produce quiver \mathcal{Q}_{42} .

8.2.1 $\overline{\min.E_7} // \text{SU}(3)$

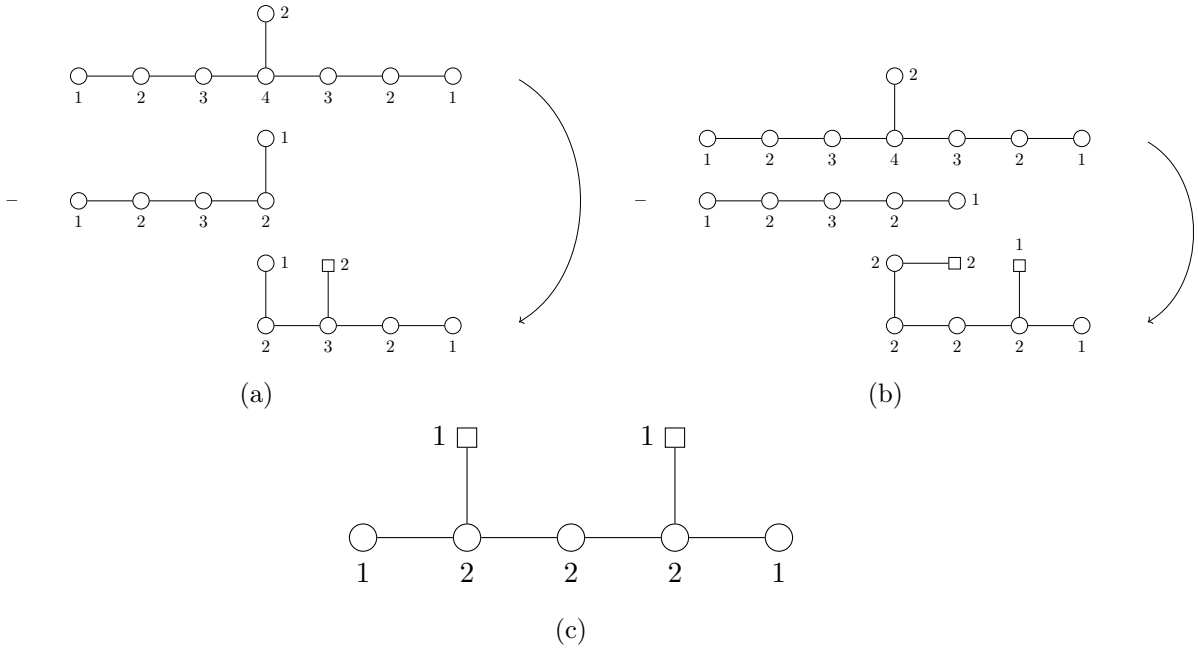


Figure 43: Both alignments of the $U(3)$ quotient quiver against $\overline{\min.E_7}$ to produce quivers \mathcal{Q}_{43a} and \mathcal{Q}_{43b} . Their intersection, reached via A_1 Kraft-Procesi transitions, is \mathcal{Q}_{43c} .

The unframed magnetic quiver for the $\overline{\min.E_7}$ permits two possible alignments for subtraction of an $U(3)$ quotient quiver, as shown in Figure 43. The resulting quivers \mathcal{Q}_{43a} and \mathcal{Q}_{43b} are magnetic quivers for the nilpotent orbits $\overline{\mathcal{O}}_{(2^3)}^{A_5}$ and $\overline{\mathcal{O}}_{(3,1^3)}^{A_5}$, respectively. We conclude that:

$$\overline{\min.E_7} // \text{SU}(3) = \overline{\mathcal{O}}_{(2^3)}^{A_5} \cup \overline{\mathcal{O}}_{(3,1^3)}^{A_5}. \quad (8.11)$$

The intersection, reached in both cases by an A_1 KP transition, is the quiver \mathcal{Q}_{43c} , which is a magnetic quiver for $\overline{n.min.A_5}$. There is an embedding of $E_7 \leftrightarrow A_5 \times A_2$ which decomposes the fundamental of E_7 as:

$$\begin{aligned}
[0, 0, 0, 0, 0, 1, 0]_{E_7} &\rightarrow [0, 0, 1, 0, 0; 0, 0]_{A_5 \times A_2} + [1, 0, 0, 0, 0; 0, 1]_{A_5 \times A_2} \\
&\quad + [0, 0, 0, 0, 1; 1, 0]_{A_5 \times A_2},
\end{aligned} \tag{8.12}$$

and we have used this to compute the HKQ using Weyl integration and to verify the above result.

8.2.2 $\overline{min.E_8} // \text{SU}(3)$

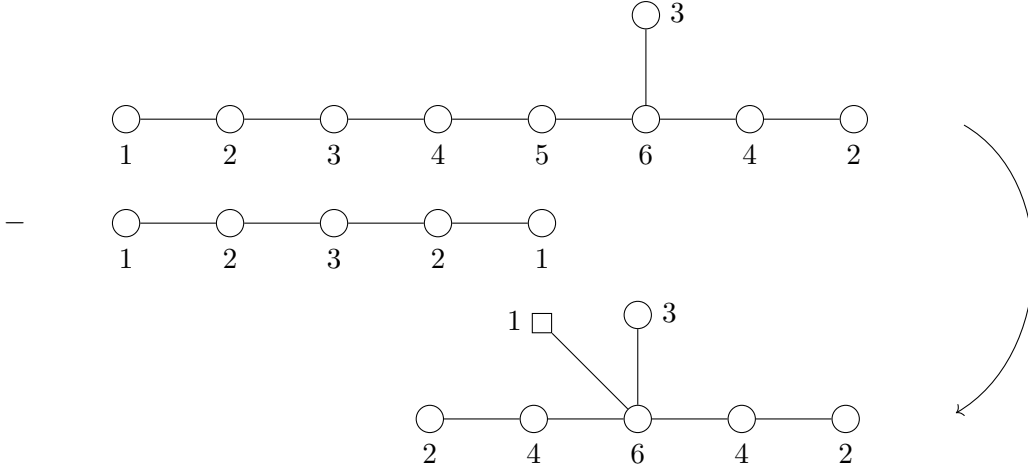


Figure 44: Quiver subtraction of the $\text{U}(3)$ quotient quiver from an unframed magnetic quiver for $\overline{min.E_8}$ to produce quiver \mathcal{Q}_{44} .

The computation of this $\text{SU}(3)$ HKQ was first done in [28] both using a diagrammatic quiver subtraction of the $\text{U}(3)$ quotient quiver from the magnetic quiver for $\overline{min.E_8}$, as reproduced in Figure 44, and explicitly using Weyl integration. The resulting diagram is not a magnetic quiver for an E_6 orbit, but turns out to be a magnetic quiver for the double cover of the 21-dimensional orbit of E_6 . The quiver \mathcal{Q}_{44} is also a slice in the affine Grassmannian of E_6 and so we find:

$$\overline{min.E_8} // \text{SU}(3) = [\overline{\mathcal{W}_{E_6}}]_{[0,0,0,0,0,0]}^{[0,0,1,0,0,0]}. \tag{8.13}$$

8.3 Exceptional Orbit $\text{SU}(4)$ HKQ

8.3.1 $\overline{min.E_8} // \text{SU}(4)$

Subtraction of the $\text{U}(4)$ quotient quiver from the unframed magnetic quiver for $\overline{min.E_8}$ has two possible alignments, as shown in Figure 45, which produce quivers \mathcal{Q}_{45a} and \mathcal{Q}_{45b} . These are both slices in the affine Grassmannian of D_5 , being $[\overline{\mathcal{W}_{D_5}}]_{[0,0,0,0,0]}^{[0,2,0,0,0]}$ and $[\overline{\mathcal{W}_{D_5}}]_{[0,0,0,0,0]}^{[1,0,0,2,0]}$, respectively. The latter can also be identified as the normalisation of the orbit $\overline{\mathcal{O}}_{(3^2,2^2)}^{D_5}$,

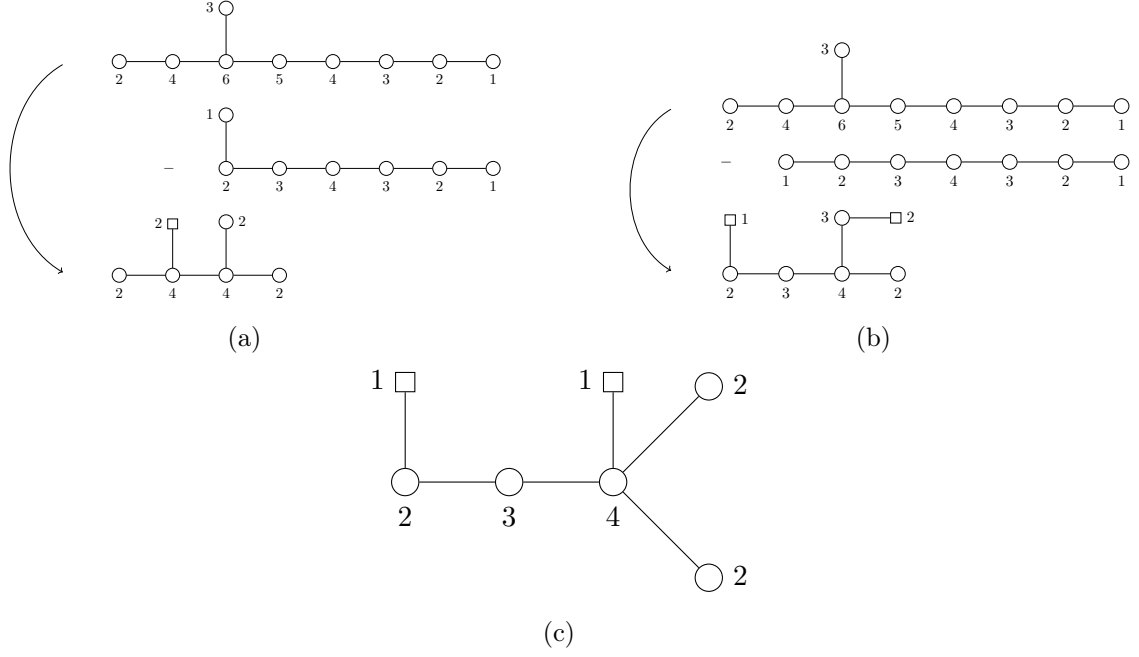


Figure 45: Both alignments of the $U(4)$ quotient quiver against $\overline{\min.E_8}$ to produce quivers \mathcal{Q}_{45a} and \mathcal{Q}_{45b} . Their intersection, reached via A_1 KP transitions, is \mathcal{Q}_{45c} .

calculated using the Nilpotent Orbit Normalisation formula [59]. We conclude that:

$$\overline{\min.E_8} // \text{SU}(4) = \overline{\mathcal{W}_{D_5}}_{[0,0,0,0,0]}^{[0,2,0,0,0]} \cup \overline{\mathcal{W}_{D_5}}_{[0,0,0,0,0]}^{[1,0,0,2,0]} \quad (8.14)$$

The intersection \mathcal{Q}_{45c} , related in both cases by an A_1 KP transition, is a magnetic quiver whose Coulomb branch is also a slice in the affine Grassmannian of D_5 , $\overline{\mathcal{W}_{D_5}}_{[0,0,0,0,0]}^{[1,0,1,0,0]}$. Comparison of the volumes of the Coulomb branches indicates it is also the double cover of the orbit $\overline{\mathcal{O}}_{(3^2,1^4)}^{D_5}$. This is in accordance with the Springer correspondence and geometric Satake equivalence, as discussed in [82].

This identity can be checked explicitly using Weyl integration under the embedding of $E_8 \leftrightarrow D_5 \times A_3$ which decomposes the fundamental of E_8 as:

$$\begin{aligned} [0, 0, 0, 0, 0, 0, 1, 0]_{E_8} &\rightarrow [0, 1, 0, 0, 0; 0, 0, 0]_{D_5 \times A_3} + [0, 0, 0, 0, 1; 0, 0, 1]_{D_5 \times A_3} \\ &+ [0, 0, 0, 1, 0; 1, 0, 0]_{D_5 \times A_3} + [1, 0, 0, 0, 0; 0, 1, 0]_{D_5 \times A_3} + [0, 0, 0, 0, 0; 1, 0, 1]_{D_5 \times A_3}. \end{aligned} \quad (8.15)$$

9 Slices in Exceptional Affine Grassmannians

Here we consider magnetic quivers for some slices in the affine Grassmannian of E-type algebras. The quivers are good by construction and many satisfy the [External Leg Rule](#) since E-type Dynkin diagrams have a long leg suitable for quotient quiver subtraction.

The cases presented are not chosen in a systematic way since a comprehensive study of affine Grassmannians is beyond the scope of this paper. Nevertheless, we draw upon these

examples in the affine Grassmannian to demonstrate the generality of our rules for quivers whose Coulomb branches are challenging to compute.

9.1 SU(2) HKQ

9.1.1 $\overline{[\mathcal{W}_{E_6}]_{[1,0,0,0,0,1]}} // \text{SU}(2)$

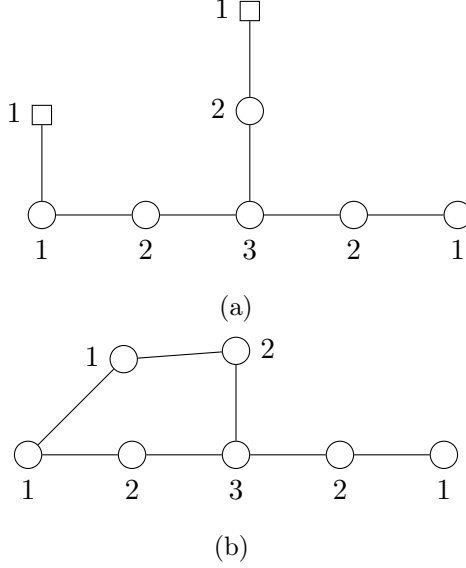


Figure 46: Framed quiver \mathcal{Q}_{46a} and unframed quiver \mathcal{Q}_{46b} for $\overline{[\mathcal{W}_{E_6}]_{[1,0,0,0,0,1]}}$

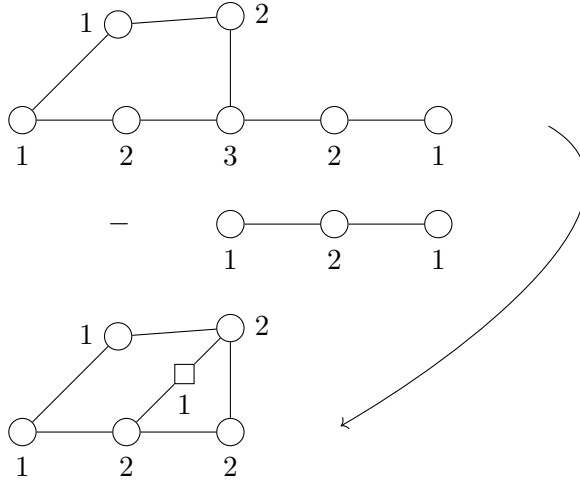


Figure 47: Subtraction of the U(2) quotient quiver from \mathcal{Q}_{46b} to yield \mathcal{Q}_{47} .

Framed and unframed magnetic quivers \mathcal{Q}_{46a} and \mathcal{Q}_{46b} for $\overline{[\mathcal{W}_{E_6}]_{[1,0,0,0,0,1]}}$ are shown in Figure 69.

The Coulomb branch global symmetry is $SO(10) \times U(1)$. By inspection of \mathcal{Q}_{46b} , we see there is only one possible alignment for an U(2) quotient quiver that obeys all of the selection

rules. This subtraction yields the quiver \mathcal{Q}_{47} shown in Figure 47. From consideration of the balance of gauge nodes of \mathcal{Q}_{47} one would expect a Coulomb branch global symmetry of at least $SU(4) \times U(1)^2$. When we compute the Hilbert series of its Coulomb branch using the monopole formula we find a global symmetry enhancement to $SU(4) \times SU(2) \times U(1)$.

The unrefined HS is:

$$HS[\mathcal{C}(\mathcal{Q}_{47})] = \frac{\left(\begin{aligned} &1 + 6t^2 + 33t^3 + 136t^4 + 541t^5 + 1862t^6 + 5913t^7 + 16736t^8 + 43638t^9 \\ &+ 103724t^{10} + 228506t^{11} + 464616t^{12} + 880496t^{13} + 1553400t^{14} \\ &+ 2568079t^{15} + 3976634t^{16} + 5792877t^{17} + 7935748t^{18} + 10255355t^{19} \\ &+ 12496990t^{20} + 14392503t^{21} + 15653956t^{22} + 16104580t^{23} \\ &+ \text{palindrome} + t^{44} \end{aligned} \right)}{(1-t)^{-6} (1-t^2)^7 (1-t^3)^8 (1-t^4)^7} \quad (9.1)$$

Noting that the $U(2)$ quotient quiver is subtracted from the balanced D_5 Dynkin diagram contained within \mathcal{Q}_{46a} , we have used the embedding (7.2) to compute the HKQ using Weyl integration and thereby to confirm the result from quotient quiver subtraction.

9.1.2 $\overline{[\mathcal{W}_{E_6}]_{[0,0,0,0,0,1]}}^{[0,0,1,0,0,0]} // SU(2)$

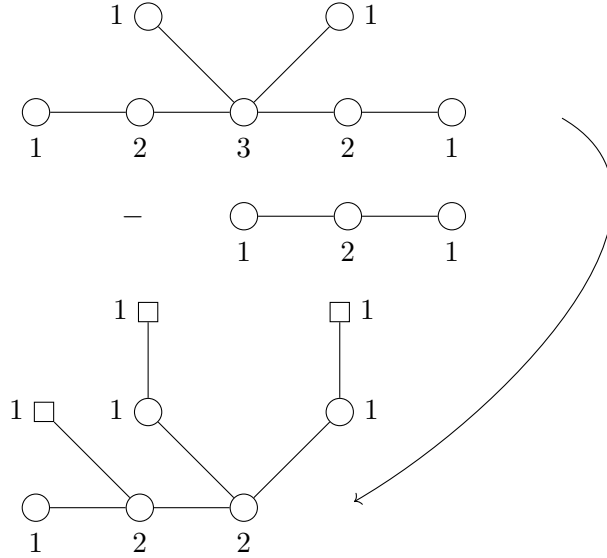


Figure 48: Subtraction of the $U(2)$ quotient quiver from the unframed magnetic quiver for $\overline{[\mathcal{W}_{E_6}]_{[0,0,0,0,0,1]}}^{[0,0,1,0,0,0]}$ to yield \mathcal{Q}_{48} .

The magnetic quiver for $\overline{[\mathcal{W}_{E_6}]_{[0,0,0,0,0,1]}}^{[0,0,1,0,0,0]}$ is shown at the top of Figure 48, together with the subtraction of the $U(2)$ quotient quiver to produce \mathcal{Q}_{48} . The global symmetry of $\overline{[\mathcal{W}_{E_6}]_{[0,0,0,0,0,1]}}^{[0,0,1,0,0,0]}$ is $SU(6) \times U(1)$. The Coulomb branch of \mathcal{Q}_{48} is $\overline{[\mathcal{W}_{D_5}]_{[0,0,0,1,1]}}^{[0,1,0,1,1]}$, and has a global symmetry of $SU(4) \times U(1)^2$. We conclude that

$$\overline{[\mathcal{W}_{E_6}]_{[0,0,0,0,0,1]}}^{[0,0,1,0,0,0]} // SU(2) = \overline{[\mathcal{W}_{D_5}]_{[0,0,0,1,1]}}^{[0,1,0,1,1]} \quad (9.2)$$

and confirm this from the unrefined Hilbert series:

$$\text{HS}[\mathcal{C}(\mathcal{Q}_{48})] = \frac{\left(\begin{aligned} &1 + 3t + 18t^2 + 55t^3 + 198t^4 + 539t^5 + 1445t^6 + 3288t^7 + 7052t^8 \\ &+ 13416t^9 + 23838t^{10} + 38390t^{11} + 57751t^{12} + 79667t^{13} + 102836t^{14} \\ &+ 122489t^{15} + 136705t^{16} + 141190t^{17} + \text{palindrome} + t^{34} \end{aligned} \right)}{(1-t^2)^2 (1-t^3)^{12} (1-t^4)^5 (1+t)^3}. \quad (9.3)$$

Noting that the $U(2)$ quotient quiver is subtracted from a leg that forms a balanced Dynkin diagram of A_5 within \mathcal{Q}_{48} , we have used the embedding (4.1) to compute the HKQ using Weyl integration, in agreement with the result from quotient quiver subtraction.

9.1.3 $\overline{[\mathcal{W}_{E_6}]_{[0,0,0,0,0,1]}}^{[0,0,0,0,0,2]} // \text{SU}(2)$

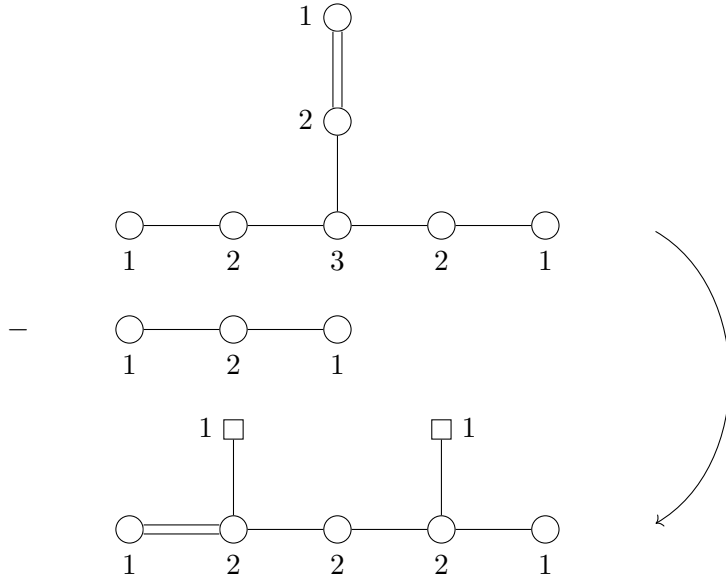


Figure 49: Subtraction of the $U(2)$ quotient quiver from the unframed magnetic quiver for $\overline{[\mathcal{W}_{E_6}]_{[0,0,0,0,0,1]}}^{[0,0,0,0,0,2]}$ to yield \mathcal{Q}_{49} .

The unframed magnetic quiver for $\overline{[\mathcal{W}_{E_6}]_{[0,0,0,0,0,1]}}^{[0,0,0,0,0,2]}$ is shown at the top of Figure 49, together with the subtraction of the $U(2)$ quotient quiver to produce \mathcal{Q}_{49} . The global symmetry of $\overline{[\mathcal{W}_{E_6}]_{[0,0,0,0,0,1]}}^{[0,0,0,0,0,2]}$ is $SU(6) \times U(1)$. The Coulomb branch of \mathcal{Q}_{49} has an $SU(4) \times U(1)^2$ Coulomb branch global symmetry. The monopole formula gives the unrefined HS:

$$\text{HS}[\mathcal{C}(\mathcal{Q}_{49})] = \frac{\left(\begin{aligned} &1 + 4t^2 + 19t^3 + 64t^4 + 212t^5 + 608t^6 + 1609t^7 + 3788t^8 + 8198t^9 \\ &+ 16140t^{10} + 29403t^{11} + 49352t^{12} + 77074t^{13} + 111680t^{14} \\ &+ 151113t^{15} + 190540t^{16} + 224913t^{17} + 248056t^{18} + 256504t^{19} \\ &+ \text{palindrome} + t^{36} \end{aligned} \right)}{(1-t^2)^4 (1-t^3)^8 (1-t^4)^4 (1+t)^4} \quad (9.4)$$

Noting the $U(2)$ quotient quiver is subtracted from an external leg which forms a balanced Dynkin diagram of A_5 , we have used the embedding (4.1) to compute the HKQ using Weyl integration, in agreement with the result from quotient quiver subtraction.

9.1.4 $\overline{[\mathcal{W}_{E_6}]_{[0,0,0,0,0,1]}}^{[0,0,0,1,1,0]} // \text{SU}(2)$

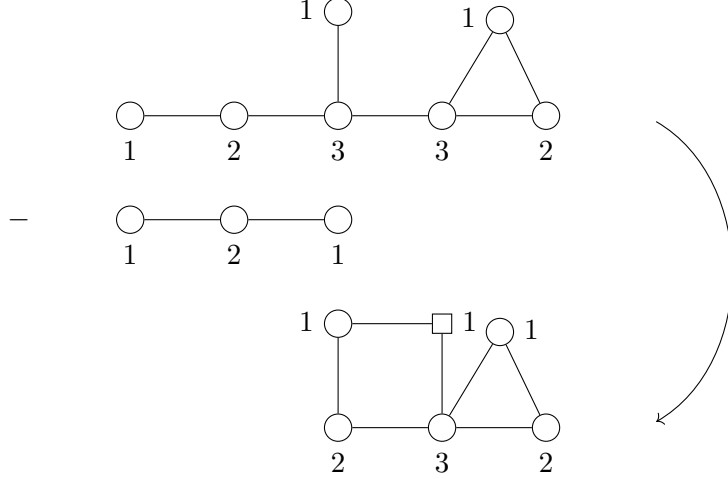


Figure 50: Subtraction of the $U(2)$ quotient quiver from the unframed magnetic quiver for $\overline{[\mathcal{W}_{E_6}]_{[0,0,0,0,0,1]}}^{[0,0,0,1,1,0]}$ to yield \mathcal{Q}_{50} .

The unframed magnetic quiver for $\overline{[\mathcal{W}_{E_6}]_{[0,0,0,0,0,1]}}^{[0,0,0,1,1,0]}$ is drawn at the top of Figure 50, together with the subtraction of the $U(2)$ quotient quiver to produce \mathcal{Q}_{50} . Note that there is only one possible alignment which respects all of the selection rules given in 2. The global symmetry of $\overline{[\mathcal{W}_{E_6}]_{[0,0,0,0,0,1]}}^{[0,0,0,1,1,0]}$ is $SU(6) \times U(1)$, and the global symmetry of the Coulomb branch of \mathcal{Q}_{50} is $SU(4) \times U(1)^2$. The latter is confirmed by the computation of the HS using the monopole formula:

$$\text{HS}[\mathcal{C}(\mathcal{Q}_{50})] = \frac{\left(\begin{aligned} &1 + 7t + 39t^2 + 170t^3 + 668t^4 + 2372t^5 + 7780t^6 + 23590t^7 + 66604t^8 \\ &+ 175712t^9 + 435301t^{10} + 1016083t^{11} + 2242404t^{12} + 4691381t^{13} \\ &+ 9328137t^{14} + 17665378t^{15} + 31926140t^{16} + 55157964t^{17} \\ &+ 91240107t^{18} + 144699995t^{19} + 220286604t^{20} + 322261559t^{21} \\ &+ 453465718t^{22} + 614264933t^{23} + 801601813t^{24} + 1008376706t^{25} \\ &+ 1223428820t^{26} + 1432240058t^{27} + 1618409691t^{28} + 1765687065t^{29} \\ &+ 1860269901t^{30} + 1892885098t^{31} + \text{palindrome} + t^{62} \end{aligned} \right)}{(1-t)^{-1} (1-t^3)^7 (1-t^4)^6 (1-t^5)^6 (1+t)^6}. \quad (9.5)$$

The $U(2)$ quotient quiver is subtracted from a leg which forms the balanced Dynkin diagram of A_5 . We have used the embedding in (4.1) to compute the HKQ using Weyl integration and find agreement with quiver subtraction.

9.1.5 $[\overline{\mathcal{W}_{E_6}}]_{[0,2,0,0,0,0]}^{[1,0,0,1,0,0]} // \text{SU}(2)$

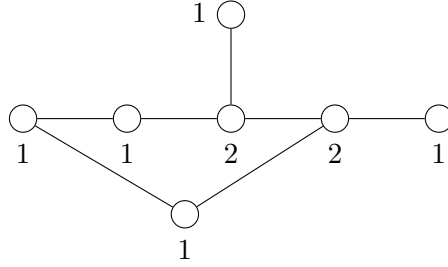


Figure 51: Unframed magnetic quiver \mathcal{Q}_{51} for $[\overline{\mathcal{W}_{E_6}}]_{[0,2,0,0,0,0]}^{[1,0,0,1,0,0]}$.

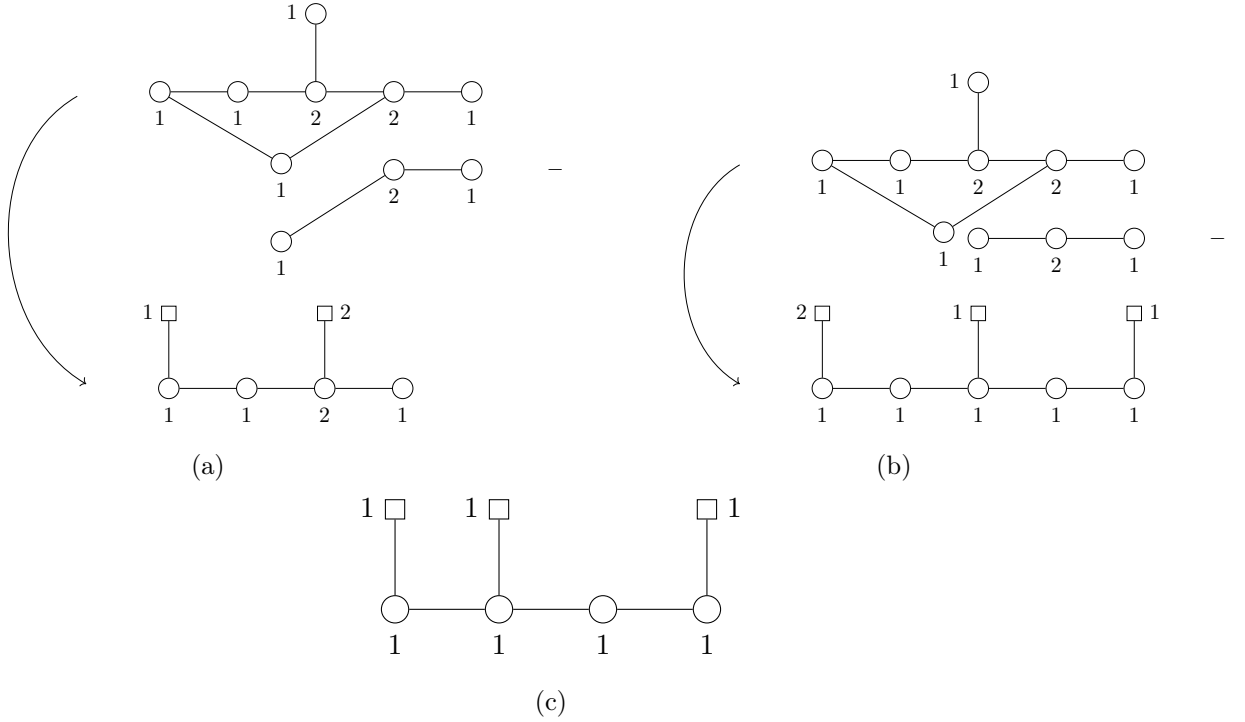


Figure 52: Both alignments of the $U(2)$ quotient quiver against the unframed magnetic quiver \mathcal{Q}_{51} for $[\overline{\mathcal{W}_{E_6}}]_{[0,2,0,0,0,0]}^{[1,0,0,1,0,0]}$, giving the quivers \mathcal{Q}_{52a} and \mathcal{Q}_{52b} . Their intersection, via A_1 KP transitions, is quiver \mathcal{Q}_{52c} .

The unframed magnetic quiver \mathcal{Q}_{51} for $[\overline{\mathcal{W}_{E_6}}]_{[0,2,0,0,0,0]}^{[1,0,0,1,0,0]}$ is given in Figure 51. The global symmetry of $[\overline{\mathcal{W}_{E_6}}]_{[0,2,0,0,0,0]}^{[1,0,0,1,0,0]}$ is $SU(5) \times U(1)^2$. There are two equivalent external legs for $U(2)$ quotient quiver subtraction respecting the rules given in 2, so either may be chosen for the subtraction. There are two possible alignments of the $U(2)$ quotient quiver, which produce the magnetic quivers \mathcal{Q}_{52a} and \mathcal{Q}_{52b} , for the affine Grassmannian slices

$[\overline{\mathcal{W}}_{A_4}]_{[0,1,0,0]}^{[1,0,2,0]}$ and $[\overline{\mathcal{W}}_{A_5}]_{[1,0,1,0,0]}^{[2,0,1,0,1]}$, respectively. We conclude that:

$$[\overline{\mathcal{W}}_{E_6}]_{[0,2,0,0,0,0]}^{[1,0,0,1,0,0]} // \text{SU}(2) = [\overline{\mathcal{W}}_{A_4}]_{[0,1,0,0]}^{[1,0,2,0]} \cup [\overline{\mathcal{W}}_{A_5}]_{[1,0,1,0,0]}^{[2,0,1,0,1]} \quad (9.6)$$

The intersection of \mathcal{Q}_{52a} and \mathcal{Q}_{52b} is \mathcal{Q}_{52c} , which is a magnetic quiver for $[\overline{\mathcal{W}}_{A_4}]_{[0,1,0,0]}^{[1,1,0,1]}$. Proceeding as before, we find the HS of the union (9.6):

$$\begin{aligned} HS & \left[\mathcal{C} \left([\overline{\mathcal{W}}_{A_4}]_{[0,1,0,0]}^{[1,0,2,0]} \cup [\overline{\mathcal{W}}_{A_5}]_{[1,0,1,0,0]}^{[2,0,1,0,1]} \right) \right] \\ &= \frac{(1+t^2)(1+5t^2+8t^3+14t^4+16t^5+23t^6+16t^7+14t^8+8t^9+5t^{10}+t^{12})}{(1-t^2)^6(1-t^3)^4} \\ &+ \frac{\left(\begin{aligned} &1+t+11t^2+22t^3+70t^4+128t^5+266t^6+398t^7+623t^8+761t^9+935t^{10}+938t^{11} \\ &+935t^{12}+761t^{13}+623t^{14}+398t^{15}+266t^{16}+128t^{17}+70t^{18}+22t^{19}+11t^{20}+t^{21}+t^{22} \end{aligned} \right)}{(1-t)^{-1}(1-t^2)^3(1-t^3)^5(1-t^4)^3} \\ &- \frac{\left(\begin{aligned} &1+2t+9t^2+24t^3+50t^4+76t^5+108t^6+120t^7 \\ &+108t^8+76t^9+50t^{10}+24t^{11}+9t^{12}+2t^{13}+t^{14} \end{aligned} \right)}{(1-t)^{-2}(1-t^2)^6(1-t^3)^4} \end{aligned} \quad (9.7)$$

$$\begin{aligned} &= \frac{\left(\begin{aligned} &1+t+11t^2+22t^3+78t^4+160t^5+353t^6+601t^7+980t^8+1335t^9+1682t^{10} \\ &+1827t^{11}+1800t^{12}+1529t^{13}+1151t^{14}+722t^{15}+372t^{16}+138t^{17}+13t^{18} \\ &-25t^{19}-28t^{20}-15t^{21}-8t^{22}-t^{23}-t^{24} \end{aligned} \right)}{(1-t)^{-1}(1-t^2)^3(1-t^3)^5(1-t^4)^3} \end{aligned} \quad (9.8)$$

The HS in the signed sum (9.7) are for $[\overline{\mathcal{W}}_{A_4}]_{[0,1,0,0]}^{[1,0,2,0]}$, $[\overline{\mathcal{W}}_{A_5}]_{[1,0,1,0,0]}^{[2,0,1,0,1]}$, and $[\overline{\mathcal{W}}_{A_4}]_{[0,1,0,0]}^{[1,1,0,1]}$, respectively.

The U(2) quotient quiver is subtracted from a leg which forms the Dynkin diagram of A_4 . One can use the embedding in (4.1) to compute the HKQ using Weyl integration and to find agreement with quiver subtraction.

9.1.6 $[\overline{\mathcal{W}}_{E_7}]_{[0,0,0,0,0,0,1]}^{[0,0,0,1,0,0,0]} // \text{SU}(2)$

The magnetic quiver for $[\overline{\mathcal{W}}_{E_7}]_{[0,0,0,0,0,0,1]}^{[0,0,0,1,0,0,0]}$ is shown at the top of Figure 53, followed by subtraction of the U(2) quotient quiver to produce \mathcal{Q}_{53} , which is a magnetic quiver for $[\overline{\mathcal{W}}_{E_6}]_{[1,0,0,0,0,1]}^{[1,0,1,0,0,0]}$. The global symmetry of $[\overline{\mathcal{W}}_{E_7}]_{[0,0,0,0,0,0,1]}^{[0,0,0,1,0,0,0]}$ is $\text{SU}(7) \times \text{U}(1)$. Note that there is only one external leg which respects the selection rules for quiver subtraction. We obtain the result:

$$[\overline{\mathcal{W}}_{E_7}]_{[0,0,0,0,0,0,1]}^{[0,0,0,1,0,0,0]} // \text{SU}(2) = [\overline{\mathcal{W}}_{E_6}]_{[1,0,0,0,0,1]}^{[1,0,1,0,0,0]} \quad (9.9)$$

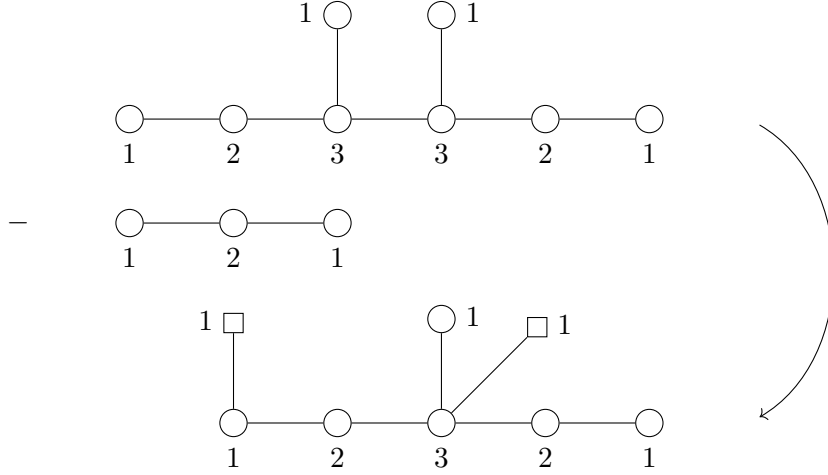


Figure 53: Subtraction of the $U(2)$ quotient quiver from the unframed magnetic quiver for $\overline{[\mathcal{W}_{E_7}]_{[0,0,0,0,0,0,1]}}^{[0,0,0,1,0,0,0]}$ to produce the magnetic quiver \mathcal{Q}_{53} .

The global symmetry of $\overline{[\mathcal{W}_{E_6}]_{[1,0,0,0,0,1]}}^{[1,0,1,0,0,0]}$ is $SU(5) \times U(1)^2$, which is verified through the computation of the HS using the monopole formula.

$$HS[\mathcal{C}(\mathcal{Q}_{53})] = \frac{\left(\begin{aligned} &1 + 4t + 29t^2 + 116t^3 + 507t^4 + 1764t^5 + 5897t^6 + 17316t^7 + 47598t^8 \\ &+ 119000t^9 + 277876t^{10} + 600000t^{11} + 1213902t^{12} + 2292834t^{13} \\ &+ 4073898t^{14} + 6800152t^{15} + 10715088t^{16} + 15929986t^{17} \\ &+ 22418427t^{18} + 29855900t^{19} + 37713801t^{20} + 45170786t^{21} \\ &+ 51383981t^{22} + 55484436t^{23} + 56938432t^{24} + \text{palindrome} + t^{48} \end{aligned} \right)}{(1-t)^{-4}(1-t^2)^7(1-t^3)^{10}(1-t^4)^7} \quad (9.10)$$

As the $U(2)$ quotient quiver is subtracted from a balanced subdiagram of the magnetic quiver for $\overline{[\mathcal{W}_{E_7}]_{[0,0,0,0,0,0,1]}}^{[0,0,0,1,0,0,0]}$, which forms the A_6 Dynkin diagram, we employ the embedding given in (4.1) to verify the result.

9.1.7 $\overline{[\mathcal{W}_{E_7}]_{[1,0,0,0,0,0,0]}}^{[0,1,0,0,0,0,0]} // SU(2)$

The unframed magnetic quiver for $\overline{[\mathcal{W}_{E_7}]_{[1,0,0,0,0,0,0]}}^{[0,1,0,0,0,0,0]}$, which has global symmetry $SO(12) \times U(1)$, is shown at the top of Figure 54. This is followed by the subtraction of the $U(2)$ quotient quiver to produce the magnetic quiver \mathcal{Q}_{54} . This has a global symmetry of $SO(8) \times SU(2) \times U(1)$, as can be determined from the Hilbert series:

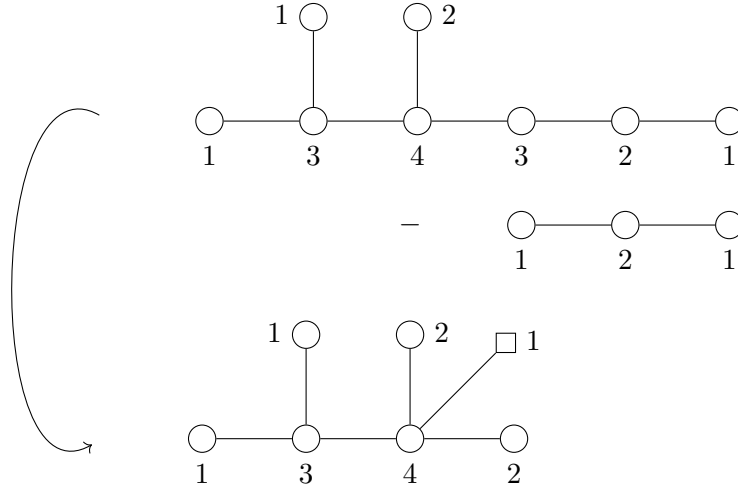


Figure 54: Subtraction of the $U(2)$ quotient quiver from an unframed magnetic quiver for $\overline{[\mathcal{W}_{E_7}]_{[1,0,0,0,0,0,0]}}^{[0,1,0,0,0,0,0]}$ to give \mathcal{Q}_{54} .

$$HS[\mathcal{C}(\mathcal{Q}_{54})] = \frac{\left(\begin{aligned} &1 + 9t + 66t^2 + 373t^3 + 1914t^4 + 8701t^5 + 36329t^6 + 138552t^7 \\ &+ 489648t^8 + 1605300t^9 + 4918751t^{10} + 14118695t^{11} + 38138780t^{12} \\ &+ 97185445t^{13} + 234361303t^{14} + 535948910t^{15} + 1165046145t^{16} \\ &+ 2411578527t^{17} + 4762032274t^{18} + 8983378907t^{19} + 16213188569t^{20} \\ &+ 28027708562t^{21} + 46461483210t^{22} + 73925927636t^{23} \\ &+ 113003617343t^{24} + 166076737959t^{25} + 234831061465t^{26} \\ &+ 319661125610t^{27} + 419130743340t^{28} + 529576399650t^{29} \\ &+ 645063463512t^{30} + 757718368534t^{31} + 858546072189t^{32} \\ &+ 938541874231t^{33} + 990021037865t^{34} + 1007788178974t^{35} \\ &+ \text{palindrome} + t^{70} \end{aligned} \right)}{(1-t)^{-9} (1-t^2)^{11} (1-t^3)^{13} (1-t^4)^{11}}. \quad (9.11)$$

Note that the pattern of balanced gauge nodes in \mathcal{Q}_{54} requires a Coulomb branch global symmetry of at least $SO(8) \times U(1)^2$, and so an enhancement has occurred.

The HKQ can be computed explicitly with Weyl integration using the embedding (7.2) to find agreement with quotient quiver subtraction.

9.2 $SU(3)$ HKQ

9.2.1 $\overline{[\mathcal{W}_{E_7}]_{[1,0,0,0,0,0,0]}}^{[0,1,0,0,0,0,0]} // SU(3)$

We can also take the unframed magnetic quiver for $\overline{[\mathcal{W}_{E_7}]_{[1,0,0,0,0,0,0]}}^{[0,1,0,0,0,0,0]}$ and consider the subtraction of the $U(3)$ quotient quiver. There are two possible alignments shown in Figure 55, producing quivers \mathcal{Q}_{55a} and \mathcal{Q}_{55b} . These are magnetic quivers for $\overline{[\mathcal{W}_{D_5}]_{[0,0,0,1,1]}}^{[0,0,2,0,0]}$ and

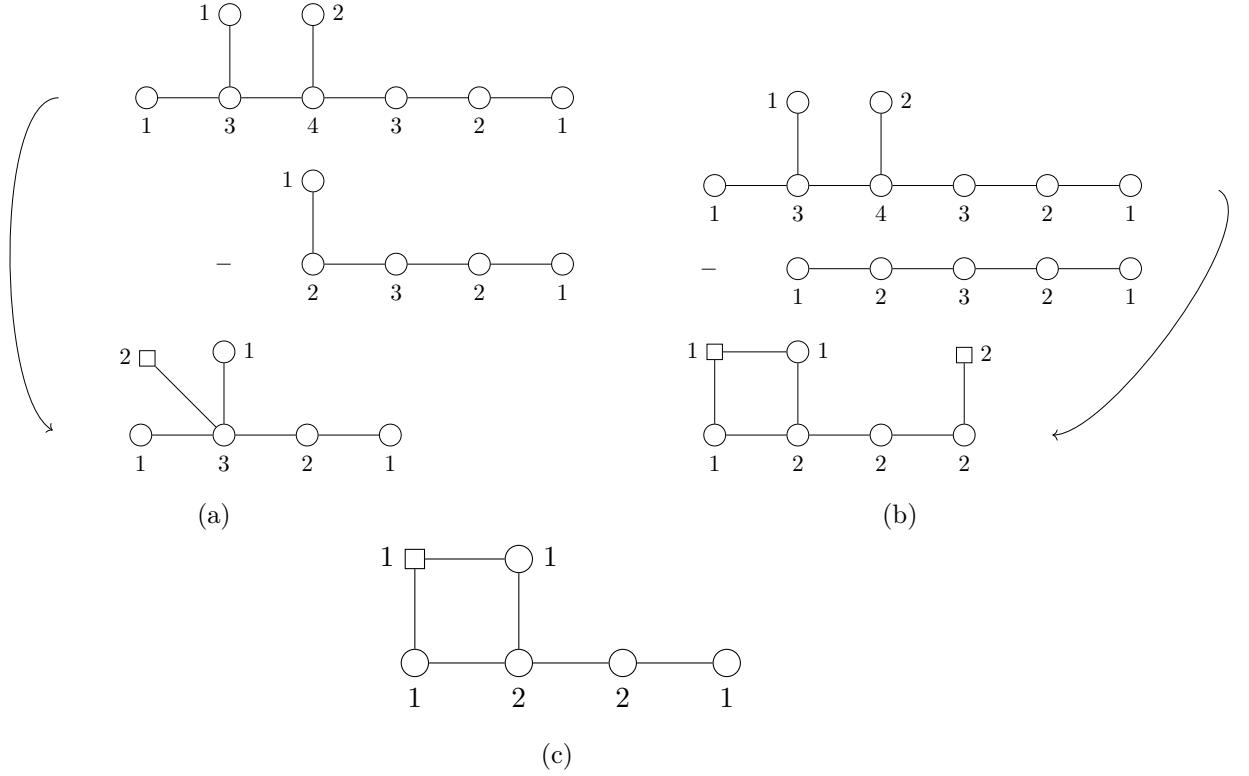


Figure 55: Both alignments of the $U(3)$ quotient quiver against the unframed magnetic quiver for $\overline{[\mathcal{W}_{E_7}]_{[1,0,0,0,0,0,0]}^{[0,1,0,0,0,0,0]}}$ to give the quivers \mathcal{Q}_{55a} and \mathcal{Q}_{55b} . Their intersection, via A_1 KP transitions, is quiver \mathcal{Q}_{55c} .

$\overline{[\mathcal{W}_{D_5}]_{[2,0,0,1,1]}^{[2,0,0,1,1]}}$ respectively. We conclude that,

$$\overline{[\mathcal{W}_{E_7}]_{[1,0,0,0,0,0,0]}^{[0,1,0,0,0,0,0]}} // \text{SU}(3) = \overline{[\mathcal{W}_{D_5}]_{[0,0,0,1,1]}^{[0,0,2,0,0]}} \cup \overline{[\mathcal{W}_{D_5}]_{[2,0,0,1,1]}^{[2,0,0,1,1]}}. \quad (9.12)$$

To compute the union we note that there is an A_1 KP transition from each of \mathcal{Q}_{55a} and \mathcal{Q}_{55b} to their intersection, which is a magnetic quiver for $\overline{[\mathcal{W}_{D_5}]_{[0,0,0,1,1]}^{[0,1,0,1,1]}}$. The monopole

formula yields the HS of the union as:

$$\begin{aligned}
& HS \left[\overline{[\mathcal{W}_{D_5}]_{[0,0,0,1,1]}}^{[0,0,2,0,0]} \cup \overline{[\mathcal{W}_{D_5}]_{[2,0,0,1,1]}}^{[2,0,0,1,1]} \right] \\
&= \frac{\left(\begin{aligned} & 1 + 3t + 15t^2 + 46t^3 + 148t^4 + 386t^5 + 954t^6 + 2064t^7 + 4183t^8 + 7649t^9 + 13081t^{10} \\ & + 20490t^{11} + 30060t^{12} + 40738t^{13} + 51804t^{14} + 61138t^{15} + 67790t^{16} + 69920t^{17} \\ & + \text{palindrome} + t^{34} \end{aligned} \right)}{(1-t)^{-3} (1-t^2)^8 (1-t^3)^7 (1-t^4)^4} \\
&+ \frac{\left(\begin{aligned} & 1 + 4t + 21t^2 + 72t^3 + 264t^4 + 792t^5 + 2276t^6 + 5728t^7 + 13478t^8 + 28656t^9 + 56852t^{10} \\ & + 103680t^{11} + 177030t^{12} + 280752t^{13} + 418307t^{14} + 582484t^{15} + 764001t^{16} + 940120t^{17} \\ & + 1091630t^{18} + 1191688t^{19} + 1228644t^{20} + \text{palindrome} + t^{40} \end{aligned} \right)}{(1-t)^{-4} (1-t^2)^6 (1-t^3)^8 (1-t^4)^6} \\
&- \frac{\left(\begin{aligned} & 1 + 3t + 18t^2 + 55t^3 + 198t^4 + 539t^5 + 1445t^6 + 3288t^7 + 7052t^8 + 13416t^9 + 23838t^{10} \\ & + 38390t^{11} + 57751t^{12} + 79667t^{13} + 102836t^{14} + 122489t^{15} + 136705t^{16} + 141190t^{17} \\ & + \text{palindrome} + t^{34} \end{aligned} \right)}{(1-t)^{-3} (1-t^3)^7 (1-t^4)^5} \tag{9.13}
\end{aligned}$$

$$\begin{aligned}
&= \frac{\left(\begin{aligned} & 1 + 4t + 21t^2 + 72t^3 + 264t^4 + 792t^5 + 2311t^6 + 5948t^7 + 14510t^8 + 32172t^9 \\ & + 67045t^{10} + 128688t^{11} + 231618t^{12} + 386696t^{13} + 605330t^{14} + 882664t^{15} \\ & + 1207465t^{16} + 1542388t^{17} + 1848901t^{18} + 2071096t^{19} + 2175454t^{20} \\ & + 2132696t^{21} + 1955542t^{22} + 1666800t^{23} + 1321273t^{24} + 964732t^{25} + 646981t^{26} \\ & + 391080t^{27} + 209934t^{28} + 94416t^{29} + 31585t^{30} + 2532t^{31} - 6746t^{32} - 7412t^{33} \\ & - 5153t^{34} - 2904t^{35} - 1378t^{36} - 568t^{37} - 206t^{38} - 64t^{39} - 19t^{40} - 4t^{41} - t^{42} \end{aligned} \right)}{(1-t)^{-4} (1-t^2)^6 (1-t^3)^8 (1-t^4)^6}, \tag{9.14}
\end{aligned}$$

where in (9.14) the HS components are those for $\overline{[\mathcal{W}_{D_5}]_{[0,0,0,1,1]}}^{[0,0,2,0,0]}$, $\overline{[\mathcal{W}_{D_5}]_{[2,0,0,1,1]}}^{[2,0,0,1,1]}$, and their intersection $\overline{[\mathcal{W}_{D_5}]_{[0,0,0,1,1]}}^{[0,1,0,1,1]}$, respectively.

There is an embedding of $D_6 \leftrightarrow A_3 \times D_3 \leftrightarrow A_3 \times A_2 \times U(1)$. We have performed the SU(3) HKQ analytically and find agreement with quiver subtraction.

10 Miscellaneous Moduli Spaces

Here we consider some miscellaneous moduli spaces and their HKQs using quiver subtraction on their magnetic quivers.

First we consider SU(2) HKQs of the generic star shaped quivers $SU(2)^N$, which for cases $N = 3, 4$ are the 4 (quaternionic) dimensional moduli space of free fields (Section 3) and the 5 dimensional $\overline{min.D_4}$ (Section 7), respectively.

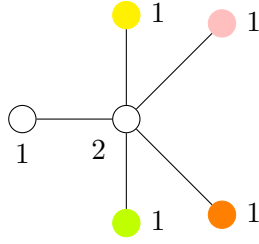


Figure 56: Unframed star shaped magnetic quiver \mathcal{Q}_{56} with global symmetry $SU(2)^5$.

10.1 Star shaped quiver $SU(2)^5//SU(2)$

The Coulomb branch of the quiver \mathcal{Q}_{56} is 6 (quaternionic) dimensional and has a global symmetry of $SU(2)^5$, with each factor of $SU(2)$ being equivalent under the outer automorphism. Quiver subtraction of the $U(2)$ quotient quiver is performed by aligning it with the uncoloured nodes and one coloured node in turn. The result of the HKQ is the union of the Coulomb branches of four possible magnetic quivers, each of which is $(\mathbb{C}_2/\mathbb{Z}_2)^3$. These have 6 two-way intersections, 4 three-way intersections and 1 four-way intersection at the origin. Summing the HWGs signed in accordance with (2.2) leads to the result:

$$HWG[\mathcal{C}(\mathcal{Q}_{56})//SU(2)] = PE[(\mu^2 + \nu^2 + \rho^2 + \sigma^2)t^2 - \mu^2\nu^2\rho^2\sigma^2t^8], \quad (10.1)$$

where we have associated the highest weight fugacities μ, ν, ρ, σ to the coloured $SU(2)$ symmetries. The moduli space is 3 (quaternionic) dimensional.

10.2 Star shaped quiver $SU(2)^{N+1}//SU(2), N > 1$

The Coulomb branch of the quiver \mathcal{Q}_{57} is $N + 2$ (quaternionic) dimensional and has a global symmetry of $SU(2)^{N+1}$, with each factor of $SU(2)$ being equivalent under the outer automorphism. Generalising the analyses for \mathcal{Q}_3 , \mathcal{Q}_{29} and \mathcal{Q}_{56} , we conjecture that the

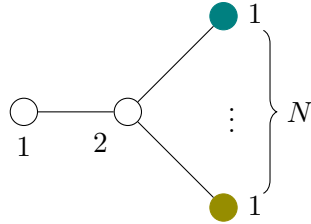


Figure 57: Unframed star shaped quiver \mathcal{Q}_{57} with global symmetry $SU(2)^{N+1}$.

HWG for the $N - 1$ (quaternionic) dimensional $SU(2)$ HKQ is:

$$HWG[\mathcal{C}(\mathcal{Q}_{57})//SU(2)] = PE \left[\sum_{i=1}^N \mu_{(i)}^2 t^2 - \left(\prod_{i=1}^N \mu_{(i)}^2 \right) t^{2N} \right], \quad (10.2)$$

where we have assigned highest weight fugacities $\mu_{(1), \dots, (N)}$ to the N coloured $SU(2)$ nodes. The interpretation of the relation at order t^{2N} in the HWG is as an invariant under the S_N outer automorphism permuting the coloured nodes.

10.3 A_{k-1} Class \mathcal{S} theory on a torus with 1 puncture

Another moduli space we consider is the A_{k-1} class \mathcal{S} theory on a torus with 1 puncture labelled by the partition $(k-2, 1^2)$. The magnetic quiver has an alternative description as an $SU(2)$ node surrounded by a bouquet of $k+1$ gauge nodes subject to an S_k discrete quotient. The case for $k=3$ is the $\overline{sub.reg.G_2}$. The $SU(2)$ HKQs of these spaces can be found using quiver subtraction.

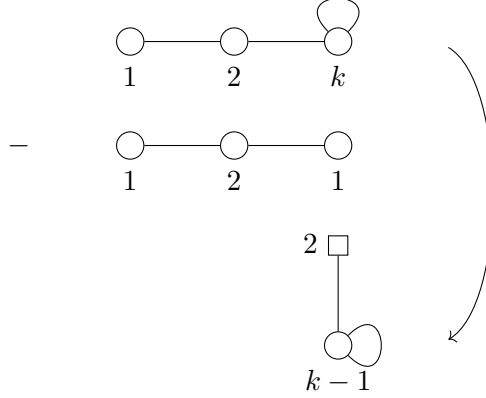


Figure 58: Subtraction of the $U(2)$ quotient quiver from the unframed magnetic quiver \mathcal{Q}_{58a} for a Class \mathcal{S} torus, with fixture symmetry $SL(k)$ and 1 puncture $(k-2, 1^2)$, to produce the magnetic quiver \mathcal{Q}_{58b} .

The unframed magnetic quiver \mathcal{Q}_{58a} for a Class \mathcal{S} theory of type A_{k-1} , on a torus (of genus 1), with 1 puncture described by the partition data $(k-2, 1^2)$, is drawn at the top of Figure 58. For the case $k=3$, where all nodes become balanced, there is an enhancement of the global symmetry of the Coulomb branch to G_2 , and the space forms the orbit closure $\overline{sub.reg.G_2}$. Apart from this case, the global symmetry of the Coulomb branch is $SU(2)^2$.

One can perform quiver subtraction by the $U(2)$ quotient quiver, which results in the magnetic quiver \mathcal{Q}_{58b} . It is known that this is an ADHM quiver and is also a magnetic quiver for $\text{Sym}^{k-1}(\mathbb{C}^2/\mathbb{Z}_2)$. Thus, we conjecture that for this family of quivers:

$$\mathcal{C}(\mathcal{Q}_{58a}) // SU(2) = \text{Sym}^{k-1}(\mathbb{C}^2/\mathbb{Z}_2), \quad k \geq 2. \quad (10.3)$$

We have checked the result by Weyl integration for small values of k , taking the HKQ w.r.t the $SU(2)$ associated to the node of rank 1 in \mathcal{Q}_{58a} .

10.4 Extended E_6 quiver $\overline{min.E_6} \times \mathbb{H}^2 // SU(2)$

One can take the affine E_6 shown in the top of Figure 40 and extend one leg by a further node of $U(2)$. This is shown in Figure 59, with the node in black having a balance of -1 . The Hilbert series of the Coulomb branch of this quiver is computed as

$$HS[\mathcal{C}(\mathcal{Q}_{59})] = \frac{\left(1 + 56t^2 + 945t^4 + 6776t^6 + 23815t^8 + 43989t^{10} + 43989t^{12} + 23815t^{14} + 6776t^{16} + 945t^{18} + 56t^{20} + t^{22}\right)}{(1-t)^4(1-t^2)^{22}}. \quad (10.4)$$

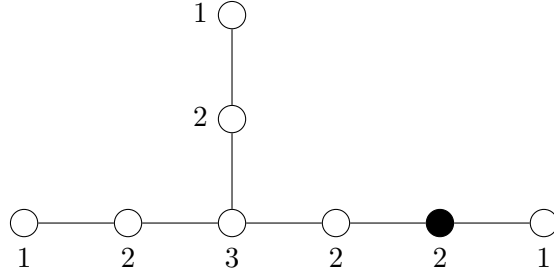


Figure 59: Magnetic quiver \mathcal{Q}_{59} for $\overline{\min.E_6} \times \mathbb{H}^2$.

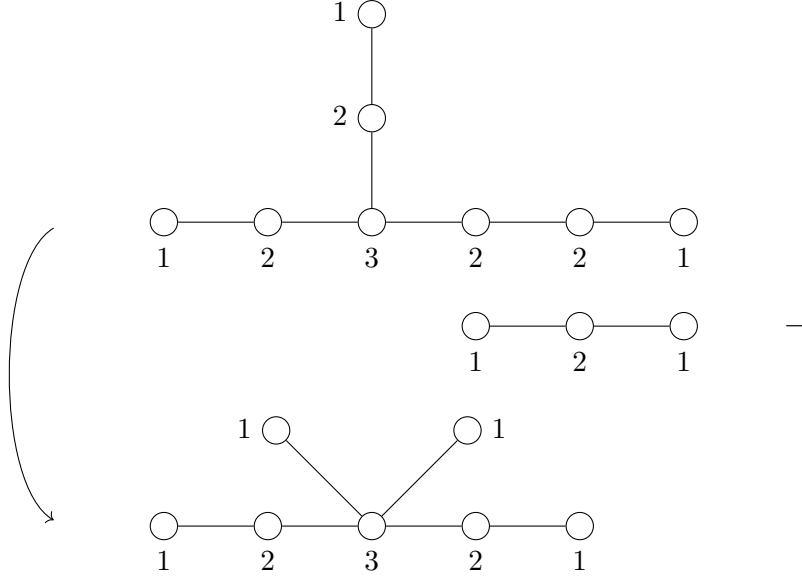


Figure 60: Subtraction of the U(2) quotient quiver from the unframed magnetic quiver \mathcal{Q}_{59} for $\overline{\min.E_6} \times \mathbb{H}^2$ to produce the magnetic quiver \mathcal{Q}_{60} .

The moduli space is $\overline{\min.E_6} \times \mathbb{H}^2$ and the global symmetry is $E_6 \times C_2$ which is confirmed from the t^2 coefficient of the above HS. One alignment and subtraction of the U(2) quotient quiver from \mathcal{Q}_{59} is shown in Figure 60 to produce quiver \mathcal{Q}_{60} . The Hilbert series of the Coulomb branch of \mathcal{Q}_{60} is

$$HS[\mathcal{C}(\mathcal{Q}_{60})] = \frac{\left(\begin{aligned} &1 + 6t + 41t^2 + 206t^3 + 900t^4 + 3326t^5 + 10846t^6 + 31100t^7 + 79677t^8 \\ &+ 183232t^9 + 381347t^{10} + 720592t^{11} + 1242416t^{12} + 1959850t^{13} + 2837034t^{14} \\ &+ 3774494t^{15} + 4624009t^{16} + 5220406t^{17} + 5435982t^{18} + \text{palindrome} + t^{36} \end{aligned} \right)}{(1-t^2)^{16}(1-t^3)^4(1+t+t^2)^6}, \quad (10.5)$$

the coefficient of the t^2 term indicates that the global symmetry of $\mathcal{C}(\mathcal{Q}_{60})$ is $A_5 \times U(1)$.

We conclude that

$$\left(\overline{\min.E_6} \times \mathbb{H}^2 \right) // \text{SU}(2) = \mathcal{C}(\mathcal{Q}_{60}). \quad (10.6)$$

The above result is verified from Weyl integration by integrating over the SU(2) in the

global symmetry of $\mathcal{C}(\mathcal{Q}_{59})$.

This result realises the Higgs branch side of the other example (alongside 8.1.4) contained in [83]. In this case the proposed duality is between $SU(3)$ gauge theory with 6 flavours at infinite coupling and the gauging of the $SU(2)$ in a rank 1 E_6 SCFT with a free fundamental hyper of $SU(2)$.

The Coulomb branch of \mathcal{Q}_{59} is exactly the Higgs branch of the latter theory. The gauging of $SU(2)$ is implemented through the quiver subtraction to produce \mathcal{Q}_{60} . The quiver \mathcal{Q}_{60} is indeed the 3d mirror for $SU(3)$ with 6 flavours.

11 Discussion and Conclusions

Quiver subtraction for $SU(n)$ HKQ In this work we have presented a new diagrammatic technique to compute the hyper-Kähler quotient by $SU(n)$ of the Coulomb branch of a quiver gauge theory. This technique works for all unitary magnetic quivers, including both "good" and "ugly" quivers, that respect the selection rules presented in Section 2. The procedure involves the subtraction of a $U(n)$ quotient quiver of the form $(1) - (2) - \dots - (n) - \dots - (2) - (1)$ from a target quiver which has been unframed w.r.t. an overall $U(1)$. Such a quotient quiver is "bad", as its central gauge node of rank n has a balance of -2 , and this method of quiver subtraction differs from the usual subtraction of "good" quivers for Kraft-Procesi transitions.

Quotient quiver subtraction requires that the target quiver should contain an external leg that forms a balanced Dynkin diagram of $SU(n)$, with nodes matching at least $(1) - (2) - \dots - (n) - \dots$.

The sum of the ranks of the gauge nodes in the $U(n)$ quotient quiver entails that the combination of this subtraction and unframing is dimensionally consistent with an $SU(n)$ HKQ.

For cases where there are multiple permissible alignments of the quotient quiver against the target quiver, the subtraction generates the HKQ as the union of the Coulomb branches of the alternative resulting quivers. The selection rules entail that these alternative quivers are related to their intersection by KP transitions, being Kleinian singularities of type A . (This follows due to the quiver subtraction being taken from a long external leg of the target quiver, along with the requirement that junctions only occur on a node of rank 2 on the quotient quiver.) The HS of the union is computed using the unions of cones formula (2.2).

Compared with HKQ via Weyl integration, the diagrammatic technique of quotient quiver subtraction is able to give additional insight into the structure of the resulting HS and/or HWG. This is because of the direct identification of the corresponding magnetic quiver(s). In cases where the HKQ is a union, this identification of the component magnetic quivers is particularly helpful and often simplifies calculation of the HS.

We have verified the validity of $SU(n)$ HKQs by quotient quiver subtraction for various classical and exceptional nilpotent orbits, and some free field moduli spaces, by comparison with the results from Weyl integration. Also, based on diagrammatic analyses, we have

been able to conjecture general results for certain families whose magnetic quivers satisfy the selection rules.

SU(n) HKQs of Free Fields We summarise some of the results from Section 3 in Table 1. These establish relationships between \mathbb{H}^n for $n \geq 4$ and the minimal nilpotent orbits of type B and D for odd and even n respectively. This is in accordance with [52].

Target Moduli Space	SU(2) HKQ	Rank
\mathbb{H}^{2k}	$\overline{\min.D_k}$	$k \geq 2$
\mathbb{H}^{2k+1}	$\overline{\min.B_k}$	$k \geq 2$

Table 1: The moduli spaces \mathbb{H}^n and their SU(2) HKQs. These fall into two families for even and odd n . These families are labelled by an integer k , with the appropriate limits on k shown.

Target Moduli Space	SU(2) HKQ	Rank
$\overline{n.\min.A_4}$	$\overline{\mathcal{O}_{(3)}^{A_2} \cup [\mathcal{W}_{D_3}]_{[0,1,3]}^{[0,1,3]}}$	$k \geq 5$
$\overline{n.\min.A_k}$	$\overline{\mathcal{O}_{(3,1^{k-4})}^{A_{k-2}} \cup [\mathcal{W}_{D_{k-1}}]_{[0,0,\dots,2]}^{[0,1,\dots,2]}}$	
$\overline{max.A_3}$	$\mathcal{S}_{\mathcal{N},(2^2)}^{A_3} \otimes \mathbb{C}^2 / \mathbb{Z}_4$	$k \geq 4$
$\overline{max.A_k}$	$[\mathcal{W}_{D_{k-1}}]_{[0,0,\dots,2]}^{[k+1,0,\dots,0]}$	
$\overline{\min.B_k}$	$\overline{n.\min B_{k-2}} \cup (\overline{\min.A_1} \otimes \overline{\min.B_{k-2}})$	$k \geq 4$
$\overline{n.\min.B_k}$	$\overline{\mathcal{O}_{(3,1^{2k-7})}^{D_{k-1}} / \mathbb{Z}_2} \cup (\overline{\min.A_1} \otimes \overline{\mathcal{O}_{(3,1^{2k-6})}^{B_{k-2}}})$	$k \geq 3$
$\overline{\min.D_k}$	$\overline{n.\min D_{k-2}} \cup (\overline{\min.A_1} \otimes \overline{\min.D_{k-2}})$	$k \geq 4$
$\overline{n.\min.D_k}$	$\overline{n.\min.B_{k-2} / \mathbb{Z}_2} \cup (\overline{\min.A_1} \otimes \overline{n.\min.D_{k-2}})$	$k \geq 4$
$\overline{sub.reg.G_2}$	$Sym^2(\overline{\min.A_1})$	
$\overline{\min.F_4}$	$\overline{n.\min.C_3}$	
$\overline{\min.E_6}$	$\overline{n.\min.A_5}$	
$\overline{\min.E_7}$	$\overline{n.n.\min.D_6}$	
$\overline{\min.E_8}$	$\overline{n.\min.E_7}$	

Table 2: Some classical and exceptional nilpotent orbits and their SU(2) HKQs. For families of orbits, labelled by their rank k , the limits on k are shown.

SU(n) HKQs of Nilpotent Orbits We summarise some of the results from Sections 4, 5, 7, and 8 in Tables 2, 3, and 4. These establish interesting relationships between classical and exceptional nilpotent orbits under SU(n) HKQ and other orbits or affine Grassmannian slices, and include many results that we have not found in the Literature.

In particular this work extends the work of Kobak-Swann [65], who find discrete quotients between nilpotent orbit closures, to include relationships under continuous hyper-Kähler quotients between nilpotent orbit closures and/or affine Grassmannian slices. Several aspects of these examples merit discussion.

Target Moduli Space	SU(3) HKQ	Rank
$\overline{max.A_5}$	$\mathcal{S}_{\mathcal{N},(2^3)}^{A_5} \otimes \mathbb{C}^2 / \mathbb{Z}_6$	$k = 6, 7, 8, 9, 10$
$\overline{max.A_k}$	$\overline{[\mathcal{W}_{E_{k-2}}]_{[0, \dots, 0, k+1, 0]}}_{[0, \dots, 0, 4]}$	
$\overline{\mathcal{O}_{(2^4, 1^{2k-7})}^{B_k}}$	$\overline{[\mathcal{W}_{B_{k-3}}]_{[0, 2, 0, \dots, 0]}}_{[0, 0, 0, \dots, 0]} \cup \overline{[\mathcal{W}_{B_{k-2}}]_{[2, 0, 0, 1, 0, \dots, 0]}}_{[2, 0, 0, 0, 0, \dots, 0]}$	$k \geq 6$
$\overline{min.E_7}$	$\overline{\mathcal{O}_{(2^3)}^{A_5}} \cup \overline{\mathcal{O}_{(3, 1^3)}^{A_5}}$	
$\overline{min.E_8}$	$\overline{[\mathcal{W}_{E_6}]_{[0, 0, 1, 0, 0, 0]}}_{[0, 0, 0, 0, 0, 0]}$	

Table 3: Some classical and exceptional nilpotent orbits and their SU(3) HKQs. For families of orbits, labelled by their rank k , the limits on k are shown.

Target Moduli Space	SU(4) HKQ
$\overline{min.E_8}$	$\overline{[\mathcal{W}_{D_5}]_{[0, 2, 0, 0, 0]}}_{[0, 0, 0, 0, 0]} \cup \overline{[\mathcal{W}_{D_5}]_{[1, 0, 0, 2, 0]}}_{[0, 0, 0, 0, 0]}$

Table 4: Exceptional nilpotent orbits and their SU(4) HKQs.

Firstly, while a number of the HKQs of orbits studied form 1-parameter families based on the rank of the target group, the first member of a family may take an irregular form. For example, consider the quotients $\overline{max.A_k} // \text{SU}(2)$. The first member of this family, consistent with the selection rules, is for $k = 3$. However, application of the general form for $k \geq 4$, which is given by the affine Grassmannian slice $\overline{[\mathcal{W}_{D_{k-1}}]_{[0, 0, \dots, 2]}}_{[k+1, 0, \dots, 0]}$, would require a slice of the semi-simple D_2 algebra, $\overline{[\mathcal{W}_{D_2}]_{[0, 2]}}_{[4, 0]}$. This description as a slice is not valid since the flavour co-weight minus the balance co-weight does not lie in the positive co-root lattice. The result for $k = 3$ is instead described by a product space with $A_1 \times \text{U}(1)$ global symmetry.

Or, consider the results in Table 3 for $\overline{max.A_k} // \text{SU}(3)$, which takes a different form for $k = 5$ compared with $k = 6, 7, 8, 9, 10$, the latter being an E-sequence of affine Grassmannian slices $\overline{[\mathcal{W}_{E_{k-2}}]_{[0, \dots, 0, k+1, 0]}}_{[0, \dots, 0, 4]}$. If we were to apply the more general form to $k = 5$, we would obtain $\overline{[\mathcal{W}_{E_3}]_{[0, 6, 0]}}_{[0, 0, 4]}$.

Interpreting the Dynkin diagram of E_3 as $A_2 \times A_1$ suggests this is the product of two affine Grassmannian slices $\overline{[\mathcal{W}_{A_2}]_{[0, 6]}}_{[0, 0]} \times \overline{[\mathcal{W}_{A_1}]_{[4]}}_{[0]}$. However, in the second term, the flavour co-weight minus the balance co-weight

is not in the positive coroot lattice of A_1 , and so, once again, this is not a valid affine Grassmannian slice.

Non-commutativity of KP transitions and SU(n) HKQ There are other aspects of these quotient quiver subtractions that merit further comment, including their commutation relations with other diagrammatic operations. Here, we examine the commutation between quiver subtraction for KP transitions and for SU(n) HKQ. Just as the order of KP transitions is important, we find that the operations of quotient quiver subtraction and KP transition quiver subtraction do not commute.

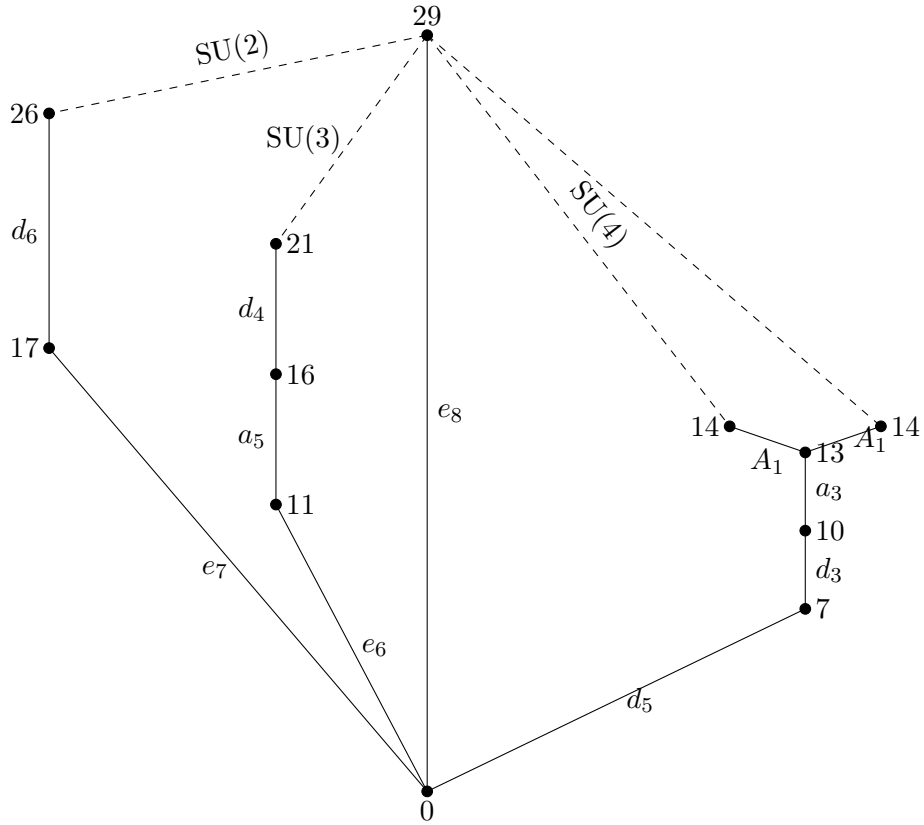


Figure 61: Hasse diagram of the $\overline{\min.E_8}$, subject to $SU(2)$, $SU(3)$, and $SU(4)$ HKQs by quotient quiver subtraction, shown by the dashed lines. The unbroken lines below each moduli space decompose their Hasse diagrams, labelled by KP transitions in the usual manner. The number next to each leaf is the quaternionic dimension of the moduli space.

By way of illustration, the Hasse diagram in Figure 61 shows the permissible KP transitions from $\overline{\min.E_8}$ before and after an initial quotient quiver subtraction for $n = 2, 3, 4$.

Without any quotient quiver subtraction and hence using KP transitions alone, only an e_8 slice can be subtracted – to the trivial leaf. Suppose instead that an $SU(n)$ HKQ, for $n = 2, 3$, or 4 , is performed first. This can then be followed by subsequent KP transitions down to the trivial leaf. Each initial $SU(n)$ HKQ takes us to a different branch of the Hasse diagram and, although the magnetic quivers at each leaf may be amenable to further $SU(n)$ HKQs, these do not generally link between the different branches. We conclude that quiver subtractions, whether for HKQs or KP transitions, do not commute.

A final comment we make is that KP transitions on nilpotent orbits of an algebra lead to other moduli spaces within the nilcone of the algebra. The difference for quotient quiver subtraction on nilpotent orbits is that one moves to a different algebra, being that of the commutant of the embedding of $SU(n)$ inside the original algebra.

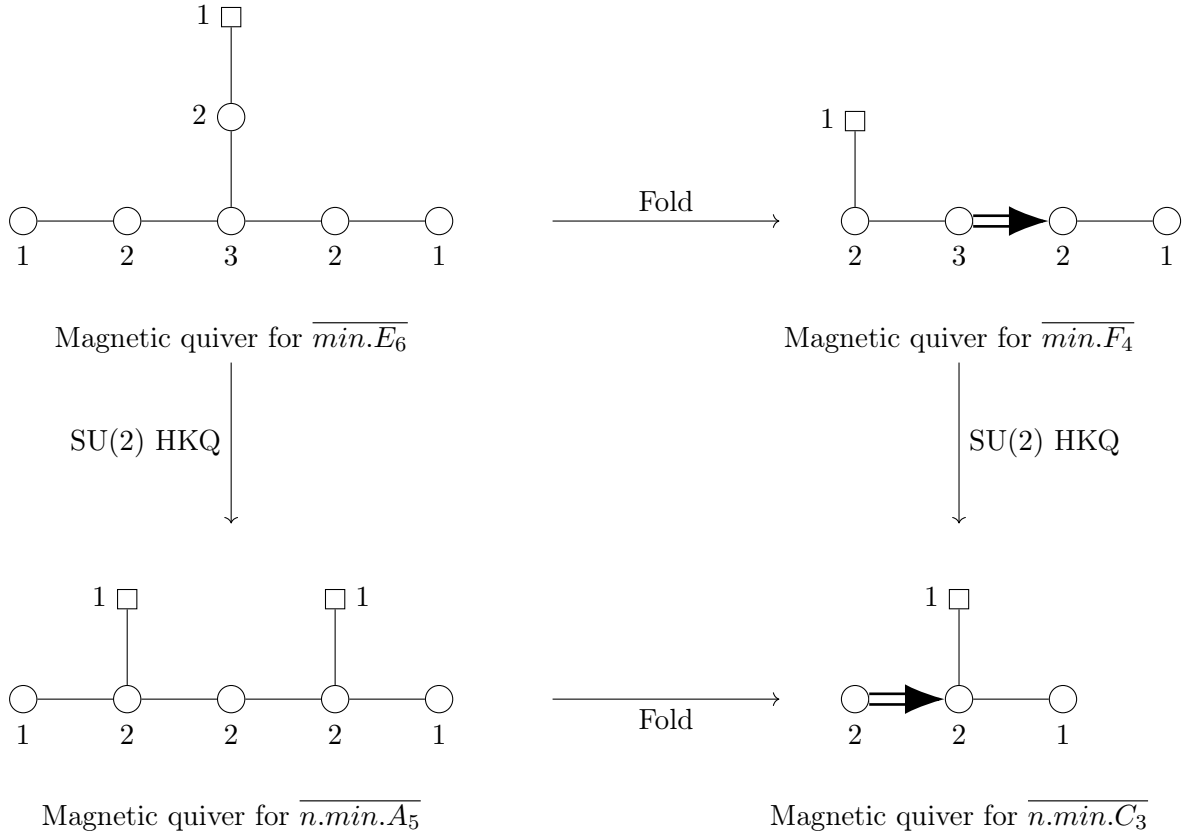


Figure 62: Commutative diagram showing folding and $SU(2)$ HKQ by quotient quiver subtraction from a magnetic quiver for $\overline{\min.E_6}$ to obtain $\overline{n.min.C_3}$.

Commutativity of Folding with $SU(n)$ HKQ A commutative diagram of the folding and $SU(2)$ HKQ of a magnetic quiver for $\overline{\min.E_6}$ is shown in Figure 62, based on results from Table 2. Applying a \mathbb{Z}_2 folding to the magnetic quiver for $\overline{\min.E_6}$ gives a magnetic quiver for $\overline{\min.F_4}$, and a subsequent $SU(2)$ HKQ by quotient quiver subtraction gives a magnetic quiver for $\overline{n.min.C_3}$. If the quotient quiver subtraction is carried out first, a magnetic quiver for $\overline{n.min.A_5}$ is obtained, but subsequent folding once again yields the magnetic quiver for $\overline{n.min.C_3}$.

A second example, shown in Figure 63, is the commutation of folding and $SU(2)$ HKQ by quotient quiver subtraction on the magnetic quiver \mathcal{Q}_{28} for $\overline{\min.D_k}$ for $k \geq 5$. Recall that there are two possible alignments of the quotient quiver, resulting in the quivers \mathcal{Q}_{30a} and \mathcal{Q}_{30b} ; so we draw commuting diagrams for each alternative. In each case, an initial folding of the magnetic quiver \mathcal{Q}_{28} for $\overline{\min.D_k}$ gives \mathcal{Q}_{19} for $\overline{\min.B_{k-1}}$. The subsequent quotient quiver subtraction gives magnetic quivers \mathcal{Q}_{20a} and \mathcal{Q}_{20b} for $\overline{n.min.B_{k-3}}$ and $(\overline{\min.A_1} \otimes \overline{\min.B_{k-3}})$, respectively. The other way around is to perform the quotient quiver subtraction first, which gives the magnetic quivers \mathcal{Q}_{30a} and \mathcal{Q}_{30b} for $\overline{n.min.D_{k-2}}$ and $(\overline{\min.A_1} \otimes \overline{\min.D_{k-2}})$, respectively. The subsequent folding once again gives \mathcal{Q}_{20a} and \mathcal{Q}_{20b} .

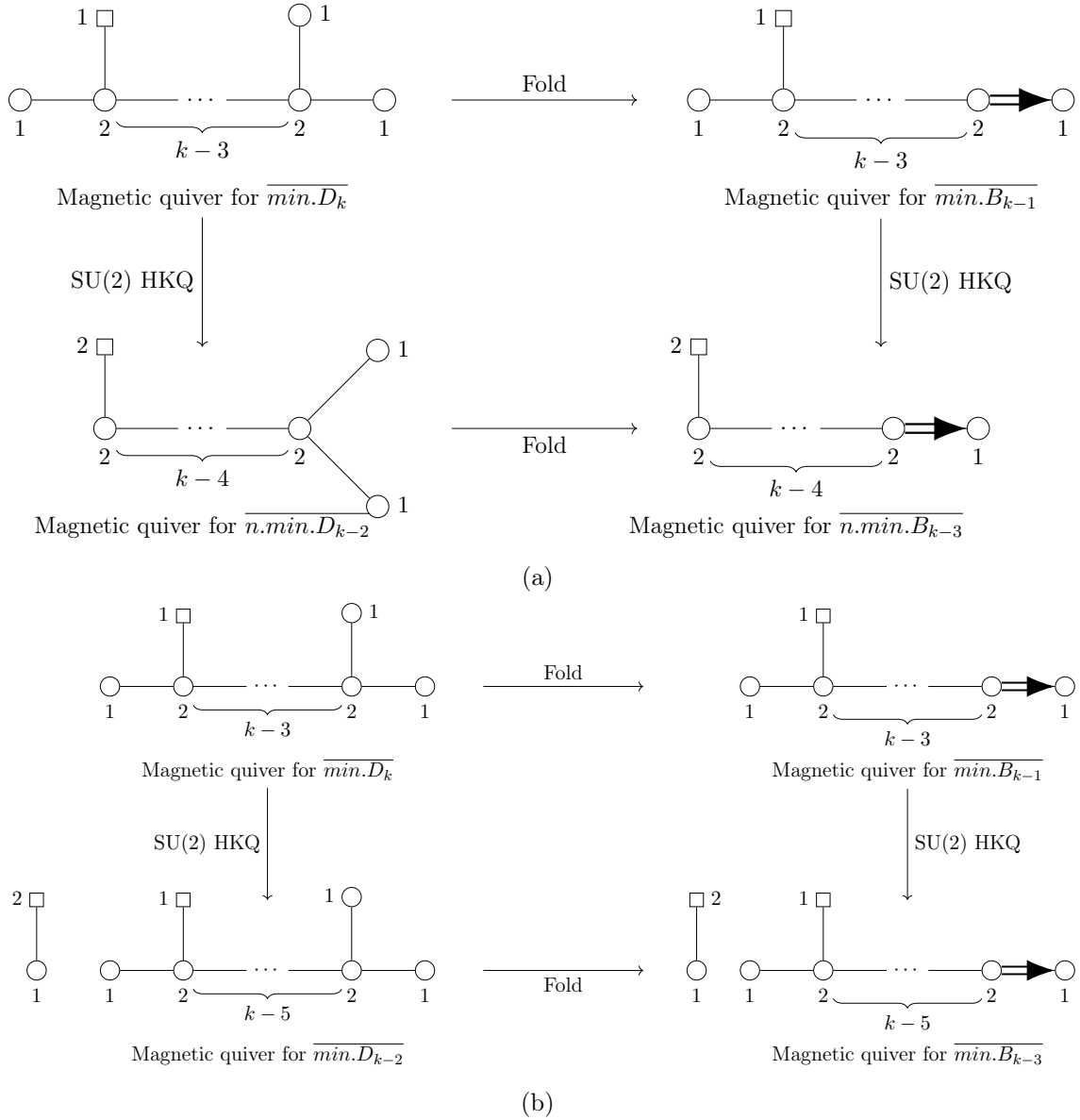


Figure 63: The quotient quiver subtraction from $\overline{\min.D_k}$ has two alignments. For each alignment we draw the commutative diagram of folding and SU(2) HKQ.

We note that the $\overline{\min.A_1}$ in \mathcal{Q}_{306} does not participate in the folding.

A more subtle example is provided by the folding and SU(2) HKQ by quotient quiver subtraction on the magnetic quiver for $\overline{n.min.D_k}$ shown in Figure 64. In this case, the initial folding is accompanied by a transformation to an alternative quiver for $\overline{n.min.B_{k-1}}$, as discussed in Section 5.1.2. The consistency of the operation marked Fold** in Figure 64a has been confirmed by analysis of the HWGs of the two magnetic quivers involved. (There is an identification of highest weight fugacities in the respective HWGs that indicates an operation on the Coulomb branch similar to folding.) However, we do not yet have a full understanding of the Fold** diagrammatic transformation.

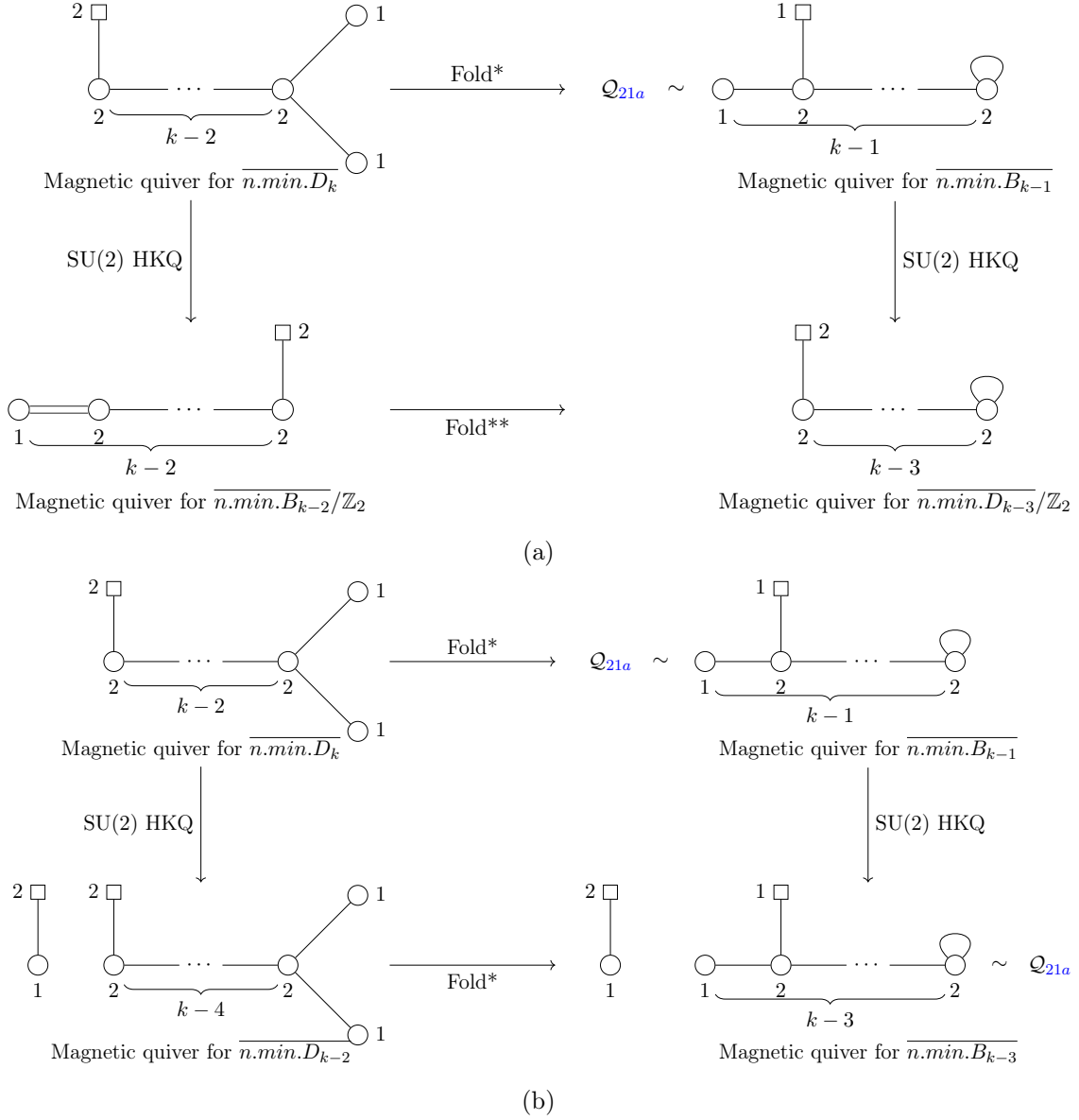


Figure 64: The $SU(2)$ quiver subtraction from $\overline{n.min.D_k}$ has two alignments. For each alignment we draw the commutative diagram of folding and $SU(2)$ HKQ. The folding operation is accompanied by a quiver loop transformation, denoted $*$ or $**$, as discussed in the text.

The fact that folding and quotient quiver subtraction often commute is not surprising. The folding of legs introduces a non-simply laced edge, with the folded nodes becoming short roots. Any subsequent quotient quiver subtraction is always taken by subtraction from the long roots and so is independent of those roots that have participated in the folding.

It should be noted that a similar commutative diagram of folding and $U(2)$ quotient quiver subtraction may be drawn for the magnetic quivers for the moduli space of free fields

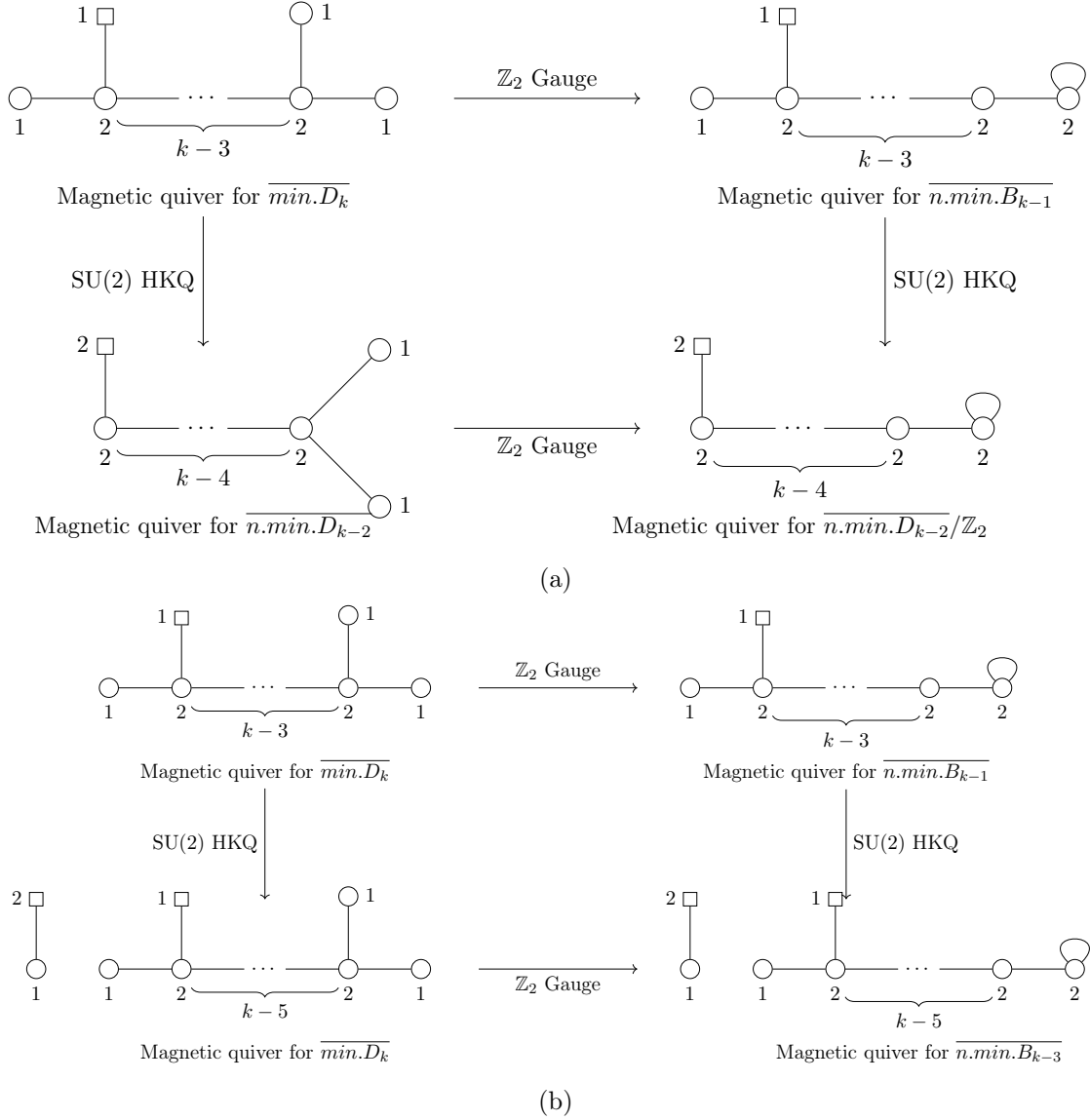


Figure 65: The $SU(2)$ quiver subtraction from $\overline{min.D_k}$ has two alignments. For each alignment we draw the commutative diagram between \mathbb{Z}_2 gauging and $SU(2)$ HKQ.

\mathcal{Q}_6 \mathcal{Q}_6 , which take the form of finite Dynkin diagrams of type D and B respectively.

Commutativity of Discrete Quotients with $SU(n)$ HKQ A similar approach can be applied to explore the commutation between discrete gauging and $SU(n)$ HKQs. Discrete gauging and quotient quiver subtraction often commute because the nodes that are discretely gauged cannot subsequently be involved in quiver subtraction and vice versa.

Consider the example in Figure 65. The magnetic quiver \mathcal{Q}_{28} for $\overline{min.D_k}$ for $k \geq 4$ contains a bouquet of two $U(1)$ gauge nodes that can be discretely gauged to give a gauge node of rank 2 with an adjoint link. This implements the Kostant-Brylinski relation $\overline{min.D_k}/\mathbb{Z}_2 = \overline{n.min.B_{k-1}}$ [64] in a diagrammatic way, and gives a magnetic quiver \mathcal{Q}_{216}

for $\overline{n.min.B_{k-1}}$. Its $SU(2)$ HKQ can be computed using quiver subtraction to yield two magnetic quivers \mathcal{Q}_{20a} and \mathcal{Q}_{20b} , whose union is $\overline{n.min.D_{k-3}/\mathbb{Z}_2} \cup \overline{min.A_1} \otimes \overline{n.min.B_{k-3}}$. Alternatively, performing the $SU(2)$ quiver subtraction first, we find the magnetic quivers \mathcal{Q}_{30a} and \mathcal{Q}_{30b} , whose union gives $\overline{n.min.D_{k-2}} \cup \overline{min.A_1} \otimes \overline{min.D_{k-2}}$. The subsequent discrete gauging of the bouquet of rank 1 nodes in these quivers once again produces \mathcal{Q}_{20a} and \mathcal{Q}_{20b} .

Here, the discrete gauging does not affect the $\overline{min.A_1}$ part of the moduli space.

It should be noted that a similar commutative diagram of discrete gauging by \mathbb{Z}_2 and $U(2)$ quotient quiver subtraction may be drawn for the magnetic quivers for the moduli space of free fields \mathcal{Q}_6 \mathcal{Q}_6 , which take the form of finite Dynkin diagrams of type D and B respectively.

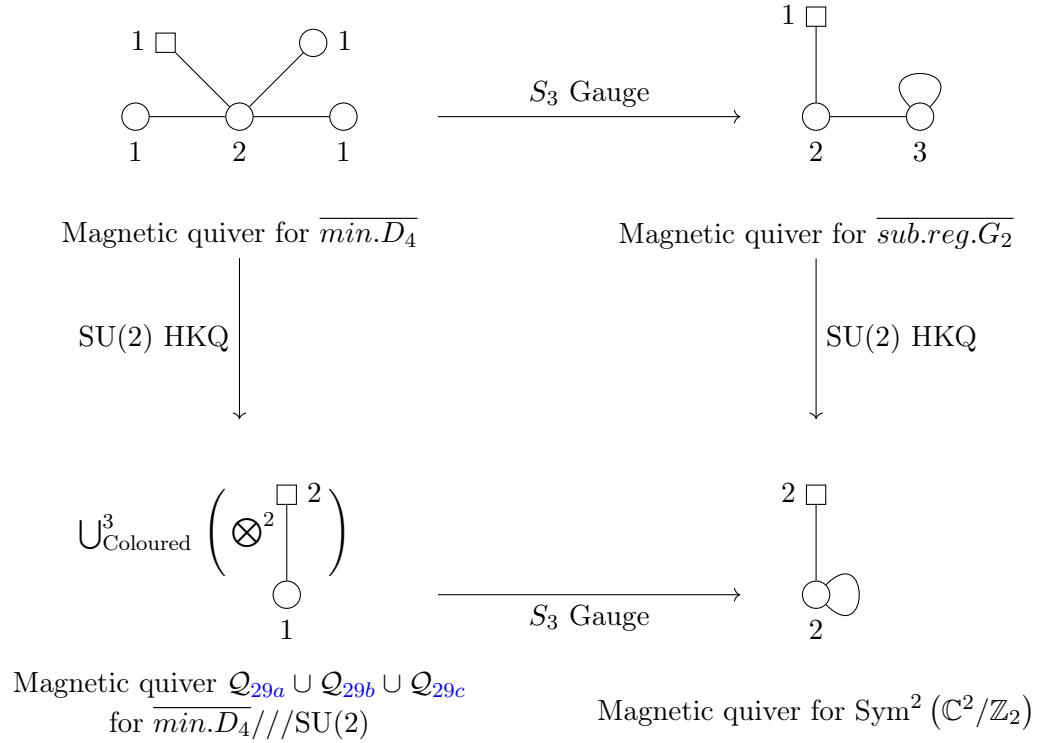


Figure 66: Commutative diagram showing S_3 discrete gauging and $SU(2)$ HKQ by quotient quiver subtraction from a magnetic quiver for $\overline{min.D_4}$ to obtain $\text{Sym}^2(\mathbb{C}^2/\mathbb{Z}_2)$.

A further non-trivial example is the commutativity of $SU(2)$ HKQ and S_3 gauging of $\overline{min.D_4}$ shown in Figure 66. If the S_3 gauging is performed on a magnetic quiver \mathcal{Q}_{29} for $\overline{min.D_4}$ a magnetic quiver for $\overline{sub.reg.G_2}$ is obtained. The quotient quiver subtraction then gives a magnetic quiver for $\text{Sym}^2(\mathbb{C}^2/\mathbb{Z}_2)$. Alternatively, carrying out the $SU(2)$ HKQ of $\overline{min.D_4}$ first, we find the union of coloured $\overline{min.A_1} \otimes \overline{min.A_1}$, as described in Section 7.1. Performing the S_3 gauging then recovers $\text{Sym}^2(\mathbb{C}^2/\mathbb{Z}_2)$.

There is no simple bouquet of $U(1)$ gauge nodes in this last step, so it is difficult to see this S_3 quotient diagrammatically. We can however check by comparing the volumes of the Coulomb branches. We do this by taking the ratio of unrefined HS in the limit $t \rightarrow 1$,

to find:

$$\frac{\text{Vol}(\overline{\text{min.}D_4}/\text{SU}(2))}{\text{Vol}(\text{Sym}^2(\mathbb{C}^2/\mathbb{Z}_2))} = \lim_{t \rightarrow 1} \frac{(1+t^2)^2(1+5t^2+12t^4-7t^6+t^8)}{1+t^2+4t^4+t^6+t^8} = 6, \quad (11.1)$$

and since $|S_3| = 6$, this is consistent with an S_3 gauging.

Moreover, we can explicitly recover the S_3 quotient using the Burnside lemma [51]. The HS of $\overline{\text{min.}D_4}/\text{SU}(2)$ can be mapped to $\text{SU}(2)$ as $[2; 0; 0]_{A_1 \times A_1 \times A_1} + [0; 2; 0]_{A_1 \times A_1 \times A_1} + [0; 0; 2]_{A_1 \times A_1 \times A_1} \rightarrow 3[2]_{A_1}$. We find the HWG:

$$\text{HWG}[\overline{\text{min.}D_4}/\text{SU}(2)]_{\rightarrow A_1} = (1 + \mu^2 t^2 + 2t^4 + 3\mu^2 t^4 + \mu^4 t^4 - \mu^2 t^6 - \mu^4 t^8) \text{PE}[2\mu^2 t^2 + t^4], \quad (11.2)$$

where μ is an $\text{SU}(2)$ highest weight fugacity. We now use the symbols $\mathbf{1}$, ε , and $\mathbf{2}$ to refer to the trivial, alternating, and fundamental representations of S_3 respectively, choose the following assignment of irreps, and perform the group average to find:

$$\begin{aligned} & (\mathbf{1}1 + \mathbf{1}\mu^2 t^2 + \mathbf{2}t^4 + \mathbf{2}\mu^2 t^4 + \varepsilon\mu^2 t^4 + \mathbf{1}\mu^4 t^4 - \mathbf{1}\mu^2 t^6 - \mathbf{1}\mu^4 t^8) \text{PE}[2\mu^2 t^2 + \mathbf{1}t^4] \\ & \rightarrow \text{PE}[\mu^2 t^2 + (\mu^4 + 1)t^4 + \mu^4 t^6 - \mu^8 t^{12}]. \end{aligned} \quad (11.3)$$

The result is the HWG for $\text{Sym}^2(\mathbb{C}^2/\mathbb{Z}_2)$, which confirms the construction.

Based on such examples, including the star-shaped quivers of $\text{SU}(2)^n$ studied in Section 10, we conjecture that $\text{SU}(2)$ HKQ and $S_{k < n}$ discrete gauging are commuting operations for quivers with bouquets of $\text{SU}(2)^n$.

One particular example of a star-shaped quiver of $\text{SU}(2)^n$ that we have studied throughout this work is for $n = 4$. This has an enhancement of the global symmetry of its Coulomb branch from $\text{SU}(2)^4 \rightarrow \text{SO}(8)$, giving a magnetic quiver for $\overline{\text{min.}D_4}$. This quiver admits two obvious discrete gauging actions of $S_2 \simeq \mathbb{Z}_2$, and S_3 , which give magnetic quivers for $\overline{n.\text{min.}B_3}$ and $\overline{\text{sub.reg.}G_2}$, respectively. These actions form part of commutative diagrams, as shown in Figure 65 (specialised to the case of $\overline{\text{min.}D_4}$) and Figure 66. There is also a discrete gauging of $\overline{n.\text{min.}B_3}/\mathbb{Z}_3 = \overline{\text{sub.reg.}G_2}$ (another Kostant-Brylinski relation) [64] which also commutes with quotient quiver subtraction. All of these results can be collected into a larger commutative diagram as shown in Figure 67.

In general, we conjecture that if two magnetic quivers are related by a discrete action, and both quivers are amenable to quotient quiver subtraction, then we expect that the quivers resulting from the HKQ are also related through the same discrete action ⁵.

SU(n) HKQs of Exceptional Affine Grassmannian Slices Further non-trivial tests of $\text{SU}(n)$ HKQs by quotient quiver subtraction are provided by target quivers which are magnetic quivers for affine Grassmannian slices of exceptional algebras.

Summaries of some of the examples computed in Section 9 are shown in Tables 5 and 6. The relationships between different affine Grassmannian slices are particularly interesting, especially when a union of affine Grassmannian slices emerges under HKQ. The quotient quiver subtraction on viable magnetic target quivers may allow one to move between affine Grassmannian slices of different algebras.

⁵As we have seen in Figure 64, this discrete action may not be obvious diagrammatically and, in such circumstances, this conjecture may assist in its identification.

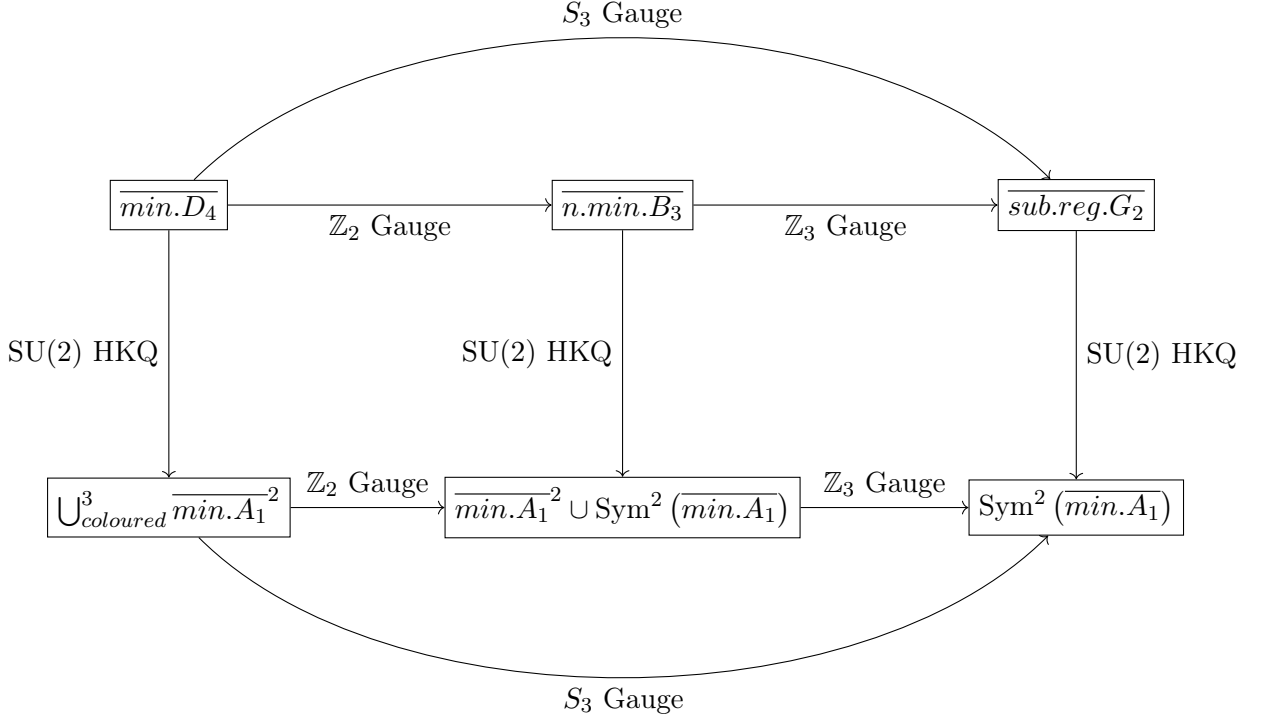


Figure 67: Commutative diagram of the discrete gauging relationships between $\overline{min.D_4}$, $\overline{n.min.B_3}$, and $\overline{sub.reg.G_2}$ and their SU(2) HKQ.

Target Moduli Space	SU(2) HKQ
$\overline{[W_{E_6}]}$ $\begin{bmatrix} 0,0,1,0,0,0 \\ 0,0,0,0,0,1 \end{bmatrix}$	$\overline{[W_{D_5}]}$ $\begin{bmatrix} 0,1,0,1,1 \\ 0,0,0,1,1 \end{bmatrix}$
$\overline{[W_{E_6}]}$ $\begin{bmatrix} 1,0,0,1,0,0 \\ 0,2,0,0,0,0 \end{bmatrix}$	$\overline{[W_{A_4}]}$ $\begin{bmatrix} 1,0,2,0 \\ 0,1,0,0 \end{bmatrix} \cup \overline{[W_{A_5}]}$ $\begin{bmatrix} 2,0,1,0,1 \\ 1,0,1,0,0 \end{bmatrix}$
$\overline{[W_{E_7}]}$ $\begin{bmatrix} 0,0,0,1,0,0,0 \\ 0,0,0,0,0,0,1 \end{bmatrix}$	$\overline{[W_{E_6}]}$ $\begin{bmatrix} 1,0,1,0,0,0 \\ 1,0,0,0,0,1 \end{bmatrix}$

Table 5: Exceptional affine Grassmannian slices and their SU(2) HKQs.

Target Moduli Space	SU(3) HKQ
$\overline{[W_{E_7}]}$ $\begin{bmatrix} 0,1,0,0,0,0,0 \\ 1,0,0,0,0,0,0 \end{bmatrix}$	$\overline{[W_{D_5}]}$ $\begin{bmatrix} 0,0,2,0,0 \\ 0,0,0,1,1 \end{bmatrix} \cup \overline{[W_{D_5}]}$ $\begin{bmatrix} 2,0,0,1,1 \\ 2,0,0,1,1 \end{bmatrix}$

Table 6: Exceptional affine Grassmannian slices and their SU(3) HKQs.

U(n) HKQ of Dynkin type Although not the focus of our study, the possibility of combining SU(n) and U(1) HKQs into a U(n) HKQ merits some comment. Often there are many ways of taking a U(1) HKQ from a unitary magnetic quiver, while the SU(n) HKQ is limited by the selection rules 2. However, in the natural case, where the embedding of U(n) follows from a Dynkin embedding into an external leg of form (1) – ... – (n) – ..., then the magnetic quiver for the U(n) HKQ can be conjectured to follow as a simple extension of the SU(n) HKQ rules herein, by omitting the step of unframing prior to the quotient quiver subtraction. This is illustrated in the examples in Appendix B, wherein care needs

to be taken regarding application of the Junction Rule to avoid HKQs where incomplete Higgsing arises.

Open problems Our method of quotient quiver subtraction imposes selection rules on the types of magnetic quiver to which it can be applied. Further work could provide diagrammatic techniques for the HKQs of the Coulomb branches of quivers that lie outside these rules.

In particular, quotient quiver subtraction requires a Dynkin type embedding of $SU(n)$ into the global symmetry of the Coulomb branch in accordance with the External Leg rule. However, there may be other embeddings of $SU(n)$ into the global symmetry G of the magnetic quiver. Is it possible to find rules that diagrammatically produce $SU(n)$ HKQs for such different embeddings?

We have explored $SU(n)$ HKQs. Are there diagrammatic techniques for HKQs by other classical groups?

We have only considered unitary magnetic quivers. Can similar diagrammatic techniques be developed for orthosymplectic quivers?

Although we have seen how to perform $SU(n)$ HKQs at the level of the quiver, these quotient quiver subtractions remain to be interpreted in the context of brane systems.

Acknowledgments

We would like to thank Julius Grimminger, Tudor Dimofte, Travis Schedler, and Marcus Sperling for discussions. The work of AH, RK, and GK is partially supported by STFC grant ST/T000791/1. The work of GK is supported by STFC DTP research studentship grant ST/X508433/1.

A $U(1)$ HKQs

Here we review the $U(1)$ and $U(1)^2$ HKQ of nilpotent orbits with a Dynkin type embedding given in Kobak-Swann [65].

The diagrammatic technique of quiver subtraction for $U(1)$ HKQ differs subtly from the diagrammatic method of non-abelian $SU(n)$ quotient quiver subtraction presented in Section 2. The $U(1)$ HKQ involves the subtraction of the quiver (1), which is the first member of the sequence of quotient quivers we use for $SU(n)$. The difference lies in that $U(1)$ gauging does not require the initial step of transforming the framed target quiver into an unframed quiver. Otherwise the subtraction procedure is similar, albeit simpler, because alternatives do not arise at junctions.

In fact, it is already known in the Literature that the gauging of a $U(1)$ can be done diagrammatically by taking a framed magnetic quiver and turning a $U(1)$ gauge node into a flavour node [73]. A selection of examples taken from Kobak-Swann are shown with target and resulting magnetic quivers in Table 7. This diagrammatic procedure for the $U(1)$ HKQ is obvious from the quivers.

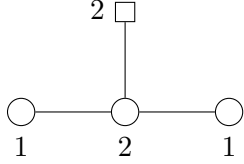
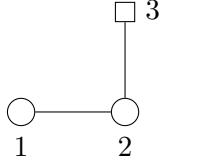
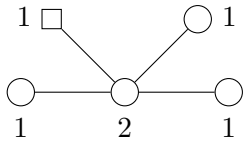
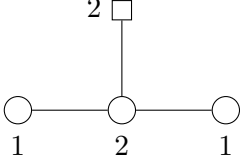
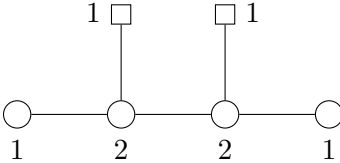
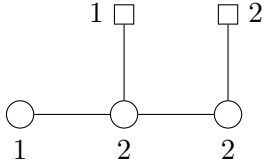
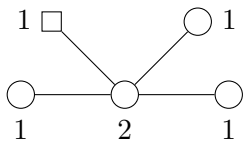
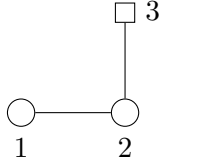
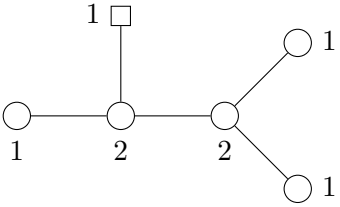
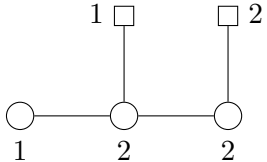
Target Orbit	Resulting Orbit	Target Quiver	Resulting Quiver	HKQ
$\overline{\mathcal{O}}_{(2^2)}^{A_3}$	$\overline{\mathcal{O}}_{(3)}^{A_2}$			U(1)
$\overline{\mathcal{O}}_{(2^2,1^4)}^{D_4}$	$\overline{\mathcal{O}}_{(2^2)}^{A_3}$			U(1)
$\overline{\mathcal{O}}_{(2^2,1)}^{A_4}$	$\overline{\mathcal{O}}_{(3,1)}^{A_3}$			U(1)
$\overline{\mathcal{O}}_{(2^2,1^4)}^{D_4}$	$\overline{\mathcal{O}}_{(3)}^{A_2}$			U(1) × U(1)
$\overline{\mathcal{O}}_{(2^2,1^6)}^{D_5}$	$\overline{\mathcal{O}}_{(3,1)}^{A_3}$			U(1) × U(1)

Table 7: Selection of U(1) and U(1)² HKQs of classical orbits with their magnetic quivers taken from Kobak-Swann [65].

B U(n) HKQ Examples

Given the diagrammatic method of performing a U(1) HKQ in Appendix A, and noting the isomorphism $U(n) \simeq SU(n) \times U(1)$, we can ask if a U(n) HKQ can be carried out diagrammatically. Complications can arise because the diagrammatic quotient quiver subtractions required by U(1) and SU(n) HKQs do not necessarily commute.

However, for cases where the target quiver possesses an appropriate external leg with U(n) symmetry, it is possible to combine the two HKQs into a single well-defined operation, as shown in the following examples.

B.1 U(n) HKQ of $\overline{max.A_k}$, $k \geq 3$

For a straightforward example of U(n) HKQ we will take the family of $\overline{max.A_k}$ orbits. The first step is the SU(n) quotient quiver subtraction which is valid for $n \leq (k+1)/2$ with the value of $n = (k+1)/2$ saturating the inequality being a special case. First for the

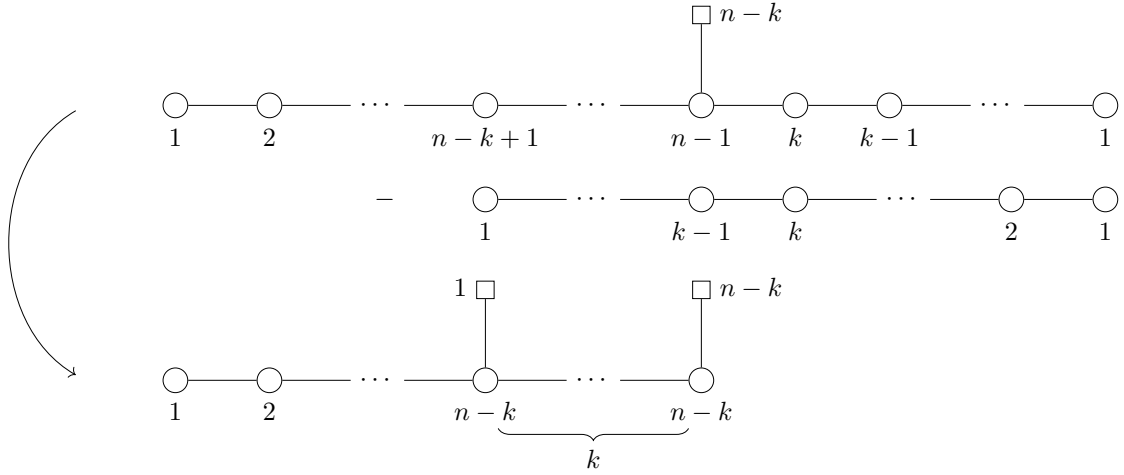


Figure 68: Quiver subtraction of the $U(k)$ quotient quiver from the magnetic quiver for $\overline{[\mathcal{W}_{A_{n+k-1}}]_{[0, \dots, 0, n-k, 0, 0, \dots, 0]}}$ to produce the magnetic quiver for $\overline{\mathcal{O}_{(n-k+1, 1^{k-1})}^{A_{n-1}}}$.

It appears that the solution in [55] for avoiding incomplete Higgsing involves making a particular choice around the breaking of the $U(k)$ gauge group, such that the HKQ implemented diagrammatically is no longer strictly that of $U(k)$.

C Violation of the Junction Rule

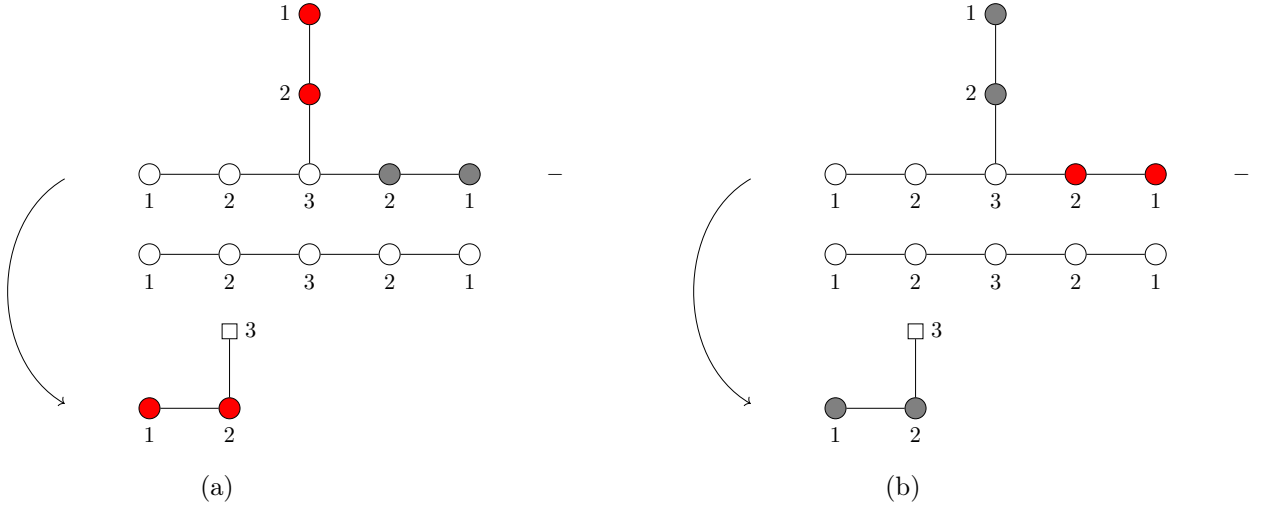


Figure 69: Both (incorrect) alignments of the $SU(3)$ quotient quiver against the unitary unframed magnetic quiver for $\overline{min.E_6}$ to give quivers \mathcal{Q}_{69a} and \mathcal{Q}_{69b} . Their intersection is trivial.

Here we give an example of the incorrect application of quiver subtraction for $SU(n)$ HKQ by explicitly breaking the [Junction Rule](#).

For our example we will take the magnetic quiver for $\overline{\min.E_6}$ and try and take the SU(3) HKQ using quotient quiver subtraction. We ignore the [Junction Rule](#) and permit the junction for the alignment of the SU(3) quotient quiver and target quiver to be located at the central node of rank 3 of the quotient quiver instead of a node of rank 2. There are two alignments of the SU(3) quotient quiver and these are related by an outer automorphism, thus we use colours for each leg of the target quiver to distinguish them. This procedure gives quivers \mathcal{Q}_{69a} and \mathcal{Q}_{69b} whose Coulomb branch is $\overline{\max.A_2}$. The incorrect application of the rules of quiver subtraction leads us to believe

$$\overline{\min.E_6} // \text{SU}(3) \stackrel{?}{=} \overline{\max.A_2} \cup \overline{\max.A_2}. \quad (\text{C.1})$$

It is simple to compute the refined HS and HWG of the union (C.1) however, to show inconsistency between Weyl integration and ignorance of the [Junction Rule](#) only the unrefined HS will suffice. We find:

$$HS [\overline{\max.A_2} \cup \overline{\max.A_2}] = 2 \times \frac{1 + 2t^2 + 2t^4 + t^6}{(1 - t^2)^6} - 1 \quad (\text{C.2})$$

$$= \frac{1 + 10t^2 - 11t^4 + 22t^6 - 15t^8 + 6t^{10} - t^{12}}{(1 - t^2)^6} \quad (\text{C.3})$$

There is an embedding of $A_2 \times A_2 \times A_2$ into E_6 which decomposes the fundamental as $[0, 0, 0, 0, 0, 1]_{E_6} \rightarrow [1, 0; 0, 0; 1, 0]_{A_2 \times A_2 \times A_2} + [0, 0; 1, 0; 0, 1]_{A_2 \times A_2 \times A_2} + [0, 1; 0, 1; 0, 0]_{A_2 \times A_2 \times A_2}$. (C.4)

This embedding is also a Dynkin type embedding. After applying this embedding, Weyl integration can be used to compute the SU(3) HKQ of $\overline{\min.E_6}$ whose HS we find to be

$$HS [\overline{\min.E_6} // \text{SU}(3)] = \frac{1 + 9t^2 + 43t^4 + 81t^6 + 20t^8 - 89t^{10} + 53t^{12} - 11t^{14} + t^{16}}{(1 - t^2)^7}, \quad (\text{C.5})$$

where the quaternionic dimension of the moduli space is 3.5, indicating that incomplete Higgsing has occurred. This does not match the prediction from quotient quiver subtraction if we fail to apply the [Junction Rule](#). We find that the application of the [Junction Rule](#) is necessary to avoid such mismatches that result from incomplete Higgsing.

D Violation of the External Leg Rule

The [External Leg Rule](#) requires that the SU(n) quotient quiver must be subtracted from nodes of the target quiver corresponding to long roots. Here we give an example where this rule is ignored.

We will attempt to subtract the SU(2) quotient quiver from the family of $\overline{n.\min.C_k}$ quivers. In order to prevent violation of the [Single Edge Rule](#) we require $k \geq 4$. The "subtraction" is shown in Figure 70 and produces quivers \mathcal{Q}_{70a} and \mathcal{Q}_{70b} . The respective Coulomb branches are identified as $\overline{n.\min.C_{k-2}}$ and $\overline{\min.C_{k-2}} \otimes \overline{\min.A_1}$. So we are lead to conjecture that:

$$\overline{\min.C_k} // \text{SU}(2) \stackrel{?}{=} \overline{n.\min.C_{k-2}} \cup \overline{\min.C_{k-2}} \otimes \overline{\min.A_1}, \quad (\text{D.1})$$

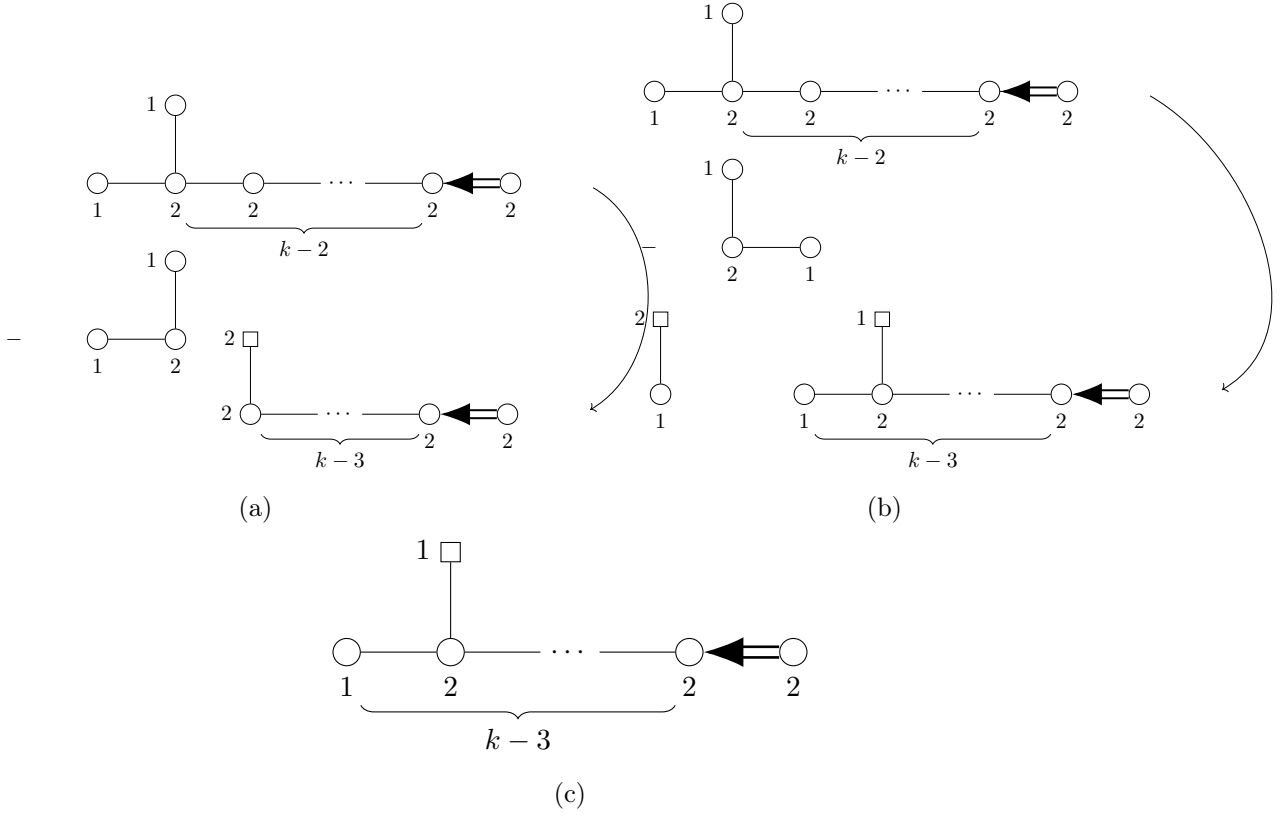


Figure 70: Both alignments of the $SU(2)$ quotient quiver against the magnetic quiver for $\overline{min.C_k}$ for $k \geq 4$ giving quivers \mathcal{Q}_{70a} and \mathcal{Q}_{70b} . Their intersection, reached via A_1 KP transitions, is quiver \mathcal{Q}_{70c} .

where the global symmetry of the union (D.1) is $Sp(k-2) \times SU(2)$.

Although it is straightforward to compute the refined HS and HWG of the union (D.1) for particular values of $k \geq 4$, calculation of the unrefined HS will suffice to demonstrate the inconsistency with Weyl integration that arises if the [External Leg Rule](#) is ignored. We present the calculation using Weyl integration and quiver subtraction for the case $k = 5$, however, we have also computed up to $k = 6$.

We find from quiver subtraction that:

$$\begin{aligned}
& HS \left[\overline{n.min.C_3} \cup \overline{min.C_3} \otimes \overline{min.A_1} \right] \\
&= \frac{\left(1 + 15t^2 + 135t^4 + 625t^6 + 1725t^8 + 3048t^{10} + 3686t^{12} \right. \\
&\quad \left. + 3048t^{14} + 1725t^{16} + 625t^{18} + 135t^{20} + 15t^{22} + t^{24} \right)}{(1-t^2)^{12}(1+t^2)^6} \\
&+ \frac{(1-t^4)}{(1-t^2)^3} \frac{(1+t^2)(1+10t^2+41t^4+10t^6+t^8)}{(1-t^2)^{10}} \\
&- \frac{(1+t^2)(1+10t^2+41t^4+10t^6+t^8)}{(1-t^2)^{10}} \tag{D.2}
\end{aligned}$$

$$\begin{aligned}
&= \frac{\left(1 + 18t^2 + 185t^4 + 1004t^6 + 3219t^8 + 6457t^{10} + 8438t^{12} \right. \\
&\quad \left. + 7094t^{14} + 3653t^{16} + 934t^{18} - 11t^{20} - 66t^{22} - 13t^{24} - t^{26} \right)}{(1-t^2)^{12}(1+t^2)^6} \tag{D.3}
\end{aligned}$$

There is a Dynkin type embedding of $C_k \leftrightarrow C_{k-1} \times A_1$ which branches the vector of C_k as:

$$[1, 0, \dots, 0]_{C_k} \rightarrow [1, 0 \dots, 0]_{C_{k-1}} + [1]_{A_1}. \tag{D.4}$$

If the embedding (D.4) is chosen for Weyl integration then the expected global symmetries do not match as Weyl integration would give a result with $\text{Sp}(k-1)$ global symmetry as opposed to the union (D.1). A second problem is that this embedding gives incomplete Higgsing as seen from the HS:

$$HS \left[\overline{n.min.C_5} // \text{SU}(2) \right] = \frac{(1+t^2)(1+22t^2+253t^4+812t^6+1058t^8+392t^{10}+36t^{12})}{(1-t^2)^{13}}. \tag{D.5}$$

This is clearly in disagreement with (D.1) which was obtained using $\text{SU}(2)$ quotient quiver subtraction but ignoring the [External Leg Rule](#). We find that the application of the [External Leg Rule](#) is necessary to avoid such pathological results where incomplete Higgsing occurs.

References

- [1] S. Cabrera, A. Hanany, and M. Sperling, *Magnetic quivers, Higgs branches, and 6d $\mathcal{N}=(1,0)$ theories*, *JHEP* **06** (2019) 071, [[arXiv:1904.12293](#)]. [Erratum: *JHEP* 07, 137 (2019)].
- [2] A. Bourget, S. Cabrera, J. F. Grimminger, A. Hanany, M. Sperling, A. Zajac, and Z. Zhong, *The Higgs mechanism — Hasse diagrams for symplectic singularities*, *JHEP* **01** (2020) 157, [[arXiv:1908.04245](#)].
- [3] A. Bourget, S. Cabrera, J. F. Grimminger, A. Hanany, and Z. Zhong, *Brane Webs and Magnetic Quivers for SQCD*, *JHEP* **03** (2020) 176, [[arXiv:1909.00667](#)].
- [4] S. Cabrera, A. Hanany, and M. Sperling, *Magnetic quivers, Higgs branches, and 6d $\mathcal{N}=(1,0)$ theories — orthogonal and symplectic gauge groups*, *JHEP* **02** (2020) 184, [[arXiv:1912.02773](#)].

- [5] J. F. Grimminger and A. Hanany, *Hasse diagrams for 3d $\mathcal{N} = 4$ quiver gauge theories — Inversion and the full moduli space*, *JHEP* **09** (2020) 159, [[arXiv:2004.01675](#)].
- [6] A. Bourget, J. F. Grimminger, A. Hanany, M. Sperling, and Z. Zhong, *Magnetic Quivers from Brane Webs with O5 Planes*, *JHEP* **07** (2020) 204, [[arXiv:2004.04082](#)].
- [7] A. Bourget, J. F. Grimminger, A. Hanany, M. Sperling, G. Zafrir, and Z. Zhong, *Magnetic quivers for rank 1 theories*, *JHEP* **09** (2020) 189, [[arXiv:2006.16994](#)].
- [8] A. Bourget, J. F. Grimminger, A. Hanany, R. Kalveks, M. Sperling, and Z. Zhong, *Magnetic Lattices for Orthosymplectic Quivers*, *JHEP* **12** (2020) 092, [[arXiv:2007.04667](#)].
- [9] E. Beratto, S. Giacomelli, N. Mekareeya, and M. Sacchi, *3d mirrors of the circle reduction of twisted A_{2N} theories of class S*, *JHEP* **09** (2020) 161, [[arXiv:2007.05019](#)].
- [10] C. Closset, S. Schafer-Nameki, and Y.-N. Wang, *Coulomb and Higgs Branches from Canonical Singularities: Part 0*, *JHEP* **02** (2021) 003, [[arXiv:2007.15600](#)].
- [11] M. Akhond, F. Carta, S. Dwivedi, H. Hayashi, S.-S. Kim, and F. Yagi, *Five-brane webs, Higgs branches and unitary/orthosymplectic magnetic quivers*, *JHEP* **12** (2020) 164, [[arXiv:2008.01027](#)].
- [12] M. van Beest, A. Bourget, J. Eckhard, and S. Schafer-Nameki, *(Symplectic) Leaves and (5d Higgs) Branches in the Poly(go)nesian Tropical Rain Forest*, *JHEP* **11** (2020) 124, [[arXiv:2008.05577](#)].
- [13] A. Bourget, S. Giacomelli, J. F. Grimminger, A. Hanany, M. Sperling, and Z. Zhong, *S-fold magnetic quivers*, *JHEP* **02** (2021) 054, [[arXiv:2010.05889](#)].
- [14] M. Van Beest, A. Bourget, J. Eckhard, and S. Schäfer-Nameki, *(5d RG-flow) Trees in the Tropical Rain Forest*, *JHEP* **03** (2021) 241, [[arXiv:2011.07033](#)].
- [15] S. Giacomelli, N. Mekareeya, and M. Sacchi, *New aspects of Argyres–Douglas theories and their dimensional reduction*, *JHEP* **03** (2021) 242, [[arXiv:2012.12852](#)].
- [16] M. Akhond, F. Carta, S. Dwivedi, H. Hayashi, S.-S. Kim, and F. Yagi, *Factorised 3d $\mathcal{N} = 4$ orthosymplectic quivers*, *JHEP* **05** (2021) 269, [[arXiv:2101.12235](#)].
- [17] F. Carta, S. Giacomelli, N. Mekareeya, and A. Mininno, *Conformal manifolds and 3d mirrors of Argyres–Douglas theories*, *JHEP* **08** (2021) 015, [[arXiv:2105.08064](#)].
- [18] G. Arias-Tamargo, A. Bourget, and A. Pini, *Discrete gauging and Hasse diagrams*, *SciPost Phys.* **11** (2021), no. 2 026, [[arXiv:2105.08755](#)].
- [19] A. Bourget, J. F. Grimminger, A. Hanany, R. Kalveks, M. Sperling, and Z. Zhong, *Folding orthosymplectic quivers*, *JHEP* **12** (2021) 070, [[arXiv:2107.00754](#)].
- [20] K. Gledhill and A. Hanany, *Coulomb branch global symmetry and quiver addition*, *JHEP* **12** (2021) 127, [[arXiv:2109.07237](#)].
- [21] M. van Beest and S. Giacomelli, *Connecting 5d Higgs branches via Fayet-Iliopoulos deformations*, *JHEP* **12** (2021) 202, [[arXiv:2110.02872](#)].
- [22] F. Carta, S. Giacomelli, N. Mekareeya, and A. Mininno, *Conformal manifolds and 3d mirrors of (D_n, D_m) theories*, *JHEP* **02** (2022) 014, [[arXiv:2110.06940](#)].
- [23] M. Sperling and Z. Zhong, *Balanced B and D-type orthosymplectic quivers — magnetic quivers for product theories*, *JHEP* **04** (2022) 145, [[arXiv:2111.00026](#)].

- [24] S. Nawata, M. Sperling, H. E. Wang, and Z. Zhong, *Magnetic quivers and line defects — On a duality between 3d $\mathcal{N} = 4$ unitary and orthosymplectic quivers*, *JHEP* **02** (2022) 174, [[arXiv:2111.02831](#)].
- [25] M. Akhond, F. Carta, S. Dwivedi, H. Hayashi, S.-S. Kim, and F. Yagi, *Exploring the orthosymplectic zoo*, *JHEP* **05** (2022) 054, [[arXiv:2203.01951](#)].
- [26] S. Giacomelli, M. Moleti, and R. Savelli, *Probing 7-branes on orbifolds*, *JHEP* **08** (2022) 163, [[arXiv:2205.08578](#)].
- [27] M. J. Kang, C. Lawrie, K.-H. Lee, M. Sacchi, and J. Song, *Higgs branch, Coulomb branch, and Hall-Littlewood index*, *Phys. Rev. D* **106** (2022), no. 10 106021, [[arXiv:2207.05764](#)].
- [28] A. Hanany and M. Sperling, *Magnetic quivers and negatively charged branes*, *JHEP* **11** (2022) 010, [[arXiv:2208.07270](#)].
- [29] J. Gu, Y. Jiang, and M. Sperling, *Rational Q -systems, Higgsing and mirror symmetry*, *SciPost Phys.* **14** (2023), no. 3 034, [[arXiv:2208.10047](#)].
- [30] M. Fazzi and S. Giri, *Hierarchy of RG flows in 6d $(1, 0)$ orbi-instantons*, *JHEP* **12** (2022) 076, [[arXiv:2208.11703](#)].
- [31] A. Bourget and J. F. Grimminger, *Fibrations and Hasse diagrams for 6d SCFTs*, *JHEP* **12** (2022) 159, [[arXiv:2209.15016](#)].
- [32] K. Gledhill and A. Hanany, *Poisson brackets for some Coulomb branches*, *JHEP* **03** (2023) 154, [[arXiv:2210.02966](#)].
- [33] M. Fazzi, S. Giacomelli, and S. Giri, *Hierarchies of RG flows in 6d $(1, 0)$ massive E -strings*, *JHEP* **03** (2023) 089, [[arXiv:2212.14027](#)].
- [34] L. Bhardwaj, M. Bullimore, A. E. V. Ferrari, and S. Schafer-Nameki, *Generalized Symmetries and Anomalies of 3d $N=4$ SCFTs*, [[arXiv:2301.02249](#)].
- [35] A. Bourget, S. Giacomelli, and J. F. Grimminger, *FI-flows of 3d $N = 4$ Theories*, *JHEP* **04** (2023) 015, [[arXiv:2302.03698](#)].
- [36] A. Bourget, J. F. Grimminger, A. Hanany, R. Kalveks, M. Sperling, and Z. Zhong, *A Tale of N Cones*, [[arXiv:2303.16939](#)].
- [37] M. Del Zotto, M. Fazzi, and S. Giri, *A new vista on the heterotic moduli space from six and three dimensions*, *Phys. Rev. D* **109** (2024), no. 2 L021903, [[arXiv:2307.10356](#)].
- [38] M. Del Zotto, M. Fazzi, and S. Giri, *The Higgs branch of heterotic ALE instantons*, *JHEP* **01** (2024) 167, [[arXiv:2307.11087](#)].
- [39] A. Hanany, G. Kumaran, C. Li, D. Liu, and M. Sperling, *Actions on the quiver – Discrete quotients on the Coulomb branch*, [[arXiv:2311.02773](#)].
- [40] C. Lawrie and L. Mansi, *The Higgs Branch of Heterotic LSTs: Hasse Diagrams and Generalized Symmetries*, [[arXiv:2312.05306](#)].
- [41] A. Bourget, M. Sperling, and Z. Zhong, *Decay and Fission of Magnetic Quivers*, [[arXiv:2312.05304](#)].
- [42] S. Benvenuti, R. Comi, and S. Pasquetti, *Mirror dualities with four supercharges*, [[arXiv:2312.07667](#)].
- [43] L. Mansi and M. Sperling, *Unravelling T -Duality: Magnetic Quivers in Rank-zero Little String Theories*, [[arXiv:2312.12510](#)].

- [44] M. Fazzi, S. Giri, and P. Levy, *Proving the 6d a-theorem with the double affine Grassmannian*, [arXiv:2312.17178](#).
- [45] A. Bourget, M. Sperling, and Z. Zhong, *Higgs branch RG-flows via Decay and Fission*, [arXiv:2401.08757](#).
- [46] S. Cremonesi, A. Hanany, and A. Zaffaroni, *Monopole operators and Hilbert series of Coulomb branches of 3d $\mathcal{N} = 4$ gauge theories*, *JHEP* **01** (2014) 005, [[arXiv:1309.2657](#)].
- [47] A. Hanany and R. Kalveks, *Highest Weight Generating Functions for Hilbert Series*, *JHEP* **10** (2014) 152, [[arXiv:1408.4690](#)].
- [48] B. Feng, A. Hanany, and Y.-H. He, *Counting gauge invariants: The Plethystic program*, *JHEP* **03** (2007) 090, [[hep-th/0701063](#)].
- [49] A. Hanany and G. Zafrir, *Discrete Gauging in Six Dimensions*, *JHEP* **07** (2018) 168, [[arXiv:1804.08857](#)].
- [50] A. Hanany and A. Zajac, *Discrete Gauging in Coulomb branches of Three Dimensional $\mathcal{N} = 4$ Supersymmetric Gauge Theories*, *JHEP* **08** (2018) 158, [[arXiv:1807.03221](#)].
- [51] A. Bourget, A. Hanany, and D. Miketa, *Quiver origami: discrete gauging and folding*, *JHEP* **01** (2021) 086, [[arXiv:2005.05273](#)].
- [52] H. Kraft and C. Procesi, *On the geometry of conjugacy classes in classical groups*, *Commentarii Mathematici Helvetici* **57** (12, 1982) 539–602.
- [53] S. Cabrera and A. Hanany, *Branes and the Kraft-Procesi transition: classical case*, *JHEP* **04** (2018) 127, [[arXiv:1711.02378](#)].
- [54] S. Cabrera and A. Hanany, *Branes and the Kraft-Procesi Transition*, *JHEP* **11** (2016) 175, [[arXiv:1609.07798](#)].
- [55] A. Bourget, A. Dancer, J. F. Grimminger, A. Hanany, and Z. Zhong, *Partial implosions and quivers*, *JHEP* **07** (2022) 049, [[arXiv:2112.10825](#)].
- [56] S. Cremonesi, G. Ferlito, A. Hanany, and N. Mekareeya, *Coulomb Branch and The Moduli Space of Instantons*, *JHEP* **12** (2014) 103, [[arXiv:1408.6835](#)].
- [57] W. Burnside, *Theory of Groups of Finite Order*. Cambridge Library Collection - Mathematics. Cambridge University Press, 1897.
- [58] A. Hanany and R. Kalveks, *Quiver Theories for Moduli Spaces of Classical Group Nilpotent Orbits*, *JHEP* **06** (2016) 130, [[arXiv:1601.04020](#)].
- [59] A. Hanany and R. Kalveks, *Quiver Theories and Formulae for Nilpotent Orbits of Exceptional Algebras*, *JHEP* **11** (2017) 126, [[arXiv:1709.05818](#)].
- [60] Y. Namikawa, *A characterization of nilpotent orbit closures among symplectic singularities*, *arXiv e-prints* (Mar., 2016) arXiv:1603.06105, [[arXiv:1603.06105](#)].
- [61] D. Kaledin, *Symplectic singularities from the Poisson point of view*, *arXiv Mathematics e-prints* (Oct., 2003) math/0310186, [[math/0310186](#)].
- [62] H. Kraft and C. Procesi, *Minimal singularities in GL_n* , *Inventiones mathematicae* **62** (1980) 503–515.
- [63] D. I. Panyushev, *On spherical nilpotent orbits and beyond*, *Annales de l'institut Fourier* **49** (1999), no. 5 1453–1476.

- [64] R. Brylinski and B. Kostant, *Nilpotent orbits, normality, and Hamiltonian group actions*, *arXiv Mathematics e-prints* (Mar., 1992) math/9204227, [[math/9204227](#)].
- [65] P. Z. Kobak and A. Swann, *Classical nilpotent orbits as hyperkähler quotients*, *International Journal of Mathematics* **07** (1996) 193–210.
- [66] S. Cabrera and A. Hanany, *Quiver Subtractions*, *JHEP* **09** (2018) 008, [[arXiv:1803.11205](#)].
- [67] A. Hanany and E. Witten, *Type IIB superstrings, BPS monopoles, and three-dimensional gauge dynamics*, *Nucl. Phys. B* **492** (1997) 152–190, [[hep-th/9611230](#)].
- [68] D. Gaiotto and E. Witten, *S-Duality of Boundary Conditions In $N=4$ Super Yang-Mills Theory*, *Adv. Theor. Math. Phys.* **13** (2009), no. 3 721–896, [[arXiv:0807.3720](#)].
- [69] A. Bourget, J. F. Grimminger, A. Hanany, M. Sperling, and Z. Zhong, *Branes, Quivers, and the Affine Grassmannian*, *Adv. Stud. Pure Math.* **88** (2023) 331–435, [[arXiv:2102.06190](#)].
- [70] A. Hanany and A. Zajac, *Ungauging Schemes and Coulomb Branches of Non-simply Laced Quiver Theories*, *JHEP* **09** (2020) 193, [[arXiv:2002.05716](#)].
- [71] R. Bielawski and V. Pidstrygach, *Gelfand-Zeitlin actions and rational maps*, *arXiv Mathematics e-prints* (Dec., 2006) math/0612365, [[math/0612365](#)].
- [72] A. Braverman, M. Finkelberg, and H. Nakajima, *Ring objects in the equivariant derived Satake category arising from Coulomb branches (with an appendix by Gus Lonergan)*, [[arXiv:1706.02112](#)].
- [73] W. Crawley-Boevey, *Geometry of the Moment Map for Representations of Quivers*, *Compositio Mathematica* **126** (2001), no. 3 257–293.
- [74] N. Jacobson, *Completely Reducible Lie Algebras of Linear Transformations*, *Proceedings of the American Mathematical Society* **2** (2, 1951) 105.
- [75] V. V. Morozov, *On a nilpotent element in a semi-simple Lie algebra*, *C. R. (Doklady) Acad. Sci. URSS (N.S.)* **36** (1942) 83–86.
- [76] D. H. Collingwood and W. M. McGovern, *Nilpotent Orbits in Semisimple Lie Algebras*. Routledge, 1993.
- [77] E. Dynkin, *Semisimple subalgebras of semisimple Lie algebras*, *Trans. Am. Math. Soc. Ser. 2* **6** (1957) 111–244.
- [78] N. Yamatsu, *Finite-Dimensional Lie Algebras and Their Representations for Unified Model Building*, [[arXiv:1511.08771](#)].
- [79] S. Cabrera, A. Hanany, and R. Kalveks, *Quiver Theories and Formulae for Slodowy Slices of Classical Algebras*, *Nucl. Phys. B* **939** (2019) 308–357, [[arXiv:1807.02521](#)].
- [80] A. Hanany and R. Kalveks, *Quiver Theories and Hilbert Series of Classical Slodowy Intersections*, *Nucl. Phys. B* **952** (2020) 114939, [[arXiv:1909.12793](#)].
- [81] A. Hanany and R. Kalveks, *Construction and Deconstruction of Single Instanton Hilbert Series*, *JHEP* **12** (2015) 118, [[arXiv:1509.01294](#)].
- [82] P. N. Achar and A. Henderson, *Geometric Satake, Springer correspondence, and small representations*, *arXiv e-prints* (Aug., 2011) arXiv:1108.4999, [[arXiv:1108.4999](#)].
- [83] P. C. Argyres and N. Seiberg, *S-duality in $N=2$ supersymmetric gauge theories*, *JHEP* **12** (2007) 088, [[arXiv:0711.0054](#)].